BIOCHEMICAL EVALUATION OF PEPTIDE-BASED CERIUM OXIDE NANOPARTICLES ON STRUCTURE AND FUNCTION OF VITAL ORGANS IN ADULT RODENT

BY

Olayinka Anthony ADEBAYO

B.Sc. (Hons), Akungba, M.Sc. (Ibadan)

A Thesis in the Department of Biochemistry,

Submitted to the Faculty of Basic Medical Sciences,

in partial fulfilment of the requirements for the award of degree of

DOCTOR OF PHILOSOPHY

of the

UNIVERSITY OF IBADAN

February, 2023

CERTIFICATION

I certify that this work was carried out by Mr. O. A. Adebayo in the Department of Biochemistry, University of Ibadan.

……

Supervisor

O. A. Adaramoye,

BSc., (Ilorin), M.Sc., Ph.D. (Ibadan)

Professor, Department of Biochemistry,

University of Ibadan, Nigeria

DEDICATION

I dedicate this research report to my father, late Dr Ezekiel Adeniyi Adebayo.

AKNOWLEDGEMENTS

I sincerely express my profound and immeasurable gratitude to my supervisor and the Head of the Department, Professor Oluwatosin Adekunle Adaramoye, first, for accepting me as a masters and PhD student under his mentorship and supervision and secondly for his overall contribution to my growth and unwavering academic, moral, financial, and spiritual support to my young family and entire Adebayo's Family. Sir your input contributed in no small measure to the successful completion of this research work. God continue to bless you and your family sir.

I appreciate Professor O. Olorunsogo for his fatherly role, love and kindness all the time. Also, to my Head of DMT unit, Professor Ebenezer Olatunde Farombi, I thank you Sir for your support throughout my postgraduate studies. I have learnt vital lessons from you Sir. I want to appreciate the Dean of my faculty, Professor Oyeronke A. Odunola, thanks in a million for your motherly role. I will also appreciate Professor Gadegesin, the postgraduate coordinator and Professor Olaiya for their constant support in the course of my studies, Thank you Sirs. My unalloyed thanks goes to Dr. Omolola A. Adesanoye for her assistance and encouragement throughout my studies. Thanks ma and God bless you plentifully. I also want to appreciate Dr A. Abolaji, Dr I. Owumi, Dr. Adedara, Dr. E. Olowofolahan and other lecturers of the Department.

I am equally grateful to Mr Eric Sabo, Rev Okewuyi and Mr Ajiboye for their technological assistance during experimentation. I love the company of my colleagues, Idowu Oyinlola (Madam), Semiu Lawal, Segun Olatoye, Comfort, Olola, Opeyemi, Emmanuel, Olagunju Bolaji, Kosemani Samson, Tolulope, Aminat, Leye, Aanu and all past undergraduate students from our laboratory. You guys made the programme easier for me. To Mr Rasak Olajide, though we couldn't spend much time together, the effect of your contribution cannot be forgotten in haste. I want to specially thank Professor Akinloye (Lagos State University) who provided the cerium oxide nanoparticles used for this study without paying a dime. God bless you Sir

Adedoyin, I really want to thank you for being the best colleague I can wish for. Right from the pre research days, through our experimentations and post animal house technicalities, you have been a huge support, sharing knowledge and expertise, making sure we don't lack any laboratory procedures and the likes. Without mincing words, you really made the time spent with you worthwhile and memorable.

To my Father, Late Dr Ezekiel Adeniyi and my mother, Mrs Janet Adebayo, who can simply be described as stereotype of God's gift to any child. I thank you both for your ever refreshing care and support. To my siblings Anike and Bukola, you guys have always been a solid support and your contributions to this programme through thick and thin cannot be forgotten.

I cannot but appreciate Professor O. Akanbi and Professor A. Olonisakin for always being there for the Adebayo's family since the demise of my father. Thank you, Sirs and God keep your families. To my spiritual fathers, Pastor Samuel, Rev Adegunloye, and Rev Idowu, thank you for your support. To my undergraduate supervisor, Dr. Omonkhua, thank you for laying the foundation on which I now build. I know you will be proud of me.

My appreciation goes to the Memento Marketing Agency, from my direct boss, Ahamedshill, and to RB, MB and M0st. Thank you all for believing in me and giving me your platform to showcase my talent. You trusted me with all your assignments despite the fact that we haven't met, God bless you all. To my ever-loving wife and support base, Olajumoke, I want to appreciate you for sticking with me through thick and thin. I have no doubt that you are God sent to me. Thank you for love and support. I also appreciate the Olotu family, most especially Dr Goke and Dr Mrs Jibola Kayode, thanks for all you do.

Finally, eternal praise be to God Almighty for His grace and love that I enjoyed throughout this programme. He alone will be my God forever.

Olayinka Anthony Adebayo

December 2022

ABSTRACT

The application of cerium oxide nanoparticle or nanoceria (CeO_2NPs) in biomedical sciences as an antioxidant agent has gained prominence in recent times. Further medical application of CeO_2NPs is still evolving. However, this approach has not been fully elucidated. In this research report, I evaluated the outcome of CeO_2NPs treatment on the liver and testis, and its ameliorative potential in diethylnitrosamine (DEN)-induced hepatotoxicity and, N-Nitroso-N-methylurea (NMU) and Benz[a]pyrene (BaP)-induced mammary toxicity.

Twenty male Swiss mice (30.0±2.1g) were divided into four groups (n=5): control, 100, 200 and 300 µg/kg CeO_2NPs. Nanoceria was administered intraperitoneally three times per week for 5 recurring weeks. Mice were sacrificed, blood was collected and testes were harvested for analyses. The second study consist of six groups (n=6) and treated thus: Control, DEN, [DEN+CeO_2NPs (100 µg/kg)], [DEN+CeO_2NPs (200 µg/kg)], CeO_2NPs (100 µg/kg) and CeO_2NPs (200 µg/kg). Mice were pre-treated with CeO_2NPs daily for eight days and, hepatotoxicity was induced by single administration of DEN (200 mg/kg, i.p). In the third study, 24 female rats were allocated into 4 groups (n=6), and treated thus: Control, [NMU+BaP], [NMU+BaP+CeO_2NPs] and [NMU+BaP+Vincristine]. The NMU and BaP were administered at 50 mg/kg thrice (at week 7, 10 and 13), while Vincristine [(positive control) (0.5 µg/kg)] and CeO_2NPs (200 µg/kg) were administered twice and thrice per week, respectively. Haematological [Haemoglobin (Hb), Packed cell volume (PCV) and red blood cell (RBC) count] and biochemical indices [Alanine Aminotransferase (ALT), urea, antioxidant enzymes and Malondialdehyde (MDA)] were determined by standard methods. Hormones: Luteinizing hormone (LH), follicle stimulating hormone (FSH) and prolactin were estimated by ELISA, while inflammatory markers; inducible Nitric Oxide Synthase (iNOS) and Cyclooxygenase-2 (COX-2), and apoptotic indices; Bcl-2 associated X-protein (Bax), p53 and Caspase-3 were determined by immunohistochemistry. Micro-section of tissues were stained with Haematoxylin and Eosin and viewed under light microscope. Data were analysed using ANOVA at $\alpha_{0.05}$.

In study one, nanoceria reduced Haemoglobin by 71% and 35%, packed cell volume by 69% and 26% and red blood cell count by 69% and 36% at 100 and 300µg/kg CeO_2NPs, respectively compared to control. The LH (11.30±1.52 and 10.30±0.57 vs

19.51±0.52), FSH (9.66±1.15 and 7.33±0.57 vs 18.40±0.50) and prolactin (6.05±1.00 and 4.33±0.57 vs 9.31±0.43) were decreased in 200 and 300μg/kg CeO_2NPs-treated mice, respectively compared to control. Testicular MDA level was increased by 67% and 78% in 200 and 300 μg/kg CeO_2NPs-treated mice respectively, and an attendant decrease in activities of antioxidant enzymes. In the second study, pre-treating using CeO_2NPs (100 and 200 μg/kg) decreased ALT activity by 24% and 23%, respectively. Likewise, CeO_2NPs at 200 μg/kg caused 35% reduction in MDA level and concomitant increase in antioxidant enzymes. The liver showed weak expression of iNOS and Cox-2 when pre-treated with CeO_2NPs. In the third study, the [NMU+BaP] decreased the activities of mammary antioxidant enzymes while increasing MDA level. Caspase-3, Bax and p53 were reduced in [NMU+BaP] animals. Histology revealed severe peri-vascular infiltration of inflammatory cells in hepatocytes of DEN-treated mice, and malignancy in mammary tissues of [NMU+BaP] animals. Treatment with CeO_2NPs (200μg/kg b.wt) attenuated altered biochemical, inflammatory and antioxidant markers, and cyto-architectures of liver and mammary tissues in DEN- and [NMU+BaP]-treated animals.

Nanoceria ameliorated chemically induced hepatic, reproductive and mammary gland toxicity in animals via induction of apoptosis and antioxidant enzymes.

Keywords: Antioxidant, Cerium oxide nanoparticles, mammary gland Apoptosis
Word count: 499

TABLE OF CONTENTS

LIST OF TABLES

LIST OF FIGURES

LIST OF PLATES

LIST OF ABBREVIATIONS

AmB:	Amphotericin
ANOVA:	Analysis of Variance
Bax	B cell lymphoma-2-associated X Protein
BBB	Blood brain barrier
Bcl-2	B cell lymphoma-2
CDNM:	1-Chloro-2, 4, -dinitrobenzene
CeO_2 NPs	Cerium oxide nanoparticles
COX:	Cyclooxygenase
DEN:	Diethylnitrosamine
DNA:	Deoxyribonucleic acid
DPA:	Diphenylamine
DTNB:	5` 5`-Dithiobis-(2-nitrobenzoic acid)
ER:	Endoplasmic reticulum
GPx:	Glutathione Peroxidase
GSH:	Reduced Glutathione
HRP:	Horseradish peroxidase
IHC:	Immunohistochemical
iNOS:	Inducible Nitric Oxide Synthase
LH:	Luteinizing Hormone
MDA:	Malondialdehyde
MPO:	Myeloperoxidase
NF-KB:	Nuclear Factor kappa B
NMU:	N-methyl-N-nitrosourea

NO:	Nitric Oxide
PCV:	Packed cell volume
QDs:	Quantum dots
ROS:	Reactive oxygen species
SA:	Salicylic acid
TBA:	Thiobarbituric acid
TCA:	Trichloroacetic acid
UV:	Ultraviolet

CHAPTER ONE

INTRODUCTION

1.1 Background of the study

The evolution of nanotechnology era is accompanied with array of potential health concerns that may arise following intentional or accidental contact with manufactured compounds. The speech by Richard Feynman at a scientific gathering in 1959 heralded the concept now referred to as nanotechnology (Feynman, 1960). Nanotechnology is defined as the research and technological manipulations of a substance at the atomic, molecular, and micro-molecular level. (Ghio *et al.,* 2010), thereby creating new substances that performs different and exciting functions. Applications of nanotechnology ranges from electronic industry where it has encouraged construction of devices which consumes less energy and have lesser weight (Bayda et al., 2019). In the Agriculture and food sector, nanotechnology has encouraged the use of nano-oriented materials as a component of food packaging in order to reduce the amount of leaked carbon (IV) oxide, thereby prolonging the shelf life of packaged foods (Li *et al*., 2022).

In addition, it has enabled textile industries to produce nano fabrics that are stain repellent and wrinkle free. (Patra and Gouda, 2013). In the energy sector, nanotechnology has encouraged the production of gasoline and diesel from low-grade materials, thereby preventing fuel shortage. (Rai *et al.,* 2016). In medicine, nanoparticles play vital functions which include fluorescent dyes, delivery of drugs and genetic materials (Yetisgin *et al.,* 2020), detection of pathogenic microorganisms (Fanelwa *et al.,* 2022), protein detection (Váradi et al., 2017), structural investigation of the genetic code, biological modification of tissues (Wang, 2017) and decontamination and separating cellular fragments (Barhoum *et al.*, 2022). New forms of nano-based metal oxides are currently being designed for a variety of innovative usage (Asim *et al.,* 2020).

Cerium, which belongs to the family of the lanthanides sequence of earth metals occupies position 58 on the periodic table of elements. Cerium oxide has found application where it has been used in diesel powered engines as catalyst to reduced particulate matter emission, and therefore, emitting cerium oxide nanoparticles (or nanoceria), which contribute to air pollution, causing a major health hazard to humans and animal in the environment. (Martina *et al.,* 2020). It also accounts for some antioxidant properties, where it can be used to protect cells from radiation induced carcinogenesis (Tarnuzzer *et al.,* 2005).

Report has it that there is increased possibility of using cerium, praseodymium, and terbium oxide-based nanoparticles to generate hydrogen for fuel cells that use solid oxide; a market that is projected to develop significantly, causing environmental dispersion of these compounds while being used (Park *et al.,* 2000). Cerium oxide nanoparticles finds applications in industrial sectors where it is being used as ceramic or polishing of glass, solar energy cells, television tubes, UV absorbing objects, and as sensors in gas containers (Corma *et al.,* 2004). Although, addition of cerium oxide nanoparticles to diesel further improves the overall output of engines, it however causes unfiltered discharge of this particle to the atmosphere. Direct exposure of humans to nanoparticles can be made possible workplace (occupational) as well as environmental discharge via breathing and absorption as main routes. Inhalation however appears to be the primary exposure route because CeO_2 NPs are weakly absorbed in the gut. A keratinocyte-based model schemes showed that cerium oxide nanoparticles can serve as an antioxidative agent and co-localizations of this particle in cellular components, including the nucleus, mitochondria, lysosomes, as well as cytoplasm has been reported (Chen *et al.,* 2013).

Cerium oxide nanoparticles can protect cellular components by promoting the removal of reactive oxygen species (ROS) owing to their characteristic antioxidative activities (Ma *et al.,* 2012). The availability of two-fold oxidation status of nanoceria or the cellular pH where the nanoparticles internalization takes place were assumed to be responsible for this defensive mechanism (Nelson *et al.,* 2016). Along the same line, researchers have suggested that smaller dimension of cerium oxide nanoparticles may not induce any side effect, nonetheless it can confer protection on cells from the harmful effects occasioned by exposure to radiation and oxidative damage, but the

mechanism of protection is cell type specific. Several studies have also revealed that nanoceria can cause oxidative injury and increase cell death in the epithelium of the human lungs (Park *et al.,* 2008; Tsai *et al.,* 2018). Owing to its ability to trigger inflammatory reactions, in-vivo investigations have shown that exposure to nanoceria via instillation or inhalation in the tracheal can cause systemic pulmonary toxicity in animals (Peng *et al.,* 2014). Due to these discrepancies, the toxic effect of CeO_2NPs remains unknown, and the particular toxicity end point pertinent to human wellbeing must be resolved.

1.1.2 Problem Statement

The recent proliferation of nano-based products due to the application of nanotechnology has increased exposure to various types of nanoparticles by people, animals as well as the ecosystem, and the risk associated to this exposure has been widely debated. Among nanoparticles that have received wide applications, cerium oxide nanoparticles have stands out due to its applications in biomedical and industrial sector. However, despite its essential properties, there has continued to be uncertainty regarding its toxic characteristics.

1.2 Rationale of this study

The increased production of new (nano) materials due to their applications in various fields has made the exposure to these materials to be on the rise. Earlier researchers focused more on the distinctive physicochemical characteristics of nano-based materials to manufacture devices that are less in weight and occupy minimal space. In recent years, scientists have beamed searchlight on the probable biomedical applications of engineered nanoparticles in various conditions, such as component of drug delivery system to target organs, a feat which biological agents could not. Therefore, the possible advantage and hazards accompanying the use of and exposure to nanomaterials have continued to generate debate in recent years. The uniqueness and biochemical characteristic of cerium oxide nanoparticles has enabled its applications in medicine. The ability of nanoceria acting as an antioxidative agent has been employed to treat and/ manage different forms of pathological conditions in experimental animals, many of which produced outstanding outcomes. However, because their hazardous properties are unknown, there are concerns that they may

cause occupational risks to factory staff and consumers exposed to cerium oxide nanoparticles.

1.2.2 Aim of the Study

This research was carried out to correctly assess the toxicological profile of cerium oxide nanoparticle in animals and also suggest the possible mechanisms of its toxicity. In addition, the health benefit of this nanoceria in chemically induced pathological conditions needs to be explored and expanded.

1.3 Study Objectives

The purpose of this research was to investigate the following.

(a) Effect of nanoceria on male reproductive function in adult mice.

(b) Evaluation of hepatic function of adult mouse following exposure to cerium oxide nanoparticles,

(c) Ameliorative potential of nanoceria in diethylnitrosamine (DEN)-induced hepatotoxicity in male wistar rats and

(d) Ameliorative potential of nanoceria following induction of mammary toxicity via injection of Benz[a]pyrene and N-Nitroso-N-methylurea to adult female rats.

CHAPTER TWO

LITERATURE REVIEW

2.1 Nanotechnology

The conception of the word ‘nanotechnology’ was initiated by Richard Feynman in a presentation titled “*There's Plenty of Room at the Bottom”* where he stated the probability of synthesising nanoparticles by direct alteration of atoms. Nanotechnology is the multi-dimensional field that encompasses arrays of diverse disciplines which includes and not limited to agriculture, engineering, biology, physics, and chemistry. It is the research and technological alteration of substances at the nuclear, molecular, or macromolecular level (Ghio *et al.*, 2010), giving rise to an entirely different entity in shape, size, and function. The research into synthesis and applications of nanoceria are likewise widespread, extending from traditional devices to wholly new systems based on molecular self assembly, from making new nano-based materials to directing matter control on the atomic level (Karakoti et al., 2008).

The National Nanotechnology Initiative (NNI) established a more universal explanation of the term ‘nanotechnology’ which describes nanotechnology as the alteration of matter within the length scale from 1-99 nanometres. The potential biomedical and industrial applications of nanotechnology have propelled the government to spend billions of dollars. Precisely, the European Union has financed to the tune of 1.2 billion dollars to its National Nanotechnology Initiative, while the US has invested 3.7 billion dollars and Japan has committed 750 million dollars (Loh *et al*., 2003).

The future implication of nanotechnology application in various industries is now being discussed among scientists. This is due to the ability of various compounds to be engineered and give rise to variety of novel products which can find applications in consumer goods, energy, electronics, agriculture, and medicine. Nanotechnology, in contrast, generates similar challenges that most innovative technologies do, such as the

toxicity of nanoparticle and environmental impact, as well as their possible implications on global economies and speculation about various scenarios of the apocalypse. These fears have triggered a debate amongst advocacy organizations and authorities on whether nanotechnology necessitates special guideline (Karakoti et al., 2008).

2.2 APPLICATIONS OF NANOTECHNOLOGY

2.2.1 Drug Delivery

The ability of nano based particles to be deployed as tool for the delivery of drugs, light chemicals, and certain cell types (e.g. cancer treatment) remains one function of nanotechnology in the medical field currently being developed (Jin *et al.,* 2020). This method assists in protecting healthy cellular units of the human body while also permitting earlier identification of disease. Nanoparticles, for example, are being developed to deliver chemotherapeutic agents directly to malignant cells (Cheng *et al.,* 2021). Targeted delivery of chemotherapeutics is undergoing testing, and final approval for usage with cancer patients is forthcoming. Various forms of nanoparticles have been deployed for delivery of medications to targeted sites to increase poorly soluble drugs uptake, specific-site drug targeting and drug bioavailability by delivering directly to the site of disease (Ould-Ouali *et al.,* 2005). Doxorubicin (Sudha et al., 2017), dexamethasone (Panyam and Labhasetwar, 2004) and paclitaxel (Tewabe *et al.,* 2021) are examples of some anticancer agents that have been effectively prepared using nanoparticles.

Dexamethasone is an active anti-cancer drug that inhibit cell proliferation and reduces inflammation. This drug attaches self to receptors within the cytoplasm, and the resulting complex so formed is conveyed to the core nucleus, thereby inducing production of specific anti-proliferative proteins (Panyam and Labhasetwar, 2004). The use of specialized chemo delivery mechanisms like micelles, vessicles, and nano particles in cancer therapy has been extensively studied (Tharkar *et al.,* 2019). Reduced toxicity, small size, biological distribution and alteration of the pharmacokinetics of the drugs are some factors that contribute to effective drug delivery (Glassman *et al.,* 2019). Chemotherapy is becoming frequently ineffective in cancer treatment because of the resistance of anti-tumour drugs to certain cancer cells.

Such resistance usually develops when tumour cells express p-glycoprotein, which has the ability to exude anti-tumor drugs rapidly as they move across the outer membrane of the cell (Mansoori *et al.,* 2017). There has increased the probability of nanoparticles to deliver anti-cancer drugs against tumor growth devoid of triggering p-glycoprotein pump, according to a recent study (Wang *et al.,* 2010).

2.2 Tissue Engineering

The surface of a normal bone frequently comprises 100m wide structures (Claeke, 2008). The natural body has the tendency to decline a smooth-surface artificially crafted bone implant (Thiel, 2000). This is due to the fact that such surfaces can probably develop fibrous tissues that covers the implant, limiting the frequency of contacts by the bone and implant, which further leads to implant loosening and inflammation (Thiel, 2000). It was shown that Introduction of nano-sized structures on the surface of artificial prosthetic bone might possibly moderate the likelihood of bone rejection while also stimulating the production of new bone cells (Qiao *et al.,* 2022).

Osteoblasts are important in bone formation and growth and are predominantly located on developing bone. Also, over ninety percent (90%) of normal bone cells on suspension attached to metal surface containing nanomaterials (Caetano-Lopes *et al.,* 2007). In orthopaedics, titanium is a common material for effective bone repair. It is ductile, highly tensile and resistant to fracture. However, it lacks biological activity, rendering it difficult for it to support growth and cell adhesion (Thiel, 2000).

2.2.3 Nanosystem in inflammation

The capacity of nanoparticles to identify and eliminate foreign particles quickly has provided a sensible method to targeting macrophages using nanoparticles. The ability of macrophages to release a variety of inflammatory proteins permits them to control inflammation in a variety of pathological disorders. As a result, macrophages could be used as a drug target in a variety of human and animal disorders. Despite the fact that macrophages can kill most bacteria, some have gained the ability to resist phagocytosis (Sarabjeet, *et al.,* 2007). These pathogenic agents subvert the molecular machinery of the macrophage, which is designed to eliminate them and end up in the already modified lysosomes. As a result, the transport of antimicrobial agents via nanoparticles in the intracellular vacuoles of pathogenic microphages could be effective in

eliminating cellular pools of inflammatory proteins (Zhang *et al.,* 2007). This technique can therefore be used to deliver exact drug concentrations directly into the infected vacuole of the macrophage as well as reduce drug-related adverse effects. Amphotericin (AmB), an antifungal agent has been formulated with nanotubes (lipid-based) to produce AmB which shows less toxicity. Mahmoud *et al.,* (2022) deployed a trilaurin-dependent lipid nanoparticles as a novel intravenous chemo-delivery approach for targeting microphages. In genetic treatment and some medically related scenarios like rheumatoid arthritis and auto-immune blood maladies, nano-based transport of toxic macrophages has proven to be a realistic mechanism of eliminating pathogenic macrophages (Sarabjeet, *et al.,* 2007).

2.2.4 Optical Imaging

In most practices, organic dyes are loaded into the sample for conventional imaging of cellular and tissue sections. Biomolecules linked to dyes like rhodamine selectively attach to cellular components via receptor-ligand connections. Insufficient fluorescence power and photobleaching are common events that often occur in this method of imaging (Oliveira *et al.,* 2017). Photobleaching involves deliberate loss of fluore-intensity at time intervals, caused by permanent alterations in the chemical structure of the dye, rendering them non fluorescent. Quantum dots (QDs), a form of nanoparticle comprises inorganic semi-conductor units. Being made up of inorganic materials, QDs can easily dissolve in aqueous solutions. Therefore, for optimal delivery of its functions in biological system, quantum dots need to be coated with materials that can dissolve in water (Wagner *et al.*, 2019).

The next stage involves coating the quantum dots using a thin layer compound that has high affinity to bind to a specific cellular component. In addition, quantum dots can serve multiple functions because each quantum dots can accommodate more than one molecule (Shashi, 2007). In one of their studies, Akerman in 2002 established that quantum dots capped in Zns and CdSe can be delivered to mice's lungs by coating its surface with amino acid sequence, CGFECVRQCPERC, which has been identified to possess the ability in binding of blood vessels of the lungs (Akerman *et al.,* 2007).

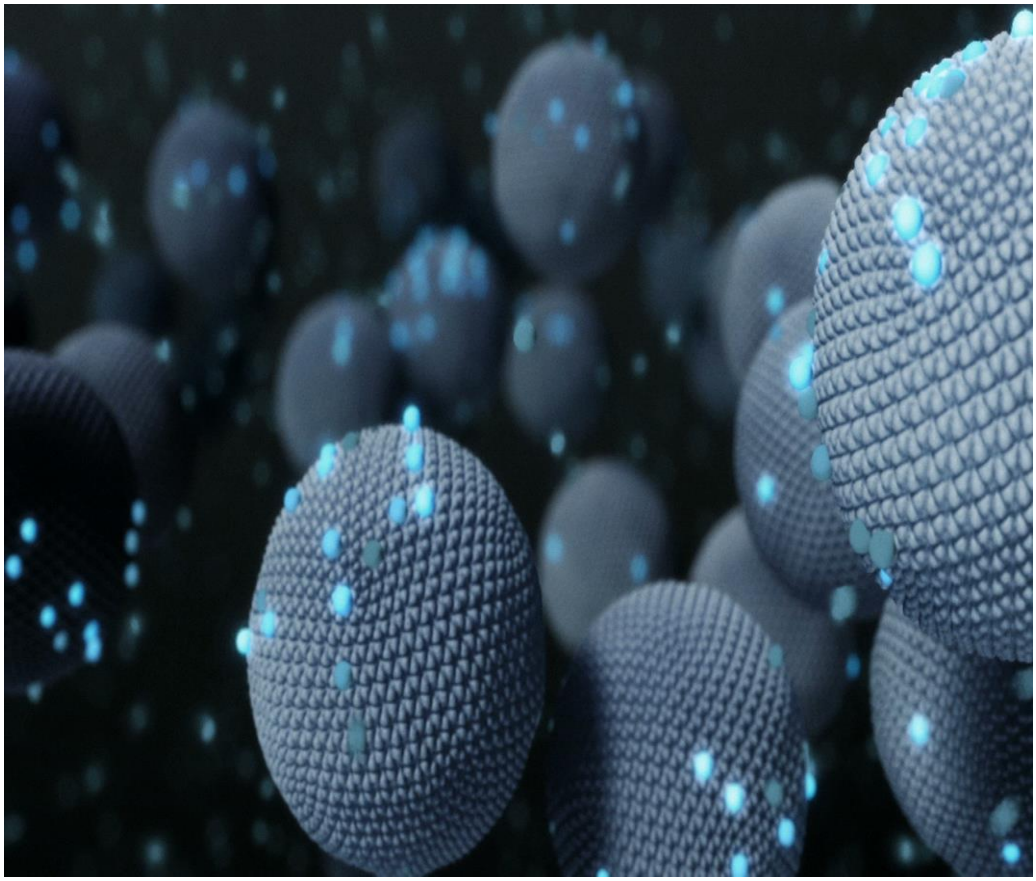

Figure 2.1: Optical Imaging using High Resolution Optical Nanoscope (Karthik and Prabaharan, 2020)

2.2. 5 Manipulation of cells and biomolecules

Functionalized metal nanoparticles offer a wide variety of functions such as probing and separation of cells (Pankhurst *et al.,* 2003). The majority of metal-based nanoparticles investigated recently have a characteristic spherical shape, which limits their prospects of being made multifunctional nanoparticles such as quantum dots discussed above. Alternatively, cylindrical nanoparticles could be constructed by deploying the electrode position of the metal to a nano-porous alumina template (Skinbinska *et al.,* 2021). Diverse ligands have the tendency to be attached to different sections due to the well-developed mechanism designed for functionalising surface chemistry of most metals. Porphyrins containing carboxyl or thiol substituents, for example, were linked simultaneously with nickel or gold sections (Qi et al., 2020). As a result, construction of magnetic nanowires with spatially separated fluorescent sections can be achieved (Ariga *et al.,* 2019)

2.2.6 Detection of protein

It is unarguable fact that proteins are important constituent of the structural architecture of the cell, therefore understanding their roles is vital in order to further advance the wellbeing of humans. Engineered gold particles are often used in immunohistochemical research to detect interactions between proteins (Thiel, 2000). However, the multi-faceted detection abilities of the approach is relatively inadequate. The improved surface Ratman Scattering spectroscopic technique is properly recognized for detecting and identifying specific molecules of dye. Merging the two strategies into a single and unique particle probe can considerably enhance the multi-plexing abilities of protein-probes.

In a study, a multifunctional probe was built around gold nanoparticle measuring 13 nanometre in length. The resultant nanoparticle was coated using dye (Rayman) on a particular end along with a small-scale molecular fragment in the terminal (Bayda *et al.,* 2019). Furthermore, the catalytically functional molecule will subsequently be layered with solution containing hydroquinone and silver iodide. The different nanoparticles are covered by means of oligonucleotides (hydrophilic) using the Raman dye at a terminal and at another end having a small molecular recognition element. Moreover, the molecule remains catalytically functional and coated using silver.

2.2.7 Nanotechnology improve fuel cells

A catalyst is used for the creating hydrogen ions from precursors such as methanol and hydrogen. The most commonly used catalyst for this process is typically the high-priced platinum. There has been recent adoption of engineered platinum particles by industries, geared towards minimising the overall amount of platinum used and thereby production cost (Zhang *et al.,* 2020). Majority of energy cells have layers that permit the free movement of hydrogen ions (figure 2.2), but it however prevents the free flow of another ions like oxygen through it (Wang *et al.,* 2017) Therefore, industries are harnessing nanotechnology to develop additional efficient barriers, allowing the production of energy cells that are long lasting and light weighted. Small-scale energy cells have been built for use in hand-held gadgets such as phones, laptops and other digital products to substitute conventional batteries (Zhang, 2017).

Most studies recommend hydrogen as the most suitable fuel for energy cell vehicles. Besides the catalyst and barrier development mentioned earlier, a light weighted, and secured hydrogen fuel storage chamber must be developed as well as a system for recharging stations. In order to construct these storage chambers, research has attempted to produce nanomaterials that are light in weight, capable of absorbing hydrogen and discharge it only when there is a demand for it (Attia *et al.,* 2020). Energy cells, like ignition engines need air and water to operate a car. For instance, in a typical hydrogen cell, the hydrogen ions move to a side of the cell while air is injected to the other compartment across the membrane (Estrada *et al.,* 2022). When on the anode, the hydrogen is oxidized and it converts to protons which travel to the cathode to generate water. Thereafter, platinum (catalyst) present at the cathode and anode aids the rapid reaction which produces electrical connection having about 60% effectiveness without any harmful waste. Heat and water are the only products emitted by this electrochemical process (Badwal *et al.,* 2014).

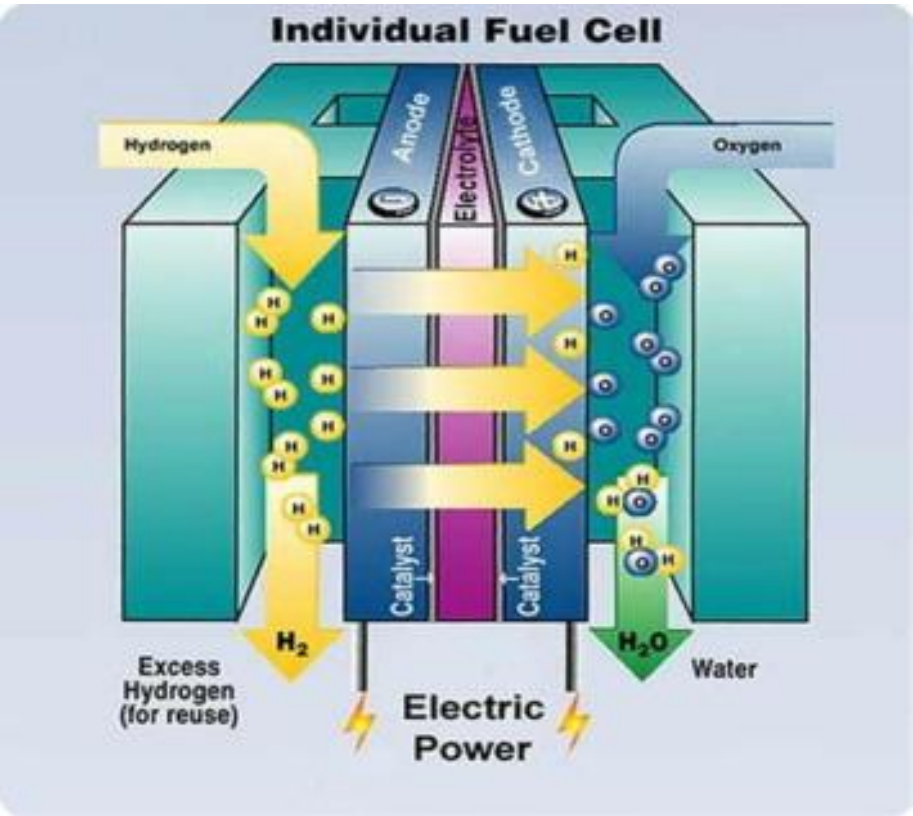

Figure 2.2 Application of nanotechnology in energy cell technology (Yeu *et al.*, 2019)

2.2.8 Food Industry

Food science has been influenced by nanotechnology in a number of ways from how food is cultivated to the packaging processes. Food-based companies now develop nanoparticles that can enhance not just the taste or flavour, but also its overall health effects to consumers. Zinc oxide nanoparticles, for example can be integrated into plastic packaging to filter UV radiation and proffer antibacterial protection while also enhancing the plastic film's strength and stability (Sirelkhatim et al., 2015). At a packaging plant, nano sensors have been recently produced to identify harmful microbes and other pollutants like salmonella typhi. This will enable frequent testing at a fraction of the cost of shipping samples to a laboratory for examination.

If done correctly, point-of-packaging analysis can drastically minimize likelihood of contaminated food stuff making way to the supermarkets. Nano-capsules carrying nutrients are developing significantly, with the goal of releasing them when nanosensors detect a vitamin deficit in the body. The food and Agricultural sector tend to be transformed by nanotechnology (Sekhon, 2010). At nano level, food security, efficacy, bioavailability, and nutritive benefits, and also production of new and improved seeds and supplements, can all be influenced. (Sirelkhatim et al., 2015). In fact, nanotechnology is enhancing food safety and handling, nutrient absorbing ability of plants, improved flavour and nutritive value, delivery techniques, infection detection, food functioning, protecting the environment, and cost of effective storage and supply.

Nanotechnology could be beneficial in creating novel, functional raw material, micro- and nano scale managing, product expansion, and modelling food-processing procedures and apparatus. Packaging of foods protects food commodities from the harsh conditions of the atmosphere, confines them, provides consumers with nutritional knowledge, and extends food storage time and overall quality (Cole and Bergesone, 2006). The application of nanotechnology in the package of food has been steadily rising in recent years. Nano-packaging had global revenues of $860 million in the year 2006, and the industry is projected to expand near $30 billion within 10 year time. (Coles *et al.*, 2003). Nanoparticles can increase the ability of packaged food to resist heat and mechanical damage by regulating the rate of both water vapour and air permeability, hence increasing the validity of the shelf life. Polymers, for instance, are

not naturally resistant to gas and vapour, however its silicate nano-composites have improved food packaging difficulty, mechanical force, and resistance to heat (Holley, 2005).

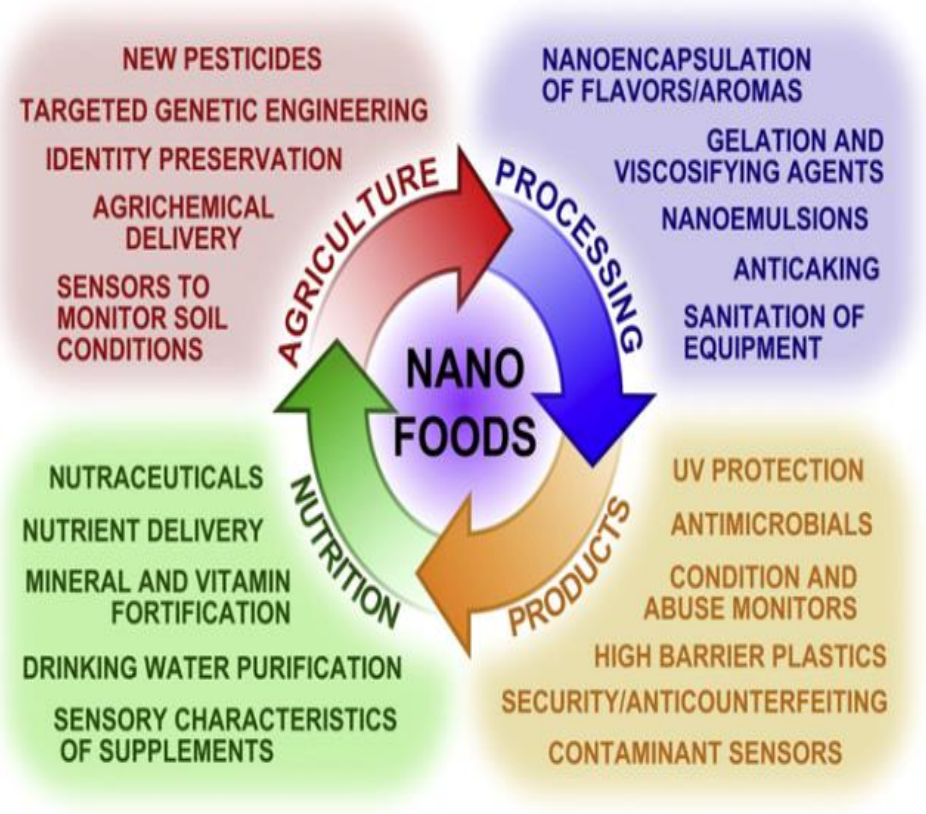

Figure 2.3: Nanotechnology has applications in food science. (Duncan, 2011)

2.3 Cerium

Cerium, (Ce) with atomic mass of fifty-eight (58), depicts a lax, pliable, shiny metallic element. When exposed to the atmosphere, cerium tarnishes quickly to be expurgated with the aid of sharp blade (Jakupec *et al.,* 2015). It takes the second position in the series of lanthanide family, possessing a characteristically dual oxidation statuses (+3 and a steady +4 that does not undergo oxidation in aqueous solution).

The biological function of cerium is unknown and studies have shown that the metallic element is particularly not very lethal (Dahle and Arai, 2015). Regardless of being constantly found associated alongside other unique earth components in mineral deposits like bastnäsite and monazite, the extraction process is simple. A distinguishing factor that differentiate cerium from other family in the rare-earth element series lies on its flipping to +4 oxidation. Cerium is most predominant element among lanthanides, with lanthanum, praseodymium, as well as neodymium following closely behind, it is the 26th most prevalent element, accounting for 66 ppm of the crust and 50% that of chlorine (Taha *et al.,* 2022)

2.3.1 Physical Characteristics

Cerium is the second among the families of the lanthanides and located between lanthanum in the left-hand and flanked in the right of the periodic table by praseodymium (Bailey *et al.,* 2022). It has 58 electrons which are organized in $[Xe]4f^{1}5d^{1}6s^{2}$ configuration, where the four electrons on the outermost shell represents the valence electrons. The 4f orbitals quickly compress and lose energy, allowing them to take part freely in various reactions. Majority of lanthanides series have the ability to utilize just three electrons to represent their valency, as subsequently the residual 4f electrons remain tightly bond. However, cerium is different because the f-shell in Ce^{4+} is empty (Bailey *et al.,* 2022).

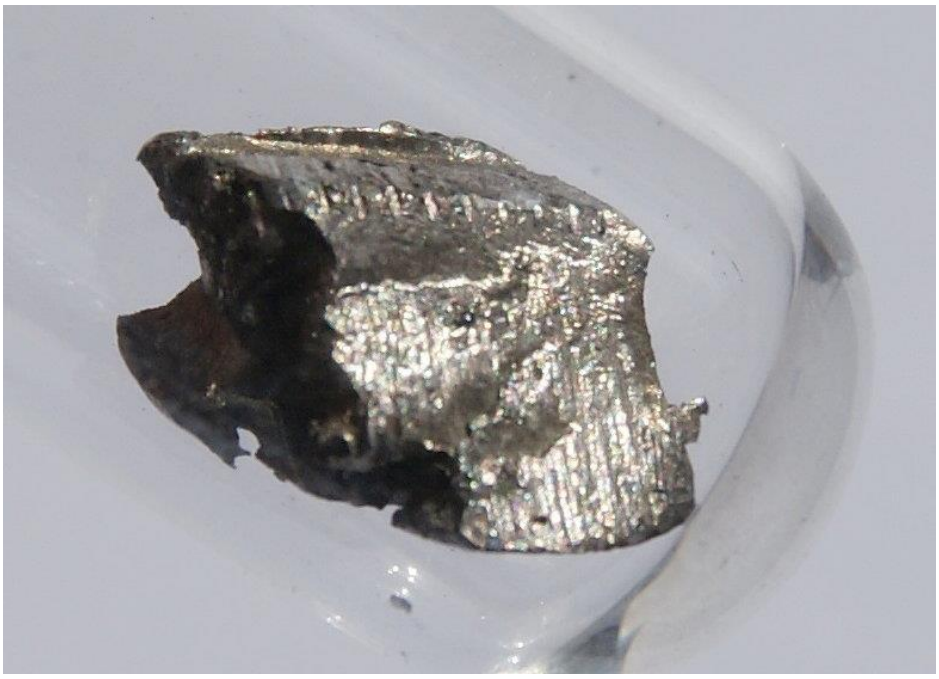

Figure 2.4: Ultrapure cerium under argon. (Juri *et al* 2009).

2.3.2 Occurrence

Among the lanthanides, cerium has the highest abundance, accounting for sixty-six parts per million of earth's layer covering; an amount that stands after copper (sixty-eight parts per million) and surpassing other regular metals such as lead (thirteen parts per million) as well as tin (thirteen parts per million) (Gschneidner, 2023). Cerium is thus present in abundance, in spite of its belonging to a family of rare earth metals. Its content in soil ranges from two to one hundred and fifty ppm, averaging fifty parts per million; seawater contains 1.5ppt cerium (Dahle and Arai, 2019). Cerium is found in a variety of reserves, however bastnasite and monazite are the most abundant sources of the element, where it accounts for nearly 50% of lanthanide concentrations. Because only cerium characteristically possesses the ability to maintain stability in aqueous medium among lanthanides, it renders extraction from its minerals easier. It is rarely eroded from the earth in comparison to the other rare earth elements because of its reduced solubility when oxidation state is at +4 (Thomas and colleagues, 2003).

2.3.4 Chemistry

While in the air, cerium tarnishes gradually, generating an oxide coating similar to iron rust. At 150 °C, cerium easily burns to generate the light yellowish cerium-dioxide, called ceria.

$$Ce + O_2 \rightarrow CeO_2$$

In the presence of hydrogen gas, cerium-dioxide can undergo reduction to produce cerium (III) oxide. The pyrophoric nature of cerium metal means that when placed on the ground or scraped, the resultant flakes catch fire (Fahlman, 2018). Cerium, belonging to the first, and therefore part of the principal lanthanides, renders its reactivity to follows periodic patterns. Cerium (IV) oxide, like other dioxides of praseodymium and terbium, has a fluorite structure. Many nonstoichiometric chalcogenides, as well as the trivalent Ce_2Z_3, are also known. Cerium exists extremely electropositive in nature which readily interacts with H_20. This reaction normally occur slowly when taking place in cold water but becomes rapid upon increase in temperature, generating cerium(III)hydroxide and hydrogen gas.

$$2\ Ce\ (s) + 6\ H_2O\ (l) \rightarrow 2\ Ce(OH)_3\ (aq) + 3\ H_2\ (g)$$

When reacted with excess fluorine, it produces a stable cerium tetrafluoride, while the other tetrahalides are unknown till present. Only the bronze-diiodide (CeI_2) is predominantly know out of the dihalides produced during the reaction. Also, cerium readily dissolves in H_2SO_4, forming solutions that contains the colourless forms of Ce^{3+} ions existing as $[Ce(H_2O)_9]^{3+}$ complexes.

$$2Ce(s) + 3H_2SO_{4(aq)} \rightarrow 2Ce^{3+}{}_{(aq)} + 3SO_2{}^{-4}{}_{(aq)} + 3H_{2\ (g)}$$

2.4 Cerium Oxide Nanoparticle

Cerium oxide nanoparticles or nanoceria for many years has found applications in different industries which include mechanical, chemical and glass polishing industries (Li *et al.*, 2022). Furthermore, there exists increased interest in the application of nanoceria-based fuel stabilizer which helps to moderate smoke emission, thereby increasing the overall efficiency of diesel engines (Jung *et al.*, 2005). Despite widespread applications, it is not until 2006 when novel studies showed the impressive biological property of cerium oxide nanoparticles in its ability to exhibit antioxidant activity (Singh *et al.*, 2020). The main property that renders cerium oxide nanoparticles in it application in biomedicine is in its ability to store oxygen in lattice (Nyoka *et al.*, 2020).

2.4.1 Biological activity of Nanoceria

The biological characteristics of nanoparticles comprises the pharmacokinetics, bio-distribution, metabolism, toxicity and excretion of the nanoparticle, depending on factors such as chemical and physical properties. It was earlier believed that the activity of a nanoparticle in the biological system is similar to its activity when synthesised. However, recent findings by scientists have shown that when nanoparticles gain access to a biological environment, they interrelate with a variety of soluble biomolecules, leading to the development of a biomolecular corona (Gao *et al.*, 2021). This corona so formed is characterised by altered charge, composition, mass as well as the nanoparticle's surface charge conferring on it a differential biological activity from its synthetic form (Spicer et al., 2018). In addition, the biomolecule-nanoparticle corona can also experience altered activity, aggregation form and

dissolution properties of the nanoparticle, influencing the biological activity of the nanoparticle.

2.4.2 Biological Identity formation for Cerium oxide nanoparticles

Biofluids are commonly made up of wide range of soluble proteins. For example, the blood plasma is made up of about 3700 distinct proteins (Anderson and Anderson, 2002). Proteins migrate towards a nanoparticle's surface when it enters a biofluid, and the most abundant proteins will reach the biofluid early. In most cases, the common proteins frequently form a weak association with the surface of the nanoparticle and dissolve quickly into solution. Higher affinity but low quantity proteins gradually take the place of lower affinity and higher quantity ones (Aggarwal *et al.,* 2009).

Although the exchange mechanism does not take place over a set amount of time, the protein corona that surrounds several formulations of nanoparticles attain equilibrium some minutes (Nguyen *et al.,* 2017). The relatively high proportion of proteins in large amount on the protein corona does not always correspond to the protein's presence contained in the biofluid. This is because the surface of the nanoparticle have high tendency to supply small proportion of proteins. This has however led to a surprising discovery that serum albumin, which is the most abundant protein in the blood plasma is found in small amount in the protein corona surrounding the bulk of nanoparticle formulations (Moman *et al.,* 2022). The protein corona surrounding the nanoceria is thought to enhance low proportions of proteins, though this has yet to be proven experimentally. These proteins are theoretically categorized into two types based on their binding affinity (Cedervall *et al.,* 2007).

Proteins contained within the corona are tightly linked to the nanoparticle and can stay bond to it for some minutes. However, proteins in the soft portion of the corona develop a systematic equilibrium alongside the nanoparticle and swiftly desorb upon removal of the biofluid. According to Casals and his colleagues, upon subjection to fetal bovine serum, the protein corona surrounding the nanoceria changes from a systematic reversible to an irreversible form over a period of time, precisely days (Casals et al., 2010; Casals *et al.,* 2011). Structural alteration and positioning of now adsorbed proteins may cause the protein corona to harden. Proteins confined in the solid corona stay linked to the particle while it interrelates with machineries of the

system biology, which includes cells due to their lengthy residence period. Therefore, the hard corona indicates in part or entirely a nanoparticle's interface in physiological environment, whereas soft portions have lesser role.

2.4.3 Role of biological character/Identity on the nanoceria's action.

In-vitro cell culture methods are commonly deployed to decipher the precise mechanism by which nanoparticles interact with cells. Silica nanoparticles (Yang *et al.,* 2011), titanium dioxide nanoparticles (Shi *et al.,* 2003). Carbon nanotube (Das *et al.,* 2017), polystyrene nanoparticles (Loos *et al.,* 2014) as well as gold nanoparticle (Fleischer *et al*., 2013) have been shown to be less associated with several cell types that are different from tissue sources when serum proteins are present in the culture media. Also, Lesniak *et al.,* (2012) proposed that some nanoparticles characterised by increased surface activity tend to associate strongly with cellular biomolecules in the membrane in the absence of serum proteins, thereby promoting nanoparticle- cell association and uptake. Proteins coat the surface of nanoparticles, increasing its hydrophilicity and forming spatial buffer that prevents association between nano-particle surface and cell membrane. Coating the surface of nanoparticle by the adsorbed proteins can help inhibit cytotoxicity that occurs due to the damage to the biomolecules on the cellular surface as well as cell membrane damage (Lesniak *et al.,* 2012).

The formation of a synthetic (biomolecular) corona has been proposed as a tool for the detoxification of nanoparticle preparations. Nevertheless, this technique should be applied with caution, as loss or degradation of the protective shield could restore its toxicity (Li *et al.,* 2020). Despite the ability of protein complex to inhibit unspecified associations between cell surface and recently formed nanoparticle's surface, it permits for selective interactions between the adsorbed proteins and the receptors on the surface of the cell. Nanoparticles become more apparent to tissue-resident macrophages of the spleen and liver due to the adsorption of plasma proteins, specifically immunoglobulins (Furumoto *et al.,* 2002).

2.4.4 Manipulating nanoceria to give rise to desired biological responses

The form of nanoparticle-protein interactions in a biofluid, as well as the structural configuration of the protein complex are determined by the chemical and physical characteristics of nanoparticles. This is due to the fact that a nanoparticle's tendency for interacting with a specific side chain of amino acid defines the relative affinities of the protein (Xia *et al.,* 2011). The relative composition of the subsequent protein corona will be influenced by hydrophobicity, chemical structure and surface charge of a nanoparticle. For example, proteins which are basic in nature preferentially adsorbs acidic polystyrene nanoparticles from blood plasma (González-García *et al.,* 2022).

There exist a high tendency for the chemical and structural composition of a protein corona to undergo changes as a result of alternation in the physicochemical properties of nanoceria. It has also been suggested that the size influences the geometry, location and arrangement of the binding sites of the proteins on the nanoparticles. As a result, the communication between nanoparticles and biomolecules differs from the communication between biomolecules and parent materials of equal physical and chemical composition. (Nguyen *et al.,* 2017). However, there exist no clear link between isoelectric point, molecular weight and the relative adsorption trend between the sizes of nanoparticles. The influence of the size of nanoparticle on individual protein is most likely a function of shape of the protein and composition of the amino acid (AA). Nevertheless, it does seem the influence of the size of nanoparticle is substantial whenever the particle size move towards that of the protein, which is often within the range of 30nm (Choi *et al.,* 2007; Lundqvist *et al.,* 2008).

2.4.5 Nanoceria mimics endogenous enzymes during oxidative defence

Several studies have reported the ability of nanoceria to mimic superoxide dismutase in its mode of function. (Singh *et al.*, 2011; Karin *et al.,* 2021; Khan *et al.,* 2022). When dioxygen undergoes reduction by single electron, a radical is formed which can induce oxidative damage to cellular components (Fridovich, 1997). It is produced as an end product of metabolism in several organelles and enzymes system such as mitochondrion (via respiratory chain) and xanthine oxidase (Kalyanaraman, 2013). Though it can break down spontaneously to produce hydrogen peroxide (H_20_2), it can also combine with other radicals which include nitric oxide radical to produce additional oxidants such as peroxynitrite. Enzymes are however produced by several

microbes and mammals to reduce the increasing abundance/ production of superoxide within the cell. However, during inflammatory process, the superoxide so produced can overwhelm the enzymatic defences, resulting to an increased presence of both ROS and RNS. The superoxide regulation in the system is thus an important factor in limiting the extent or amount of inflammation. The study carried out by Korsvik and colleagues was the first to report the ability of nanoceria to mimic superoxide dismutase in its activity. (Korsvik *et al.,* 2007). Using the X-ray photoelectron spectroscopy (XPS) analysis, two different preparations of cerium oxide nanoparticles were analysed-one containing very small amount of cerium Ce^{+3} on the surface and the other containing higher amount of cerium atoms in Ce^{+3} (Fifere *et al.,* 2021).

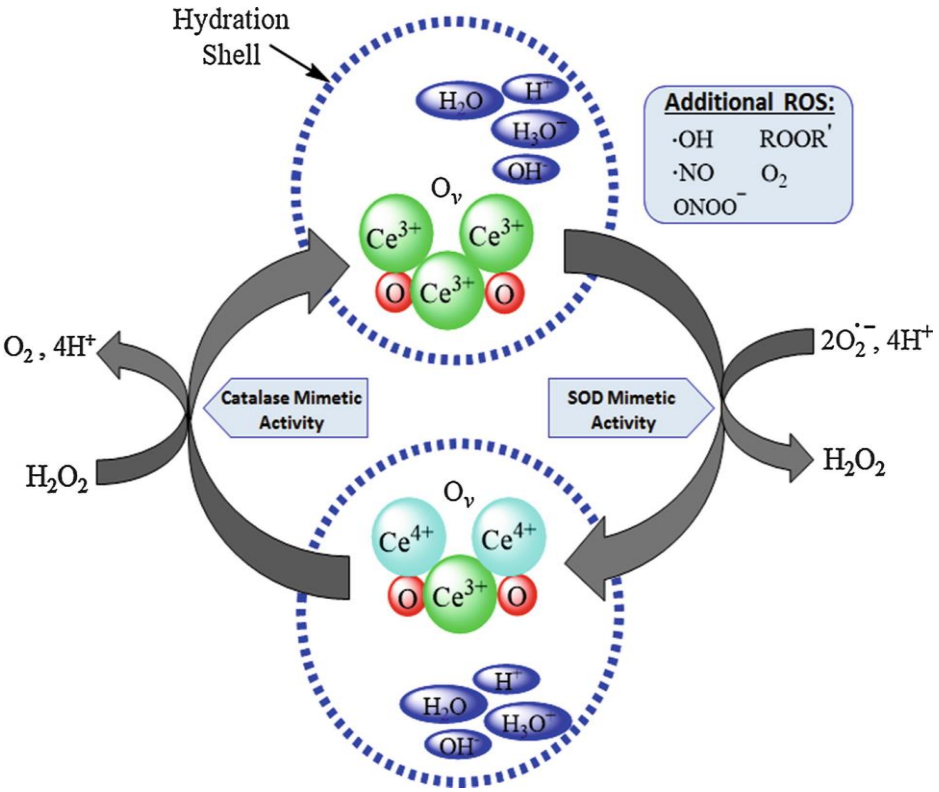

Figure 2.5: Mechanism of SOD mimetic properties of cerium oxide nanoparticles. (Estevez *et al.*, 2019)

2.4.6 *In vivo* evidence of SOD mimetic action

Estevez *et al* (2011), reported that nanoceria displayed significant activity of superoxide dismutase in an experimental ischemic brain model (Estevez *et al.*, 2011). Also, Estevez *et al*, (2019), described the ability of cerium oxide nanoparticle to imitate superoxide dismutase in its activity using a similar experimental model as Li and discovered that exposing cerium oxide nanoparticle caused in substantial reduction in superoxide concentration (Estevez *et al.*, 2019). Their study confirmed the initial findings that nanoceria can imitate superoxide dismutase in various assay methods and demonstrate the tendency of such activity to occur in vivo (Batinić *et al.*, 2010).

Although, there exist substantial amount of data linking superoxide dismutase activity to surface chemistry of cerium oxide nanoparticles, however the exact reaction mechanism is yet unknown. The reaction of cerium oxide nanoparticles with superoxide was investigated using a combined density functional theory and molecular dynamics as well as chemical tests. (Baldim *et al.*, 2018). The presence of water droplets on the nanoceria was reported in Baldim's experiment and findings imply that nanoceria formed in water is made up of reactive patches that changes when hydrated. A water-based cerium oxide nanoparticle was produced and found to imitate superoxide dismutase activity just prior to dehydration, confirming previous predictions (Dutta *et al*., 2016). However, the superoxide dismutase mimic activity of nanoceria was considerably diminished upon removal of water from the mixture (Batinić-Haberl *et al.*, 2010). These findings can therefore serve as a pivot and channel to more research on the mechanism underlying such activity.

2.4.7 The Nanoceria's Mimetic property

Cerium oxide nanoparticles also have catalytic activities similar to the enzyme catalase (Pirmohamed *et al.*, 2010). Peroxiredoxins, GPx and CAT are enzyme classes involved in the regulating H_20_2 levels in mammalian cells. The total catalytic activity of cerium oxide nanoparticles was initially thought to be insignificant in contrast to the highly efficient catalytic activity of catalase, thereby suggesting that such activity might not be relevant (Pirmohamed *et al.*, 2010). According to a recent research by Juan *et al.*, (2022) peroxides were found to be the most readily available and stable reactive oxygen species (ROS) *in vivo*, hence a catalyst that can regulate the level of peroxide could be important during inflammatory process to inhibit metal-catalysed oxidative

reactions (Fenton reaction). Due to the increasing roles of peroxide in innate system, there exist the need to regulate their production and degradation. This process is carried out by variety of enzymes which includes peroxiredoxins, glutathione peroxidases and catalase, many requiring glutaredoxin and thioredoxin as reducing agents (Song *et al.,* 2007).

Furthermore, with reference to surface charge of cerium, the tendency of nanoceria to mimic SOD is quite opposite to that of catalase. Precisely, catalase mimetic activity of nanoceria is weaker when the concentration of cerium atoms at the surface of the nanoparticle, Ce^{+3} oxidation state is higher (Singh *et al.,* 2020). Phosphate has the ability to undergo interconversion of cerium oxide nanoparticles from superoxide dismutase to catalase mimetics, according to a continuation study, which correlates with the reduced state of cerium (Singh *et al.,* 2011). This generally showed that the vacant oxygen sites on reduced cerium do not actually contribute to the ability of nanoceria to imitate catalase in its activity, therefore, reducing the nanoparticle's reactivity.

This also implies that if the level of phosphate in almost all living system is within the 5mM value, the reaction kinetics between phosphate and cerium oxide nanoparticles should be considered when comparing chemical reactions in vitro to in vivo. In a recent study, Saifi *et al*., (2018) reported that a non-water based synthesised nanoceria showed a promising catalase mimetic activity, thereby proposing that the oxygen defect on nanoceria are important to its interaction with hydrogen peroxide. In another study, aqueous solutions of nanoceria can mimic both superoxide dismutase and catalase (Gil *et al.,* 2017). Also, the exertion that cerium can exist in 3+ oxidation state has been questioned by a group of researchers (Szymanski. *et al,* 2017), indicating an undiscovered likelihood of an underlying property of nanoceria.

CHAPTER THREE

Materials and Methods

3.1.1 Reagents and Chemicals

The cerium oxide nanoparticle (CeO_2NPs) used for this research was obtained as a gift from a collaborator in the Biomedical Sciences Department, UA, Canada. Diethylnitrosamine (DEN), Trichloroacetic acid, (TCA), N-methyl-nitrosourea, (NMU) were acquired from Sigma Aldrich in the United States of America. Reduced glutathione (GSH), tris buffer, thiobarbituric acid (TBA), Sulphosalicyclic acid, hydrogen peroxide and Griess reagent were also acquired from Sigma Aldrich in USA, while Ellman's reagent, sodium potassium tartarate, 1-chloro-2,4-dinitrobezene were obtained from the British Drug House Chemical in the United Kingdom. However, the remaining chemicals and reagents used in the course of this research were of analytical grade and purest quality available.

3.1.2 Experimental Animals

Adult BALB/c mice weighing between 26g and 30g were purchased from the Animal house of the Department of Veterinary Physiology, University of Ibadan, Nigeria. They were kept in well ventilated cages at room temperature (25-30^{o}C) and maintained on normal laboratory chow (Ladokun Feeds, Ibadan, Nigeria) and water *ad libitum*. Animal handling and treatments conform to guidelines of the National Institute of Health (NIH publication 85-23. 1985) for laboratory animal and use and the Animal Care and Use Regulatory Committee of the University of Ibadan ratified this research with approval (UI-ACUREC/18/0039)

3.2 Blood Collection and Preparation of excised tissues

At the end of each study, feed were withdrawn from the animals overnight and were sacrificed by dislocating the cervical vertebra. Blood was obtained by way of ocular bleeding, a portion was collected in a plain bottle (without anticoagulant), allowed to

coagulate and later spun for fifteen minutes at a speed of 3, 000 Revolution per minute) to obtain the serum used for biochemical analysis. The second portion of the blood was withdrawn into laboratory bottles containing Ethylenediamine tetraacetic acid for assessing haematological indices. The testis, liver and mammary gland were cautiously removed, rinsed with a solution of potassium chloride (1.15%), (see appendix 1) allowed to dry by blotting on filter paper and later weighed. A portion of the tissues was homogenised (see appendix 2) with the aid of an electric homogenizing machine. The resulting homogenized tissues were then spun at 10,000 rev/m for ten minutes. The resultant homogenates were used for estimation of biochemical indices. The liver and the mammary gland were placed in formalin (10%) while the testis was placed in Bouin's solution for histopathological studies.

3.2.1 Effect of nanoceria on male reproductive function in adult mice

Procedure

Twenty (20) adult mice were allotted into four separate groups, comprising five (5) animals apiece. The group one, which is control was given normal saline, group 2 received (100 µg/kg bd/wt) group 3 (200 µg/kg bd/wt) and 4 (300 µg/kg bd/wt) of cerium oxide nanoparticles respectively, three times per week via intraperitoneal injection for five weeks. After the termination of treatment, the mouse were euthanized using ethyl ether and, serum and testis preparations for biochemical analysis were performed according to methods outlined on page 27 in section for tissue processing.

3.2.2 Evaluation of hepatic function of adult mouse following exposure to cerium oxide nanoparticles

Procedure

Twenty (20) adult mice were allotted into four separate groups, comprising five (5) animals apiece. The group one, which is control was given normal saline, group 2 received (100 µg/kg bd/wt) group 3 (200 µg/kg bd/wt) and 4 (300 µg/kg bd/wt) of cerium oxide nanoparticles respectively, three times per week via intraperitoneal injection for five weeks. After the termination of treatment, the mouse were euthanized using ethyl ether and, serum and liver preparations for biochemical analysis were performed according to methods outlined on page 27 section for tissue processing.

3.2.3 Ameliorative potential of cerium oxide nanoparticles in diethylnitrosamine (DEN)-induced hepatotoxicity in male wistar rats

A total of thirty-six (36) adult male mice were assigned equally into six groups and were exposed as follows: Control (Normal saline), DEN(200 mg/kg), CeO_2 NPs 1 (100µg/kg) + DEN(200 mg/kg bd/wt), CeO_2 NPs 2 (200 µg/kg bd/wt) + DEN, CeO_2 NPs (100 µg/kg bd/wt) as well as CeO_2 NPs (200 µg/kg bd/wt). The CeO_2NPs was administered intraperitoneally. Pre-treatment of animals with cerium oxide nanoparticles was performed for eight days, and thereafter, diethylnitrosamine was administered as a single does (200 mg/kg) 48hr before the termination of the experiment and the animals were sacrificed twenty four hours after DEN administration. The liver was carefully removed and processed for biochemical, histological and immunohistochemical examinations. Blood was obtained and processed to serum for biochemical analysis.

3.2.4 Ameliorative potential of cerium oxide nanoparticles following induction of mammary toxicity in female via injection of Benz[a]pyrene and N-Nitroso-N-methylurea to adult female rats.

A total of 24 female Wistar rats were randomly allocated to four groups of 6 animals each and were treated as follows: Group 1 (Control), group 2 [(NMU (50 mg/kg b.wt) + BaP (50 mg/kg bd/wt)], group 3 [(NMU + BaP (50 mg/kg bd/wt) + CeO_2NPs (200 mg/kg bd/wt)] and group 4 [(NMU + BaP + Vincristine (5 mg/kg bd/wt)]. The rats were pre-treated with NMU (50 mg/kg) and benz(a)pyrene (50 mg/kg bd/wt) using the intraperitoneal route three times at week 7, 10 and 13 old. Thereafter, cerium oxide nanoparticles were administered intraperitoneally 5 times weekly for thirteen weeks. Vincristine was administered intraperitoneally twice per week for the same period.

3.3 DETERMINATION OF HEMATOLOGICAL INDICIES

3.3.1 Haematocrit

Haematocrit or PCV was determined using the capillary tube technique. Briefly, the whole blood samples of experimental mice were filled into heparinized capillary tube by using capillary attraction until being 3-quarter filled. The tube end devoid of blood was closed by means of plasticine. Another alternative of sealing could be by rotating the tube in a flame but charring and burning of the tube should be avoided. The sealed capillary tube was centrifuged using microhematocrit centrifuge at 300 rpm for 15 minutes. The PCV was read directly using the microhematocrit graph reader, and the result was expressed in percentage. (Jain *et al*., 2009).

3.3.2 Haemoglobin Count.

The HB count was estimated following the use of cyamethaemoglobin by method outlined by Jain (2009)

Working principle

Following red cell hemolysis, the presence of cyanide in the diluted solution catalyses the conversion of hemoglobin to cyamethaemoglobin

Test procedure

About 0.02 mL of blood reacted with Drabkin's diluent (4ml), with the used pipette rinsed several times and resulting mixture allowed to stay for ten minutes. Thereafter, the optical density was measured with the aid of SP 600 spectrophotometer at 540nm using Drabkin's diluents as standard. Calculation of hemoglobin count was done using the formula in appendix 3

3.3.3 Erythrocyte Count.

This was performed using the hemocytometer in a method outlined by Jain *et al*., (1986).

Working Principle

Very large numbers of Red Blood Cells are present in the Blood Specimen. Practically, counting this number of red cells directly under the microscope is highly impossible. So, the Red Blood cells are counted by using a special type of chamber, designed for

the counting of blood cells in the specimen, known as Hemocytometer or Neubauer's chamber.

Test Protocol

Blood was pipetted with the of the rubber stopper attached to the tail end until reaching the 0.5 unit. Maintaining the horizontal position, the Haymen's reagent was aspirated until it reached 101unit, with caution taken to avoid exceeding the mark. In this position, the rubber stopper was carefully detached with zero pressure. Thereafter, the pipette containing the mixture was spun within two minutes in order to ensure homogeneity of the mixture. This was followed by the careful introduction of diluted blood inside the (counting) chamber and covered using a neat cover slip. Counting of the red cell was performed with the use a compound microscope with x40 magnification. This was done using a set of five small rectangles that contains eighty smaller squares, The cells overlying the ones at the topmost and that of the left sides were quantified whereas, the ones overlapping the bottommost and on the right side were not quantified. Method for calculating the red blood count is shown in appendix 4

3.3.4 Total White Cell Count

Quantification of white cells was performed by the use of a hemocytometer, following the method used previously for red cells

Working Principle

The basic principle is that the blood is diluted with acid solution which removes the red cells by haemolysis and also accentuates the nuclei of the white cells; thus, the counting of the white cells becomes easy.

Procedure

The procedure followed was similar to that of red cell count. The ratio of dilution was 1:20 and each of the 4 white cells counting areas bounded by a single thoma line.

3.4 ASSAYS OF SERUM ENZYMES

3.4.1 Aspartate aminotransferase activity Estimation

The aspartate aminotransferase enzyme activity present in the serum of tested animals was estimated following the guidelines as presented by of Reitman and Frankel, (1957) using standard laboratory Kit.

Assay principle

The reaction between aspartate and α-oxoglutarate produces 2, 4-dinitrophenylhydrazine and oxaloacetate hydrazone, and the assay principle is consequently built on measuring the amount of oxaloacetate hydrazone so formed.

α-oxoglutarate + L-aspartate $\xrightarrow{\text{AST}}$ Oxaloacetate + L-glutamate

Test Procedure

Diluted sample (100 µL) was combined with Aspartate (0.1 mL), sodium phosphate buffer solution (0.1 mL of 100 mmol/L at 7.4 pH), and 2 mL of α-oxoglutarate to make the reacting mixture. This was followed by thirty minutes of incubation at a temperature of 37^0C. Later on, a volume of 500 µL of 2, 4-dinitrophenylhydrzine was introduced into the reacting mixture and left on the bench for about twenty minutes at a temperature of twenty-five degree centigrade. An additional (5.0 mL) NaOH was introduced, then the optical density (546 nm) was recorded alongside the (reagent) blank within five minutes.

3.4.2 Alanine Aminotransferase activity estimation

The enzyme activity was estimated by the method of Reitmann and Frankiel, (1957)

Assay Principle

The alanine aminotransferase activity was measured via determining the rate of pyruvate hydrazones production alongside 2, 4 – dinitrophenylhydrazine when alanine reacts with α-oxoglutarate in the presence of ALT

α-oxoglutarate + L -alanine $\xrightarrow{\text{ALT}}$ Pyruvate + L - glutamate

Test Procedure

Diluted sample (100 µL) was reacted with L -alanine (0.1 mL), sodium phosphate buffer solution (0.1 mL of 100mmol/L at 7.4 pH), and 2 mL of α-oxoglutarate to make the reaction mixture. This was followed by thirty minutes of incubation at a temperature of 37^0C Later on, a volume of 500 µL of 2, 4-dinitrophenylhydrzine was introduced into the reaction mixture and left on the bench for about twenty minutes at a temperature of twenty-five degree centigrade. An additional (5.0 mL) NaOH was introduced, then the optical density (546 nm) was recorded alongside the (reagent) blank within five minutes.

3.4.3 Estimation of Creatinine Level in the serum

The creatinine level present in the serum of test animals was estimated following the guidelines as described by Barrtels *et al* (1972) using standard laboratory Kit.

Assay Principle

The reaction between creatinine and picric acid (in alkaline pH) readily produces a coloured complex. The concentration of creatinine is therefore proportionate to the measure of the formed complex.

Test Procedure:

In this reaction, diluted sample (0.1 mL) was reacted with a solution containing exact volume (0.1mL) of 0.32 mol/L sodium hydroxide and 35mmol/L picric acid solution. Thirty seconds after, the first absorbance (at 520 nm) of the sample and that of standard was recorded and retaken after two minutes alongside the blank.

3.4.4 Estimation of Urea in the serum

The amount of urea present in the serum of tested animals was estimated following the procedure described by Fawcet and Scott. (1960) using standard laboratory Kit.

Assay Principle

Urease hydrolyses urea to ammonia and CO_2. The ammonia formed further reacts with a phenolic chromogen and hypochlorite to form a green coloured complex. The intensity of the colour formed is directly proportional to the amount of urea present in the sample.

Test Procedure

Sample (10 µL) was added to 100 µL of 116 mmol/L EDTA, mixed and heated at 37^0C for ten minutes. Thereafter, 2.50 mL of diluted phenol (120 mmol/L) was then added, followed by 2.50 mL of diluted sodium hypochlorite (27 mmol/L). The entire solution was gently stirred and incubated at temperature of 37^0C for 15 minutes. The absorbance was taken spectrophotometrically 546nm.

3.4.5 Assessing Malondialdehyde Generation

The amount of malondialdehyde generated during lipid peroxidation was measured by determining the thiobarbituric acid reactive substances (TBARS) synthesized as described by Buege and Aust, (1978).

Assay Principle

When the reaction product of malondialdehyde (MDA) and thiobarbituric acid (TBA) is heated under an acidic pH medium, it produces a pink colour complex, having an absorbance peak at 532 nm. In this medium, it can be extracted in organic diluents, with butanol. Malondialdehyde is normally used in calibrating this assay, while result from this test is presented as the level of malondialdehyde produced. (See appendix 6)

Test Procedure

A diluted sample of 0.4mil was added up to 1.6 ml of Tris-potassium buffer (0.15M at pH 7.4. This was followed by further addition of 0.5 ml Trichloro-acetic acid (10%). A volume of 0.5 ml containing 0.75 by percentage of thiobarbituric acid was thereafter added to the mixture and put in boiling bath (80^0C) and allowed to stay for 45 mins. The reaction mixture was then allowed to cool on ice and separated via centrifugation technique for 15 minutes at 3000 g. This gives a pure pink solution and the absorbance of which was read at 532nm against dH_2O (Reference blank). See Appendix 3.5 for calculation of malondialdehyde concentration.

3.4.6 Estimation of Superoxide Dismutase activity

Circulating superoxide dismutase in the organs under study was estimated following the method described McCord and Fridovich, 1(969).

Assay Principle

In alkaline medium (pH 10.2), superoxide dismutase prevents the auto-oxidation of adrenalin, a baseline mechanism for this assay. Following the reaction of xanthine oxidase, the superoxide-radical thereof produced induces the production of adrenochrome from epinephrine, whereby the total amount of the adrenochrome so formed increases alongside increasing alkaline medium (Aitken et al., 1993), ditto further epinephrine addition. Epinephrine auto-phosphorylation occurs in two separate mechanistic pathways, whereby one involves a free-radical based chain reaction mechanism with superoxide radical playing an important role, and therefore the function of superoxide dismutase. This could be found in appendix 3.6

Test Procedure

The test samples were diluted in ratio 1:10 using distilled H_20. Thereafter a known volume measuring 0.2 mL was reacted with 2.5mL sodium carbonate buffer (0.05 M, pH 10.2) and allowed for homogeneity. The reaction was initiated by the addition of 0.3 mL formulated adrenaline (0.3M) to the solution, followed by inversion to ensure homogeneity. The whole process took place in the spectrophotometer and the optical density was observed and recorded at thirty seconds intervals for a period of 150 secs. To prepare the reference sample, 2.5 mL of buffer system was mixed with 0.3 mL adrenaline and water (0.2 mL). Preparation of reagents: See appendix 5

3.4.7 Assessment of activity of circulating Catalase

The activity of circulating catalase in the organs under study was estimated following method described Aebi H (1974).

Test principle

This assay principle is on the basis of loss of absorbance (at 240nm) that takes place during the splitting of H_20_2 by catalase. At 240nm wavelength, H_20_2 does not have peak absorbance. Despite this, the absorbance relates abundantly with the concentration, allowing it to be a useful assay for quantitative analysis.

Assay Procedure

A volume of 2.95mL of 19m.M of hydrogen peroxide solution was drawn to a (quartz) cuvette and followed by addition of 50 µL sample. The resulting mix was inverted thrice to ensure homogeneity, and later inserted into its chamber in a spectrophotometer machine. The change in optical density was recorded at one-minute intervals for a period of five minutes. Reagent preparations can be found on appendix 3.7

3.4.8 Estimation of activity of circulating glutathione -s- transferase

The activity of circulating glutathione -s- transferase in the organs under study was estimated following Habig *et al.,* (1974.).

Test Principle

The interaction between 1-chloro-2,4-dinitrobenzene (CDNB) and families of glutathione -s- transferase has been themed to generate high activity. This therefore account for using CDNB as substrate in every assay that tends to assess the activity of glutathione -s- transferase. Once this compound is conjugated alongside reduced GSH, it absorbs maximal at a higher wavelength and peaks at 340nm; the increased absorbance at this wavelength therefore correlates with the activity of the enzyme

Assay Procedure

The reaction mixture contained 30 mL reduced GSH (0.1M) with 150 mL (20 mM) of 1-chloro-2,4-dinitrobenzene. Thereafter, 2.82 mL phosphate buffer (0.1 M, pH 6.5) was included, followed by a gentle mix with 30 mL of Cytosol/Microsomes. The whole mixture in the cuvette was then placed in a spectrophotometer (340 nm) and the absorbance taken every 60sec against sample blank. The ambient temperature of the environment was maintained roughly at 30^0C for optimum result. Preparation of reagents can be found on appendix 3.8

3.4.9 Estimating circulating glutathione peroxidases(GPx)

The activity of circulating GPx in the organs under study was estimated following Rotruck *et al*.,(1973)

Test Principle

The reaction catalysis that occurs when glutathione is oxidised to GSSH by the oxidative action of hydrogen peroxide is catalysed by the glutathione peroxidase. During this process, DTNB freely interacts with the abundant GSH, giving rise to 5-thio-2-nitrobenzoic acid whose optical density is spectrophotometrically estimated at 412nm (Chen *et al.,* 2008).

Assay Procedure

The reaction mixture was prepared by adding 0.5 mL phosphate buffer, sodium azide (0.1 mL), 0.2 mL reduced glutathione, 0.1 mL hydrogen peroxide, sample aliquot (0.5 mL) and dH_20 (0.6 mL). After achieving homogeneity, incubation of the mixture followed at temperature of about 37^0C within the space of three minutes. Thereafter, 0.5mL TCA (2M) was further added before being spun at a speed of 3000 rpm for a period of 300 seconds. About 1 mL of the liquid phase was reacted with 1 mL of dinitrobenzene and 2 mL of dipotassium hydrogen phosphate. The solution was thoroughly mixed and the optical density was taken and recorded. Preparation of reagents can be found on appendix 3.9.

3.5.10 Evaluating activities of reduced glutathione

The glutathione concentrations in the organs under study were estimated following method of Moron *et al*., (1979)

Test Principle

The non-protein components of most sulfhydryl groups are highly enriched with reduced glutathione. The principle of this assay is consequently dependent on the formation of a rather even yellowish colouration which develops after the addition of Elman's reagent to compounds containing these sulfhydryl groups. The yellow colouration that results from this reaction between reduced glutathione and Elman's reagent has an absorbance that peaks within the range of 412 nm which corelates to the amount of glutathione present in the sample under investigation.

Assay Procedure

After 1:10 dilution of the test sample, 3 mL of sulphosalicyclic acid (4%) in solution was mixed with the sample in order to remove native proteins from it. This was followed by 10 minutes centrifugation at 300 rpm. The reaction mixture was

reconstituted by the addition of 0.4 mL phosphate buffer (0.1 M at pH 7.4) to the resulting supernatant (0.5 mL) and addition of 4.5 mL Ellman reagent. Preparation of blank followed same process. However, distilled water was added in place of the sample. Due to the unstable nature of the colour that developed, the spectrophotometric measurement was done within five minutes. The amount of reduced glutathione corelates with the absorbance peak at 412nm. Preparation of reagents can be found in appendix 3.10

3.4.11 Determination of Seminal Qualities

Procedure

Semen was collected from the epididymis immediately after sacrifice and 1 drop of saline was added to determine sperm count and motility of spermatozoa microscopically (x400), according to the method described by Franken and co-workers (2011). Eosin-Nigrosin stain was later added to microscopically (x400) determine the live-dead spermatozoa and for the morphological analysis of the number of sperm abnormalities, including sperm head (tailless head), mid-piece (curved mid piece and bent mid-piece) and tail (headless, rudimentary, bent, curved as well as looped) as described by Wyrobek *et al.*, (1975).

3.4.12 Determination of serum concentration of reproduction hormones.

The concentrations of serum reproductive hormones assessed in this research was determined using ELIS kits in method described by Bichara (1989).

Test Principle

The method exploits the unique specificity and affinity of a monoclonal antibody against a discrete antigen located on the hormone. The serum is permitted to freely interact concurrently with the two antibodies, which result to the sandwiching of the molecule (hormone) in between now enzyme -linked antibodies and solid phase. This is followed by the addition of Tetramethylbenzidine in citric acid buffer containing hydrogen peroxide (TMB substrate) and thereafter placed into the water bath for incubation, giving rise to blue colour development. The stop solution is then added to halt the enzymatic action with a swift change of colour into yellowish solution. The intensity of colour of the ensuing sample under investigation, which has absorbance peak at 450 nm correlates to the hormone concentration.

Assay Procedure

Four serum hormones namely prolactin, follicle stimulating hormone, luteinizing hormone and testosterone were examined with the use of ELISA test kit according to the manufacturer's instruction. The wells for calibrator, control and test samples were configured to run in duplicates. Two wells were added to accommodate TMB control. The vacant micro wells were returned into the package, containing silica gel drier and stored at 2-8^{0}c until expiration date. Each calibrator, control serum and samples (0.025ml or 25µl) were pipetted into appropriate wells. This was followed by the addition of the conjugate solution (0.100ml or 100 µl) to the wells, with exception of the blank. The experimental setup was shaken gently to ensure homogeneity for about thirty seconds, covered and incubated at room temperature for one hour. Thereafter, the content inside the microplate was decanted and followed by adding 0.3ml (300 µl) of washing solution and then decantation.

Addition of washing solution and decantation was done for a total of five times. TMB-substrate (0.100 or 100 µl) was added into each well at timed intervals (shaking of the plate was avoided after adding TMB-substrate). Incubation was performed in a dark chamber for about thirty minutes under room temperature, after which 0.150 ml of a stop solution was applied to all wells. The incubation mixtures were swirled gently for about ten seconds and the absorbance read at 450nm.

3.4.13 Nitric oxide Determination

Circulating amounts of NO_3^- and NO_2^- was measured as an index of nitric oxide (NO) synthesis in a methodby Palmer *et al*., (1987).

Test Principle

The unstable nature of nitric oxide in aqueous medium makes it to recombine swiftly into more stable nitrates and nitrites. Palmer *et al.*,1987. Therefore, in estimating the level of nitric oxide in the serum, the concentrations of its nitrites and nitrates are quantified following Griess reaction.

Assay Procedure

This was performed by reacting (0.5mL) Griess solution with 0.5 mL serum sample and placed inside water bath for 20 min at 37^{0}C. The absorbance (550nm) was taken

spectrophotometrically. The concentration of nitrite was therefore calculated by comparing the absorbance of samples to that of standard of a recognised sodium NO_2^- concentration.

3.4.15 Estimating the activity of circulating myeloperoxidase

The presence myeloperoxidase in the serum is indicative of the accumulation of morphonuclear leukocytes, following a method outlined by Trush *et al., (*1994)

Test Principle

The myeloperoxidase is exceptional as it catalyses the oxidation of chloride ion into the non radical oxidant called hypochlorous acid (HOCl), an essential bactericide. The over production of this oxidant can lead to oxidative stress and concomitant organ or tissue injury. The preparation of the reagents can be seen in appendix 3.11

Assay Procedure

An aliquot containing 50 µL dH_2O_2 and 200 µL o- dianisidine was mixed with 7 µL sample homogenate in a quartz cuvette and inverted to allow homogeneity. The mixture was later placed inside a spectrophotometer and change in absorbance at 460 nm was recorded every sixty seconds within the space of three minutes.

3.4.16 Sialic acid estimation in the testis

The testicular sialic acid content was measured following Aminoff's method (1961).

Test Procedure

The testis homogenates (500 µL) were briefly treated using 250 µL periodate solution, followed by incubation in boiling water bath (37^0C) for 30 minutes. The excessive periodate so formed was removed by the addition of 2% solution of sodium arsenate in 0.5 N HCl). Immediately the yellowish colouration of the iodine precipitate started to fade off, 2 ml of 0.1 M solution of 2-thiobarbituric acid was added and was positioned in boiling chamber for eight minutes. The mixture was allowed to cool on ice and swirled with 5 mL acidified butanol and centrifuged to ensure the separation of the mixture. The intensity of the colour in the butanol segment was used to measure the amount of sialic acid which absorbs maximally at 549 nm. The sialic content in the testis was estimated by the use of extinction coefficient as expressed in micro gramme per milligram protein. Preparation of reagents can be found in appendix 3.12.

3.5 IMMUNOHISTOCHEMICAL (IHC) ASSAY OF inflammatory and apoptotic proteins

The method of Chakravarthi *et al.* (2010) has been used with some modifications.

Principle

The principle is based on the specification of the manufacturer of a ratio 1:10 dilution of a primary antibody binding to specific antigens.

Procedure

Immunohistochemical labelling of formalin-fixed tissue slices from the liver and mammary tissue was employed to investigate expression of the selected proteins. A secondary enzyme-conjugated antibody is then treated with the antibody-antigen combination. In the presence of substrate and chromogen, the enzyme works on the substrate to produce coloured deposits at the locations of antibody-antigen contact, which were observed using a binocular microscope. Positive antigen locations in the cell cytoplasm, cell membrane, and nuclei were well-defined in colour when compared to Controls. Xylene was used to deparaffinize tissue slides (twice; 5 minutes each). After that, the tissue slides were examined. After that, the tissue slides were washed twice in ethanol at varying concentrations for 3 minutes each time (ethanol: 100%, 95% and 70%). The slides were rinsed with PBS for 5 minutes (0.01 M; pH 7.4). The antigens were retrieved by heating the slides to 97°C for 5 minutes in sodium citrate buffer (0.05 M; pH 6.0), then cooling them in the retrieval buffer for 20 minutes before being rinsed twice with wash buffer for 5 minutes each time. Before incubation, the slides were soaked in 10% BSA in PBS (blocking buffer) for 15 minutes at 37°C in a humidified environment, then washed with wash buffer. After that, the primed tissue slides were probed with diluted primary antibody and incubated for an hour at room temperature in a temperature Controlled environment. The biotinylated + streptavidine HRP secondary was diluted and applied to the segments on the slides, then incubated for the time specified after the slides had been rinsed twice with wash buffer for 5 minutes (polymer-single layer for 30 minutes). After washing the slides with wash buffer, the slide sections were incubated for further 15 minutes with 130 L of diluted Sav-HRP conjugates. For colour development, the tissue pieces were painted with a

freshly made DAB substrate solution (130 L) until the appropriate colour strength was achieved. The slides were washed three times for two minutes each time under running water. Hematoxylin was used to counterstain the nuclei for 20 seconds before rinsing, Dehydrated with 95 %, 95 %, 100 % and 100 % ethanol for 5 minutes after being rinsed under running water for 10 minutes. Before being mounted with a cover slip and mounting solution, the slides were xylene-cleared three times. The colour of the antibody staining on the tissue slides was viewed and photographed.

Scoring of slides:

The cells were scored based on haematoxylin staining. No staining if there is less than 5% staining, weak staining if there is 6-24% staining (light yellow), moderate staining if there is 25-49% staining (yellow-brown), strong staining if there is 50-74% staining (Brown) and very strong staining if there is 75-100% staining.

3.6 STATISTICAL ANALYSIS

All values data presented in this research were analysed with one–Way ANOVA and SPSS 20 was used to compare the various across the group. Tables, graphs and slates were used to present the data. Duncan multiple range test was used for the post hoc.

CHAPTER FOUR

RESULTS

4.1 Effect of nanoceria on male reproductive function in adult mice

Results

Result on weight and haematological indices

The result from table 1 shows that cerium oxide nanoparticles had ($p< 0.05$) increasing effect on animal weights treated with 100 µg/kg bd/wt of the particle, relative to control while groups administered 200 µg/kg bd/wt and 300 µg/kg bd/wt cerium oxide nanoparticles showed no difference ($p>0.05$) in their weight after exposure. Also, there was no observable difference ($p>0.05$) in the organosomatic weight and weight of the testis of the exposed animals relative to control. In Table 2, haematological analysis presented that exposure of animals has significant decreasing ($p<0.05$) effect on PCV across all groups exposed to 100, 200 and 300 µg/kg b.wt to cerium oxide nanoparticles by 68.8%, 25.9% and 30.3% respectively relative to control. Similarly, haemoglobin level of cerium oxide nanoparticles exposed animals significantly ($p<0.05$) was reduced by 70.9% and 35.0% at 100µg/kg b.wt and 300µg/kg b.wt relative to control.

Table 4.1: The animal and testicular weight indices following exposure to cerium oxide nanoparticles

Grouping	Initial(g)	Final(g)	Wt Diff(g)	Testis(g)	Organo-Somatic Wt.
Control	30.1±1.19	32.3±1.12	2.10±0.81	0.23±0.02	0.697±0.008
CeO_2 NPs 1	28.66±0.96	31.58±2.28	3.10±0.62	0.23±0.03	0.721±0.067
CeO_2 NPs 2	30.24±0.49	31.56±1.08	1.80±0.62	0.22±0.04	0.690±0.100
CeO_2 NPs 3	31.24±0.92	33.10±1.62	1.52±0.44	0.22±0.03	0.667±0.099

Values are means ± STDEV of 5 replicates. Control=mice that obtained normal saline, CeO_2 NPs 1, 2 and 3 = Cerium oxide nanoparticles at 100µg/kg, 200µg/kg and 300µg/kg. P value<5% was adjudged significant. *= Significantly different from control

Table 4.2: Hematological indices of mice following exposure to cerium oxide nanoparticles

Groupings	PCV (L/L)	HB (g/DL)	RBC (cells/µL)	WBC (mcL)	Platelets (K/mcL)
Control.	41.±12.5	13.5±3.9	6.74±1.8	48.1±7.9	10.66±1.01
CeO_2 NPs 1.	24.7±4.10*	7.90±1.22*	3.99±0.4*	49.8±1.8	10.66±1.20
CeO_2 NPs 2.	32.0±8.190*	10.5±2.57*	5.26±1.1	57.0±2.6	10.00±2.10
CeO_2 NPs 3.	30.7±4.16*	10.0±1.50*	4.95±0.6*	47.3±15.4	10.33±1.80

Values Values are means ± STDEV of 5 replicates. Control=mice that obtained normal saline, CeO_2 NPs 1, 2 and 3 = Cerium oxide nanoparticles at 100µg/k, 200µg/kg and 300µg/kg. P value<5% was adjudged significant. *= Significantly different from control

Result on semen analysis and hormonal profile

Results on sperm quality revealed that administration of cerium oxide nanoparticles resulted in decrease (significant) in sperm volume (Figure 4.2), sperm count (Figure 4.4) and motility (Figure 4.5) across all exposed groups, relative to control. Also, sperm count and motility were decreased significantly (p,0.05) across the exposed groups, relative to control. Specifically, sperm count decreased by 20.4%, 50.1% and 38% in mice administered with 100, 200 and 300µg/kg b.wt respectively, while sperm motility decreased by 20%, 58% and 71% in 100, 200 and 300µg/kg b.wt cerium oxide nanoparticle respectively. Exposure to cerium oxide nanoparticle also led to significant ($p<0.05$) increasing effect in total sperm abnormality (figure 4.3) of animals administered 200 µg/kg b.wt in comparison to control.

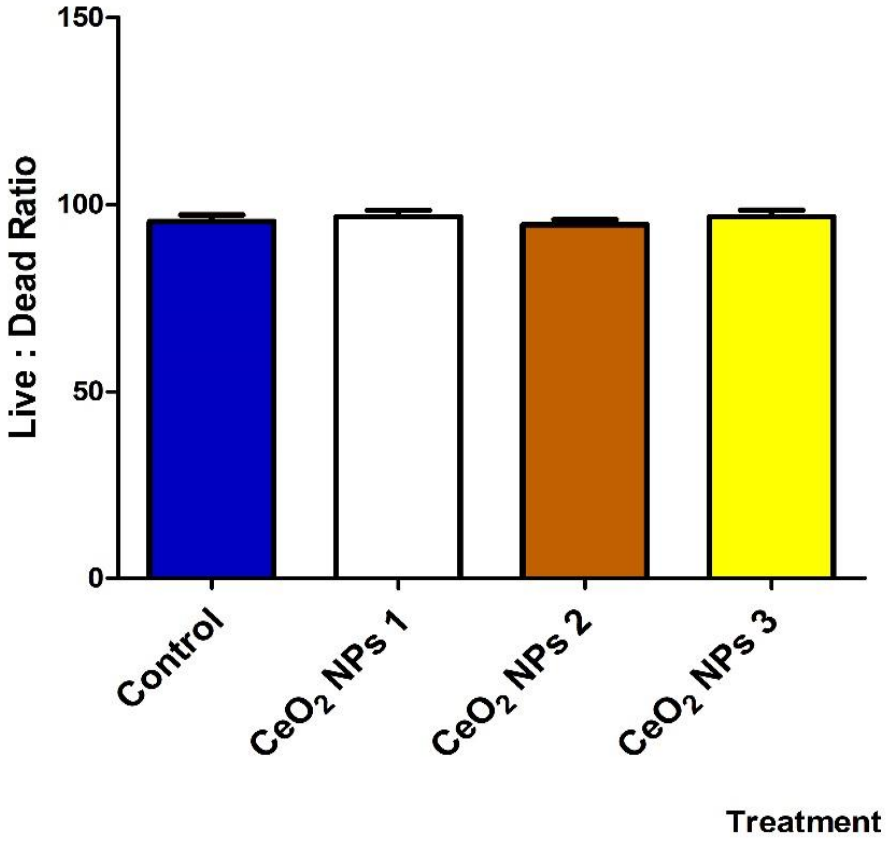

Figure 4.1: Live: Dead ratio of spermatozoa in adult male mice following exposure to cerium oxide nanoparticles.

Values are means ± STDEV of 5 replicates.Control=mice that obtained normal saline, CeO_2 NPs 1, 2 and 3 = Cerium oxide nanoparticles at 100µg/kg, 200µg/kg and 300µg/kg b.wt. P value<5% was adjudged significant. *= Significantly different from control

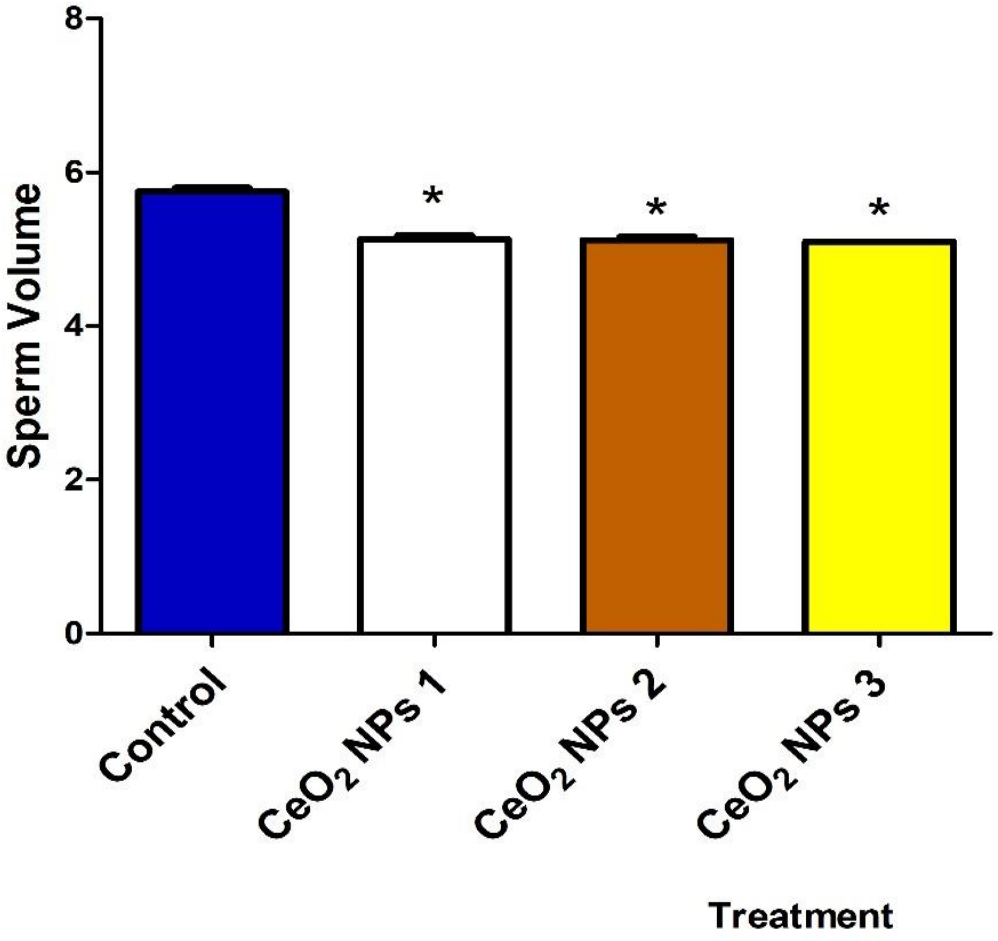

Figure 4.2: Sperm volume in adult male mice following exposure to cerium oxide nanoparticles

Values are means ± STDEV of 5 replicates. Control=mice that obtained normal saline, CeO_2 NPs 1, 2 and 3 = Cerium oxide nanoparticles at 100µg/kg b.wt, 200µg/kg b.wt and 300µg/kg b.wt. P value<5% was adjudged significant. *= Significantly different from control

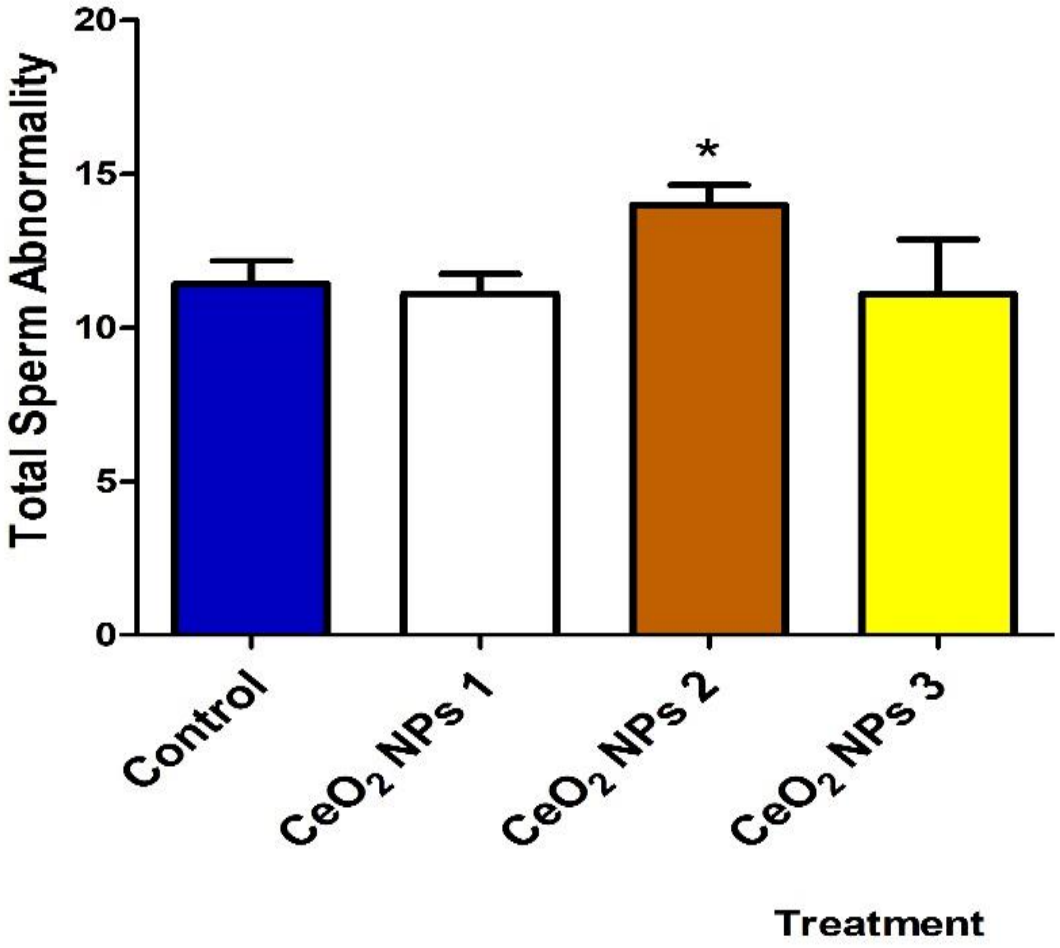

Figure 4.3: Total sperm abnormality in adult male mice following exposure to cerium oxide nanoparticles.

Values are means ± STDEV of 5 replicates. Control=mice that obtained normal saline, CeO_2 NPs 1, 2 and 3 = Cerium oxide nanoparticles at 100µg/kg, 200µg/kg bd/wt and 300 µg/kg bd/wt. P value<5% was adjudged significant. *= Significantly different from control

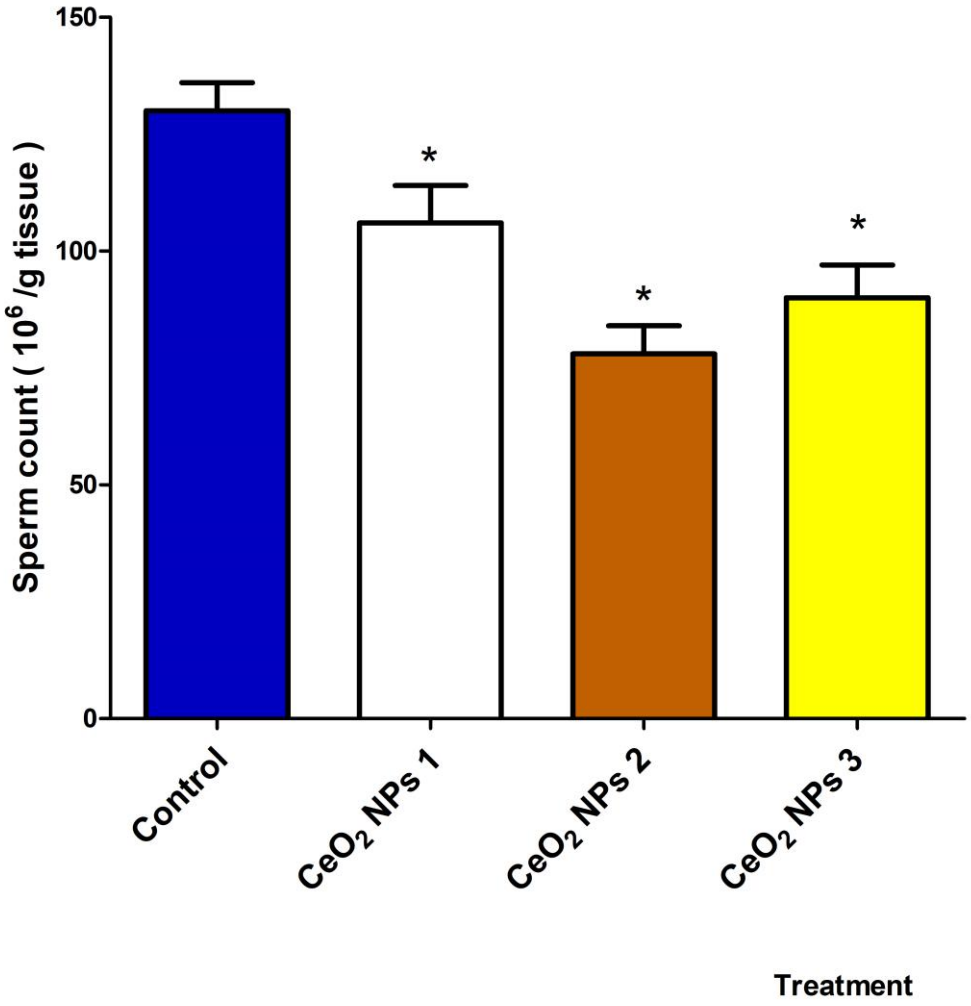

Figure 4.4: Sperm count in adult male mice following exposure to cerium oxide nanoparticles.

Values are means ± STDEV of 5 replicates. Control=mice that obtained normal saline, CeO_2 NPs 1, 2 and 3 = Cerium oxide nanoparticles at 100µg/kg bd/wt, 200 µg/kg bd/wt and 300µg/kg bd/wt P value<5% was adjudged significant. *= Significantly different from control

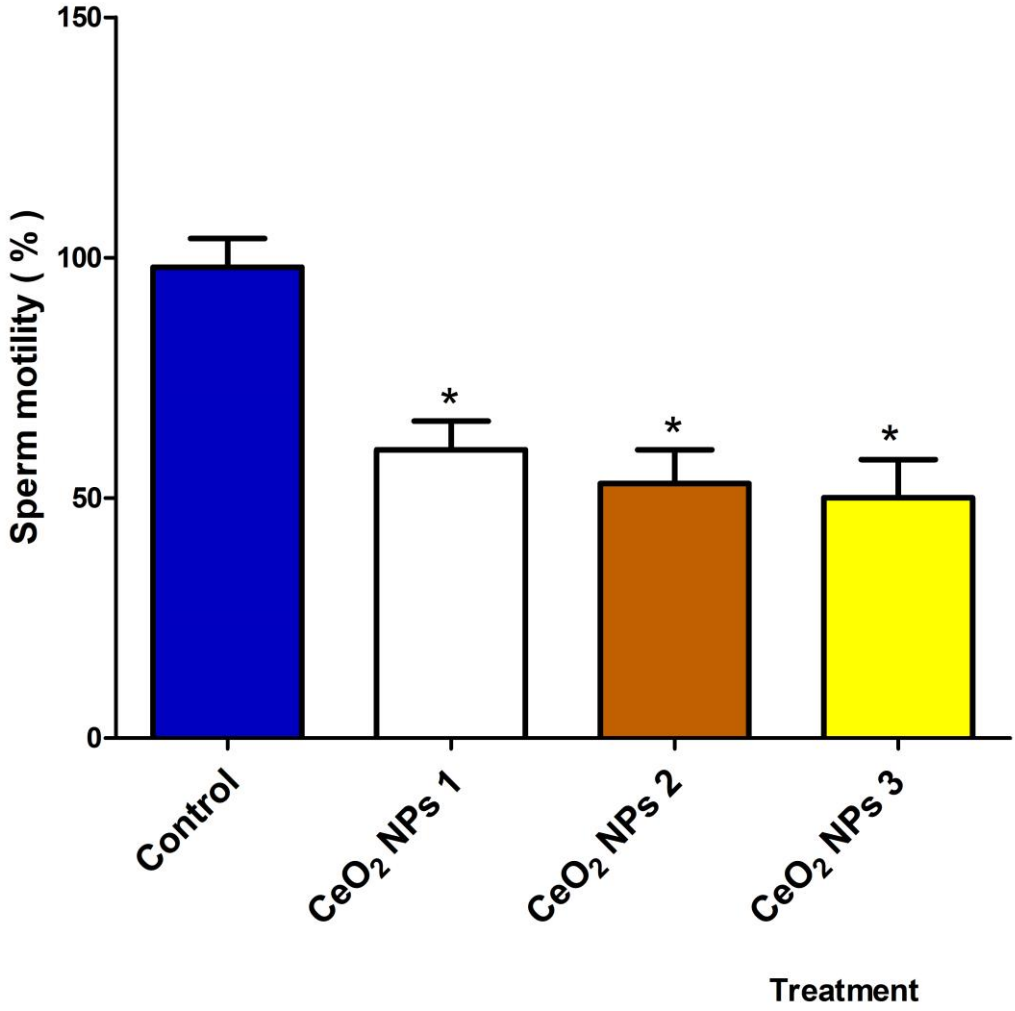

Figure 4.5: Sperm motility in adult male mice following exposure to cerium oxide nanoparticles.

Values are means ± STDEV of 5 replicates. Control=mice that obtained normal saline, CeO_2 NPs 1, 2 and 3 = Cerium oxide nanoparticles at 100µg/kg bd/wt, 200 µg/kg bd/wt and 300µg/kg bd/wt P value<5% was adjudged significant. *= Significantly different from control

Serum hormonal analysis showed that administration of cerium oxide nanoparticles at 200µg/kg bd/wt and 300µg/kg bd/wt significant ($p<0.05$) decreasing consequence on both luteinising (Figure 4.6) and follicle stimulating hormone (Figure 4.8) with respect to control. In addition, testosterone (Figure 4.9) increased significantly($p<0.05$) in mice administered with 100µg/kg bd/wt and 200µg/kg bd/wt of cerium oxide nanoparticle relative to control. However, only animals exposed to 300 µg/kg nanoceria had a decreased ($p<0.05$) prolactin level (figure 4.7) relative to the control.

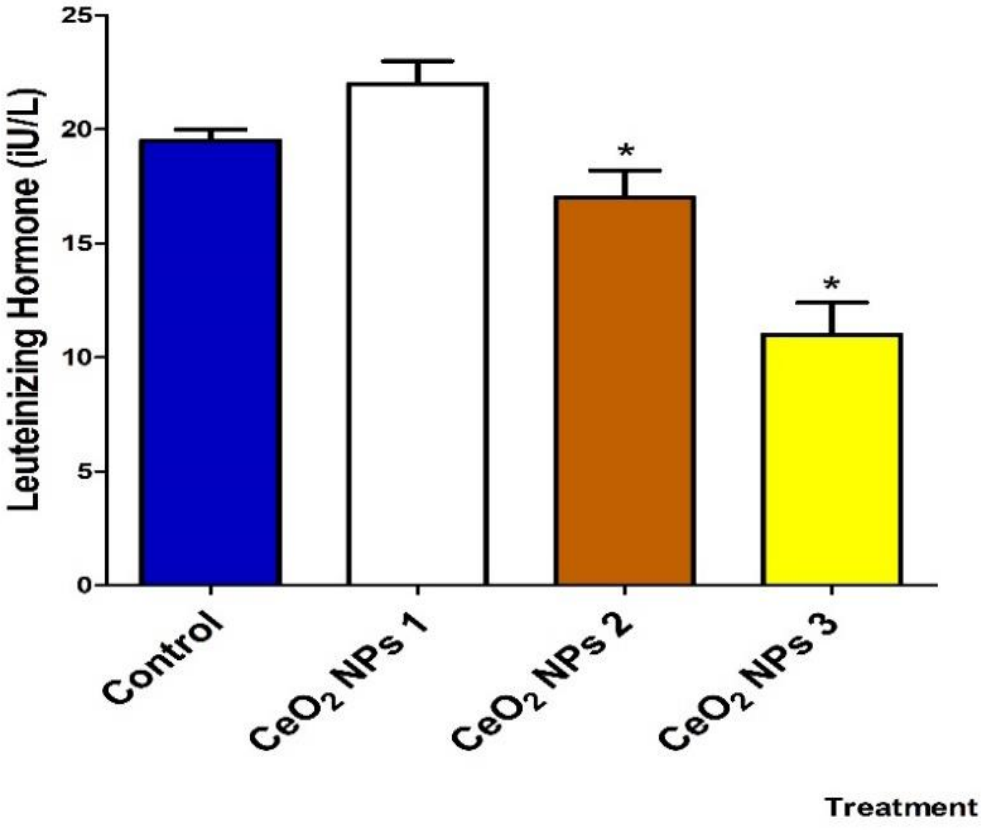

Figure 4.6: Effect of nanoceria on serum Luteinizing hormone level in adult mice

Values are means ± STDEV of 5 replicates Control=mice that obtained normal saline, CeO_2 NPs 1, 2 and 3 = Cerium oxide nanoparticles at 100µg/kg bd/wt, 200 µg/kg bd/wt and 300µg/kg bd/wt P value<5% was adjudged significant. *= Significantly different from control

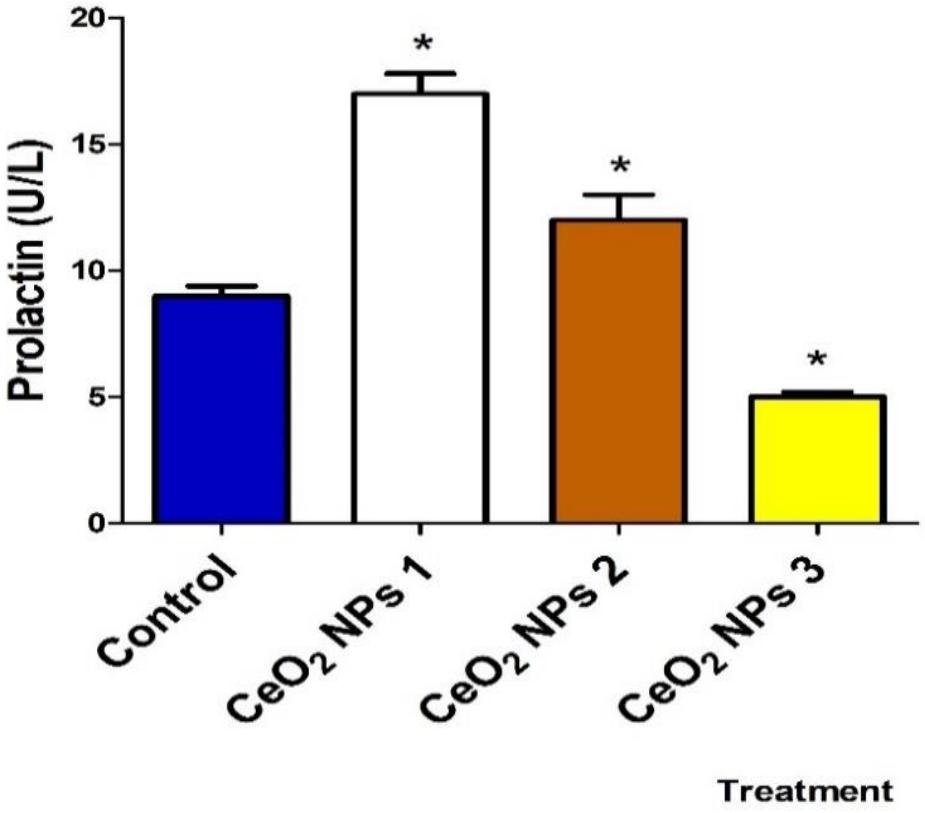

Figure 4.7: Effect of Nanoceria on serum prolactin level in adult male mice.

Values are means ± STDEV of 5 replicates. Control=mice that obtained normal saline, CeO_2 NPs 1, 2 and 3 = Cerium oxide nanoparticles at 100µg/kg bd/wt, 200 µg/kg bd/wt and 300µg/kg bd/wt P value<5% was adjudged significant. *= Significantly different from control

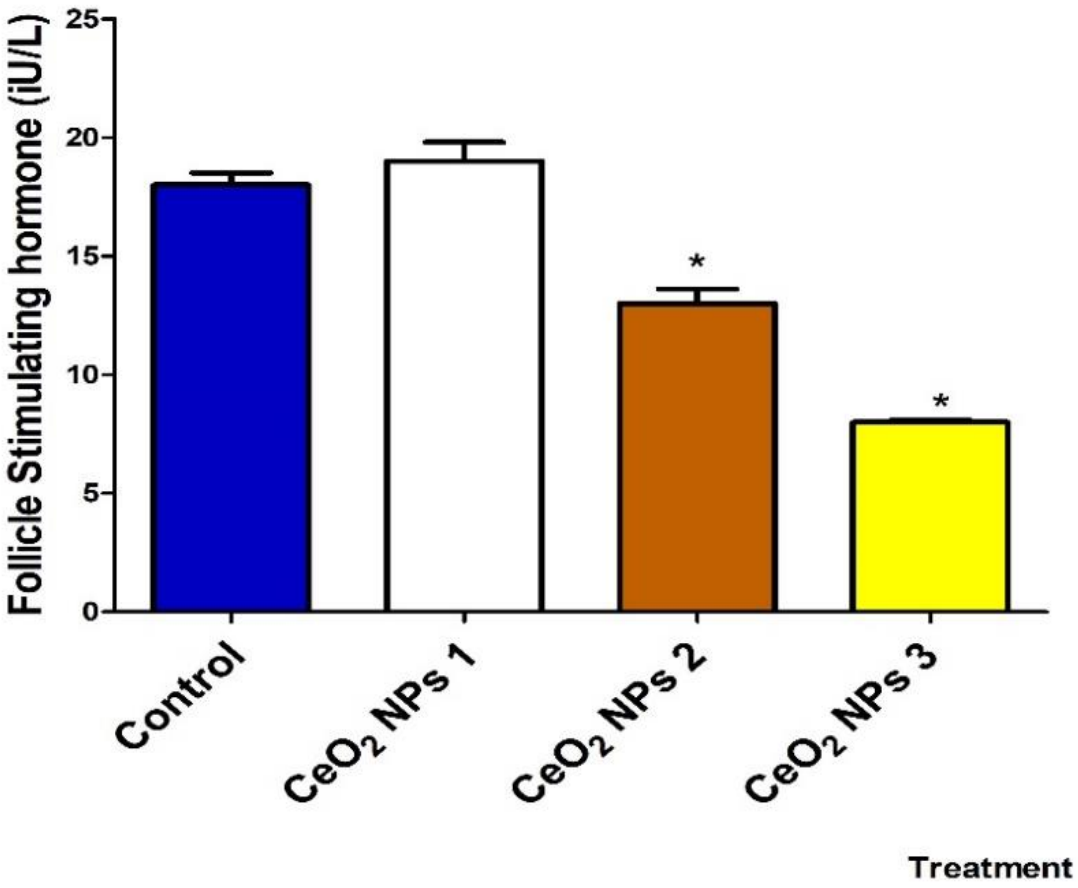

Figure 4.8: Effect of Nanoceria on serum follicle stimulating hormone levels in adult male mice.

Values are means ± STDEV of 5 replicates. Control=mice that obtained normal saline, CeO_2 NPs 1, 2 and 3 = Cerium oxide nanoparticles at 100µg/kg bd/wt, 200 µg/kg bd/wt and 300µg/kg bd/wt P value<5% was adjudged significant. *= Significantly different from control

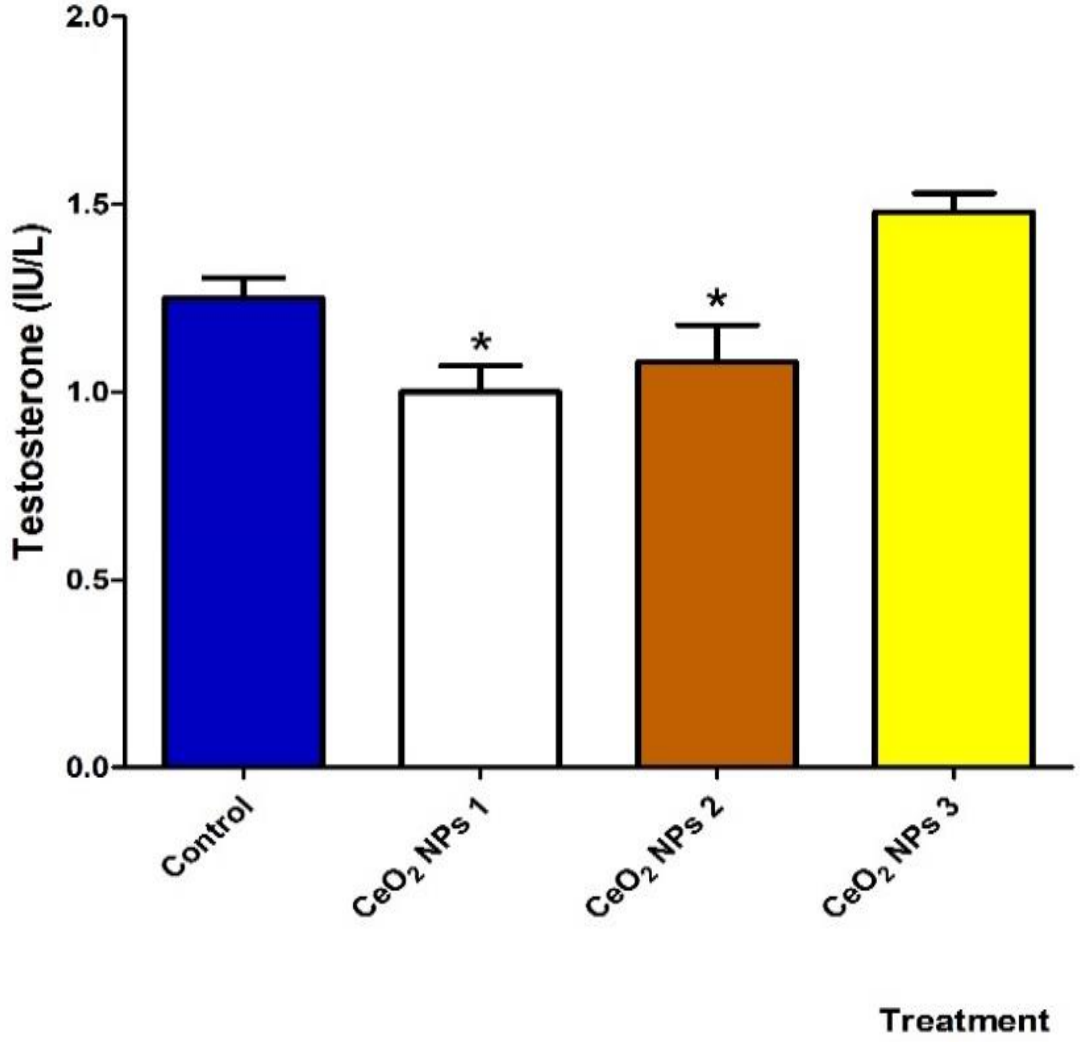

Figure 4.9: Effect of Nanoceria on serum testosterone level in adult male mice

Values are means ± STDEV of 5 replicates. Control=mice that obtained normal saline, CeO_2 NPs 1, 2 and 3 = Cerium oxide nanoparticles at 100µg/kg bd/wt, 200 µg/kg bd/wt and 300µg/kg bd/wt P value<5% was adjudged significant. *= Significantly different from control

Markers of testicular inflammation, myeloperoxidase (MPO), nitric oxide (NO) and oxidative stress, malondialdehyde (MDA) decreased across the group with respect to the control. MPO activity (Figure 4.11) increased in 100µg/kg bd/wt and 300µg/kg bd/wt by 50% and 60% respectively relative to control. However, testicular MDA level (figure 4.12) increased by 96%, 340% and 460% in mice administered 100, 200 and 300µg/kg bd/wt cerium oxide nanoparticles respectively.

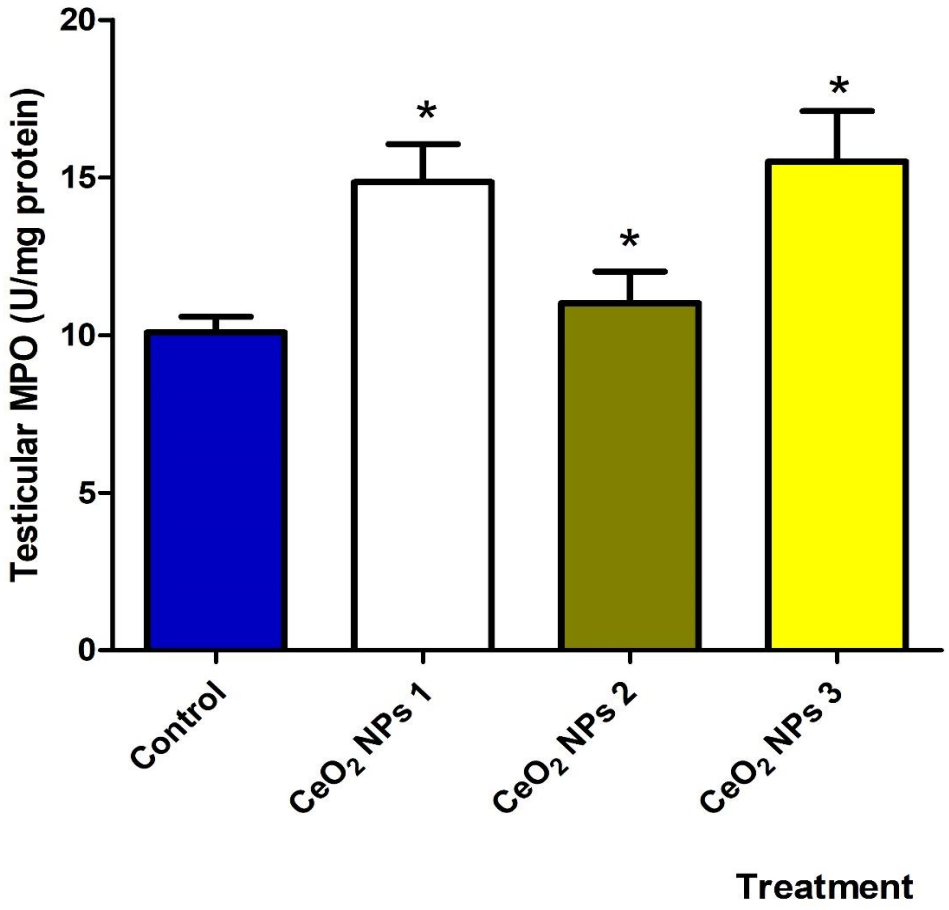

Figure 4.10 Effect of Nanoceria on testicular myeloperoxidase activity in adult male mice

Values are means ± STDEV of 5 replicates. Control=mice that obtained normal saline, CeO_2 NPs 1, 2 and 3 = Cerium oxide nanoparticles at 100µg/kg bd/wt, 200µg/kg bdwt and 300µg/kg bdwt. P value<5% was adjudged significant. *= Significantly different from control

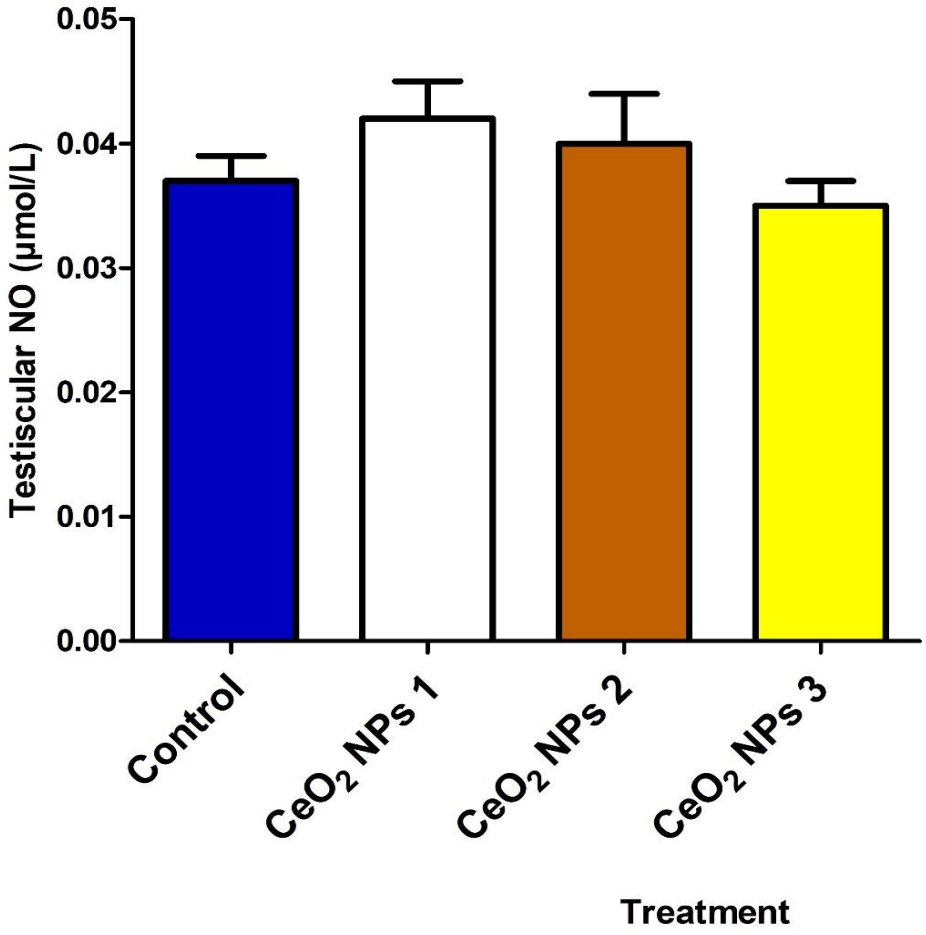

Figure 4.11: Effect of Nanoceria on the level of nitric oxide in testis of adult male mice.

Values are means ± STDEV of 5 replicates. Control=mice that obtained normal saline, CeO_2 NPs 1, 2 and 3 = Cerium oxide nanoparticles at 100µg/kg bd/wt, 200µg/kg bdwt and 300µg/kg bdwt. P value<5% was adjudged significant. *= Significantly different from control

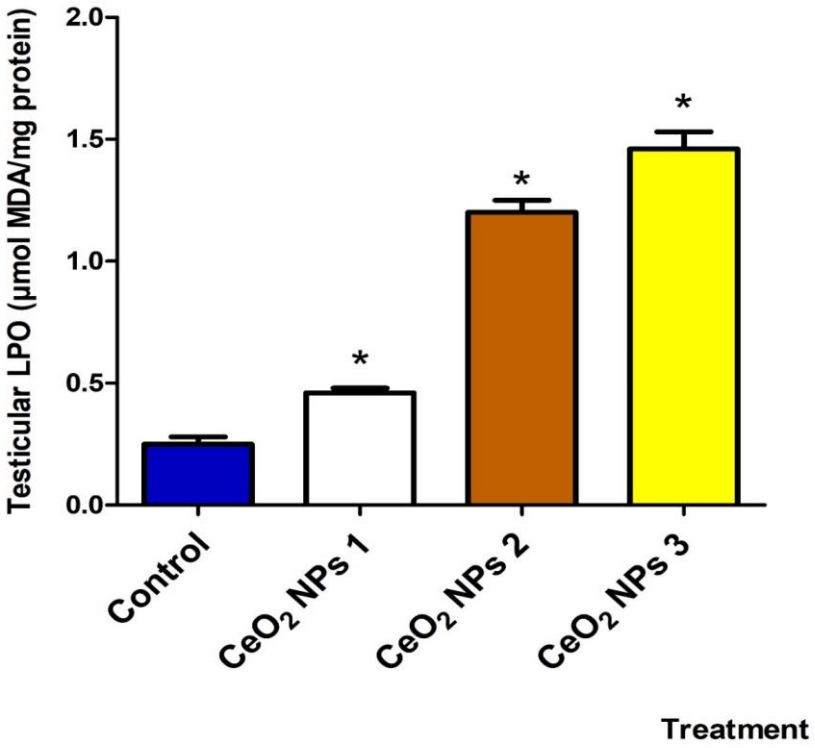

Figure 4.12: Effect of Nanoceria on malondialdehyde level in testis of adult male mice

Values are means ± STDEV of 5 replicates. Control=mice that obtained normal saline, CeO_2 NPs 1, 2 and 3 = Cerium oxide nanoparticles at 100µg/kg bd/wt, 200µg/kg bdwt and 300µg/kg bdwt. P value<5% was adjudged significant. *= Significantly different from control

Result on oxidative stress and antioxidant enzymes

Increased MDA level was accompanied also with a dose dependent and significant ($p<0.05$) decreasing effect in superoxide dismutase (figure 4.14) and catalase (figure 4.13) activities in the testis across exposed animals relative to control. Specifically, CAT activities increased in 100µg/kg, 200µg/kg and 300µg/kg cerium oxide nanoparticles treated animals by 62.2%, 66.2% and 89.1% respectively, while SOD activity was decreased in 100 µg/kg, 200 µg/kg and 300µg/kg treated animals by 28%, 67.7% and 73% respectively relative to control. Also, cerium oxide nanoparticle displayed a significant increasing effect on glutathione peroxidase (figure 415) in the testis across the treated groups, relative to control. Specifically, GPx activity decreased by 25.3%, 41.5% and 38.7% in mice administered 100µg/kg, 200µg/kg and 300µg/kg cerium oxide nanoparticles respectively.

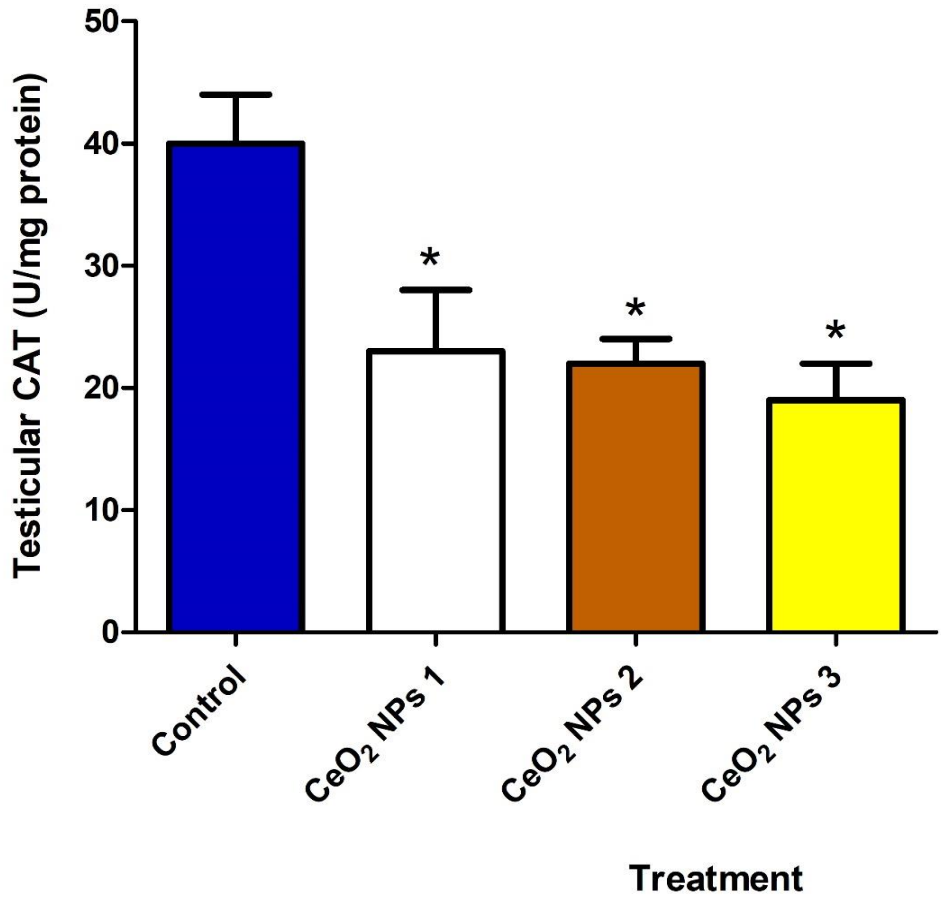

Figure 4.13: Effect of Nanoceria on testicular activity of catalase in adult male mice.

Values are means ± STDEV of 5 replicates. Control=mice that obtained normal saline, CeO_2 NPs 1, 2 and 3 = Cerium oxide nanoparticles at 100µg/kg bd/wt, 200µg/kg bdwt and 300µg/kg bdwt. P value<5% was adjudged significant. *= Significantly different from control

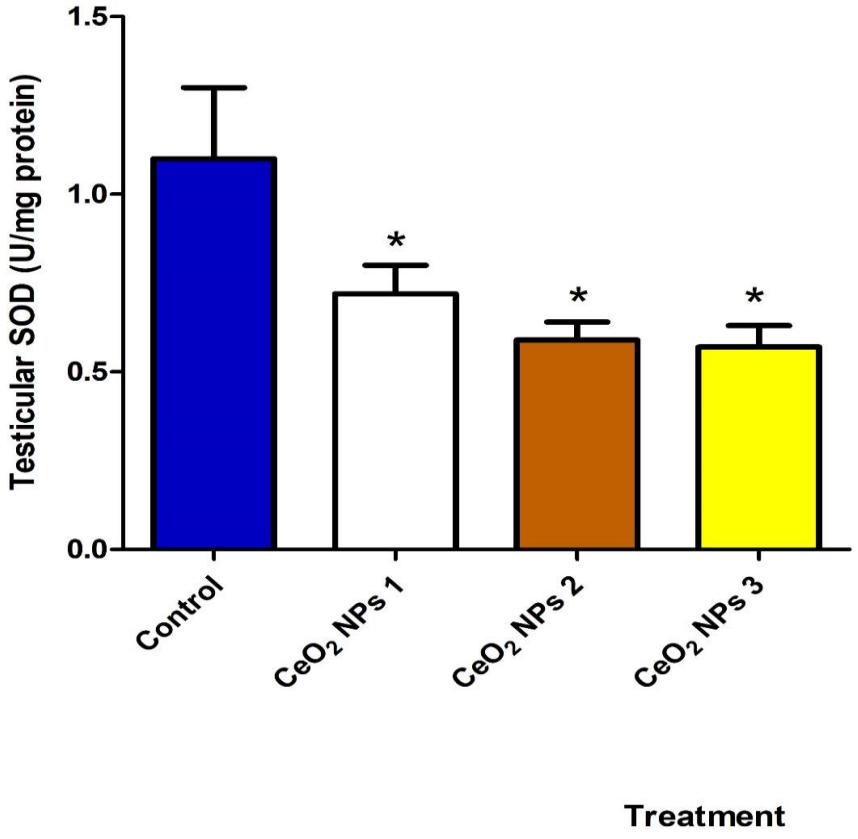

Figure 4.14: Effect of Nanoceria on testicular superoxide dismutase (SOD) activity in adult male mice

Values are means ± STDEV of 5 replicates. Control=mice that obtained normal saline, CeO_2 NPs 1, 2 and 3 = Cerium oxide nanoparticles at 100µg/kg bd/wt, 200µg/kg bdwt and 300µg/kg bdwt. P value<5% was adjudged significant. *= Significantly different from control

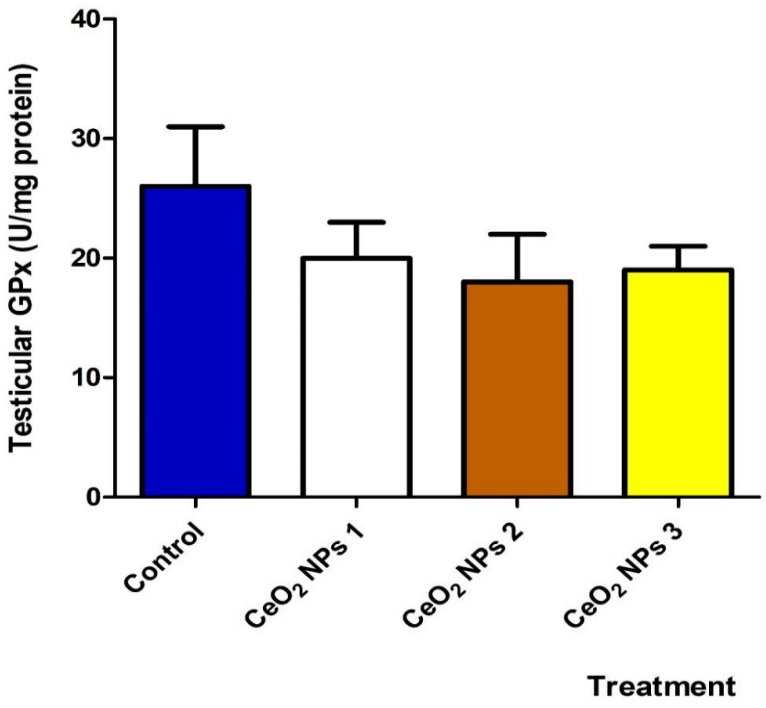

Figure 4.15: Effect of Nanoceria on glutathione peroxidase activity in testis of adult male mice

Values are means ± STDEV of 5 replicates. Control=mice that obtained normal saline, CeO_2 NPs 1, 2 and 3 = Cerium oxide nanoparticles at 100µg/kg bd/wt, 200µg/kg bdwt and 300µg/kg bdwt. P value<5% was adjudged significant. *= Significantly different from control

Result on antioxidants and histology

In a similar manner, testicular glutathione -s- transferase (figure 4.17) decreased in a significant manner by 78.2%, 82.5%% and 67.3% in mice administered 100 µg/kg, 200 µg/kg and 300 µg/kg body weight respectively. Also, administration of cerium oxide nanoparticle significantly decreased reduced GSH (figure 4.16) in mice treated with 100µg/kg, 200µg/kg and 300µg/kg body weight cerium oxide nanoparticles by 41.7%, 42.7%% and 48.5%, relative to control. The sialic acid content of the testis showed significant ($p<0.05$) decrease in all the exposed animals. Specifically, sialic acid concentration (figure 4.18) decreased by 89%, 53.9% and 65.6% in 100µg/kg, 200µg/kg and 300µg/kg body weight in mice administered cerium oxide nanoparticles respectively. Histopathological examination of the testis (plate 4.1) revealed intact spermatocytes in the control, while in 100µg/kg and 200µg/kg body weight cerium oxide exposed animals, there were necrosis and loss of the cells of the germinal epithelium from the basal compartment into the luminal compartment.

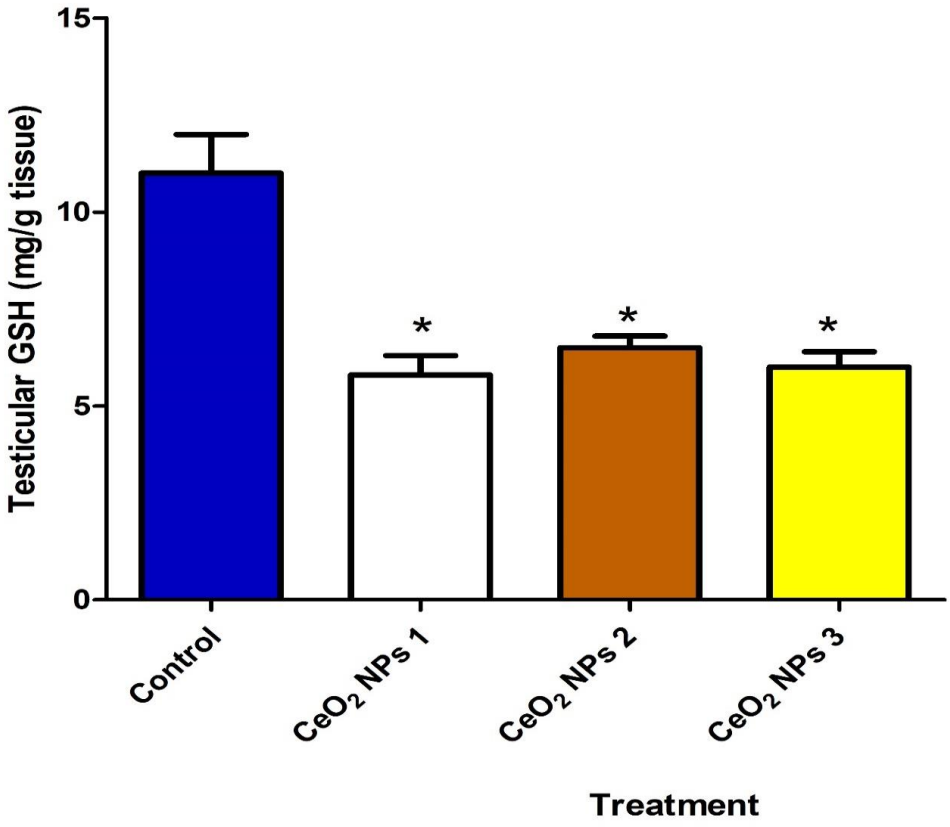

Figure 4.16: Effect of Nanoceria on testicular reduced GSH level of adult male mice.

Values are means ± STDEV of 5 replicates. Control=mice that obtained normal saline, CeO_2 NPs 1, 2 and 3 = Cerium oxide nanoparticles at 100µg/kg bd/wt, 200µg/kg bdwt and 300µg/kg bdwt. P value<5% was adjudged significant. *= Significantly different from control

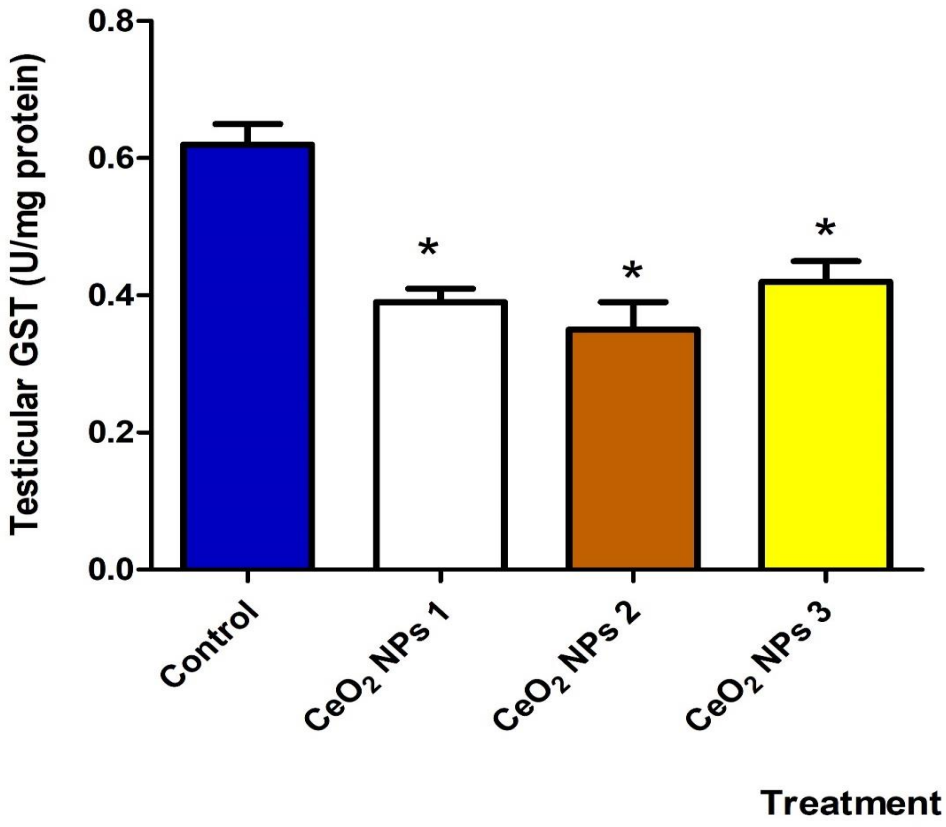

Figure 4.17: Effect of Nanoceria on testicular glutathione -s- transferase activity in adult male mice

Values are means ± STDEV of 5 replicates Control=mice that obtained normal saline, CeO_2 NPs 1, 2 and 3 = Cerium oxide nanoparticles at 100µg/kg bd/wt, 200µg/kg bdwt and 300µg/kg bdwt. P value<5% was adjudged significant. *= Significantly different from control

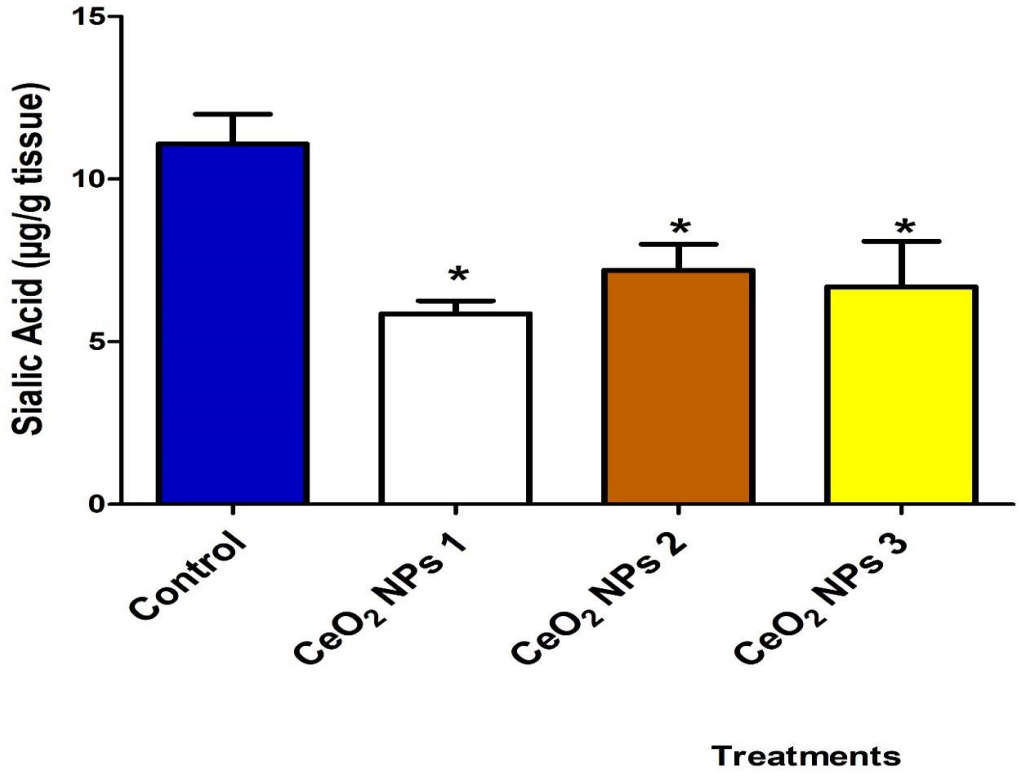

Figure 4.18: Effect of Nanoceria on sialic acid content of the testis in adult male mice

Values are means ± STDEV of 5 replicates. Control=mice that obtained normal saline, CeO_2 NPs 1, 2 and 3 = Cerium oxide nanoparticles at 100µg/kg bd/wt, 200µg/kg bd/wt and 300µg/kg bdwt. P value<5% was adjudged significant. *= Significantly different from control

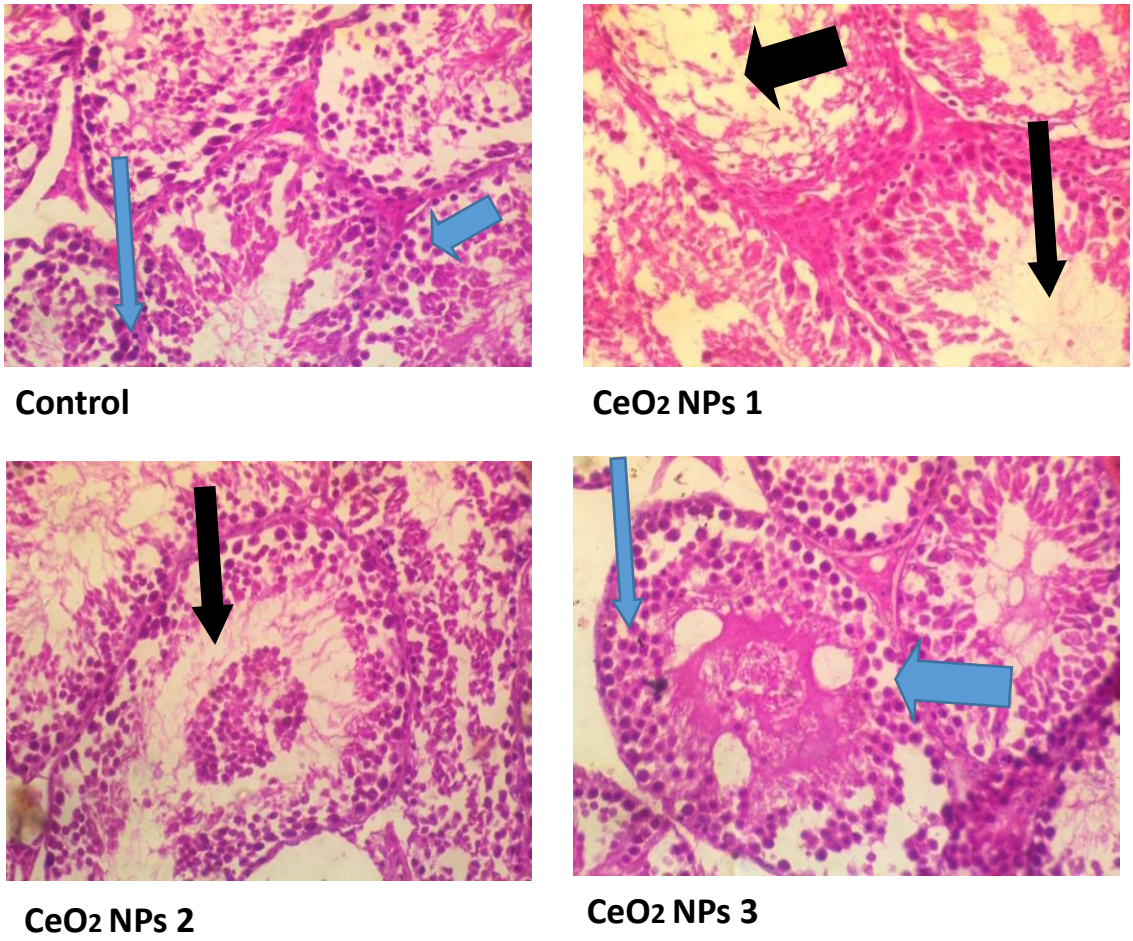

Plate 4.1: Representative photomicrographs of testes from mice treated with nanoceria at different doses. (M x 400)

Control=mice that obtained normal saline, CeO_2 NPs 1, 2 and 3 = Cerium oxide nanoparticles at 100µg/k, 200µg/kg and 300µg/kg. In the control, normal morphology of the testis was observed. However, there were treatment-related lesions such as degenerated seminiferous tubules and distorted testis in CeO_2NPs exposed animals, especially at 200µg/kg bd/wt and 300µg/kg bd/wt

4.2. Evaluation of hepatic and renal function of adult mouse following exposure to cerium oxide nanoparticles

Result

Weight and serum enzyme analysis

Figure 4.2.1 shows that cerium oxide nanoparticles had significant ($p<0.05$) increasing effect on animal weights exposed to 100 µg/kg of the particle, relative to control while groups administered 200µg/kg bd/wt and 300µg/kg bd/wt cerium oxide nanoparticles had no difference in their weight after exposure. There was no observable decrease in the organ somatic weight and liver weight of all exposed animals. Also, cerium oxide nanoparticles showed no significant effect in activities of serum urea, AST (figure 4.19), ALT (figure 4.20) and urea (figure 4.21) in the test groups, relative to control. However, the nanoparticles significantly ($p<0.05$) increased creatinine level (figure 4.22) in 100 µg/kg, 200 µg/kg body weight test groups, relative to control. Result from figure 4.23 showed that nanoceria caused significant and dose dependent decreased total bilirubin across test groups, relative to the control.

Table 4.3: Body and liver weights of adult mouse following exposure to cerium oxide nanoparticles

Groupings	Initial (g)	Final (g)	Diff (g)	Liver (g)	Organo-Somatic
Control	29.0±1.08	31.2±2.21	2.10±0.81	1.61±0.13	5.19±0.797
CeO_2 NPs 1	28.66±0.96	31.58±2.28	3.10±0.62*	1.69±0.24	5.14±1.071
CeO_2 NPs 2	30.24±0.49	31.56±1.08	1.80±0.62*	1.79±0.40	5.66±1.293
Ce O_2 NPs 3	31.24±0.91	33.10±1.62	1.52±0.44*	1.74±0.12	5.71±0.684

Values are means ± STDEV of 5 replicates. Control=mice that obtained normal saline, CeO_2 NPs 1, 2 and 3 = Cerium oxide nanoparticles at 100µg/kg bd/wt, 200µg/kg bd/wt and 300µg/kg bd/wt. P value<5% was adjudged significant. *= Significantly different from control

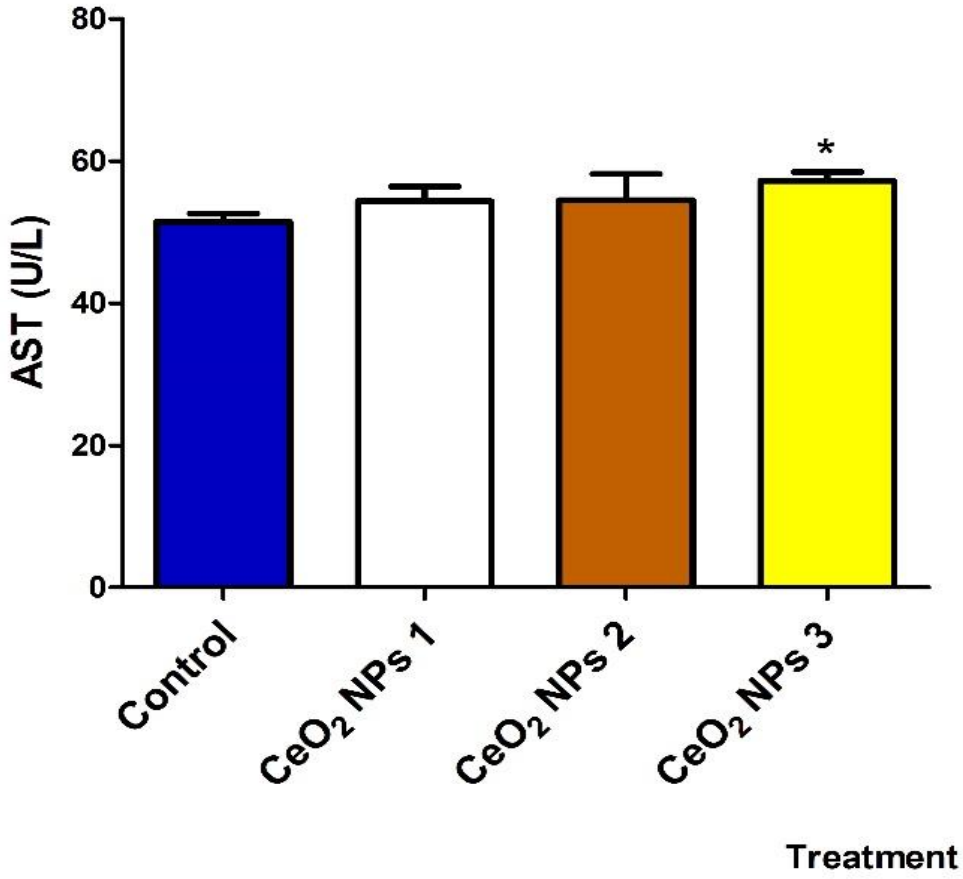

Figure 4.19: Effect of Nanoceria on serum aminotransferase (AST) activities of adult mice

Values are means ± STDEV of 5 replicates. Control=mice that obtained normal saline, CeO_2 NPs 1, 2 and 3 = Cerium oxide nanoparticles at 100µg/kg bd/wt, 200µg/kg bd/wt and 300µg/kg bd/wt. P value<5% was adjudged significant. *= Significantly different from control

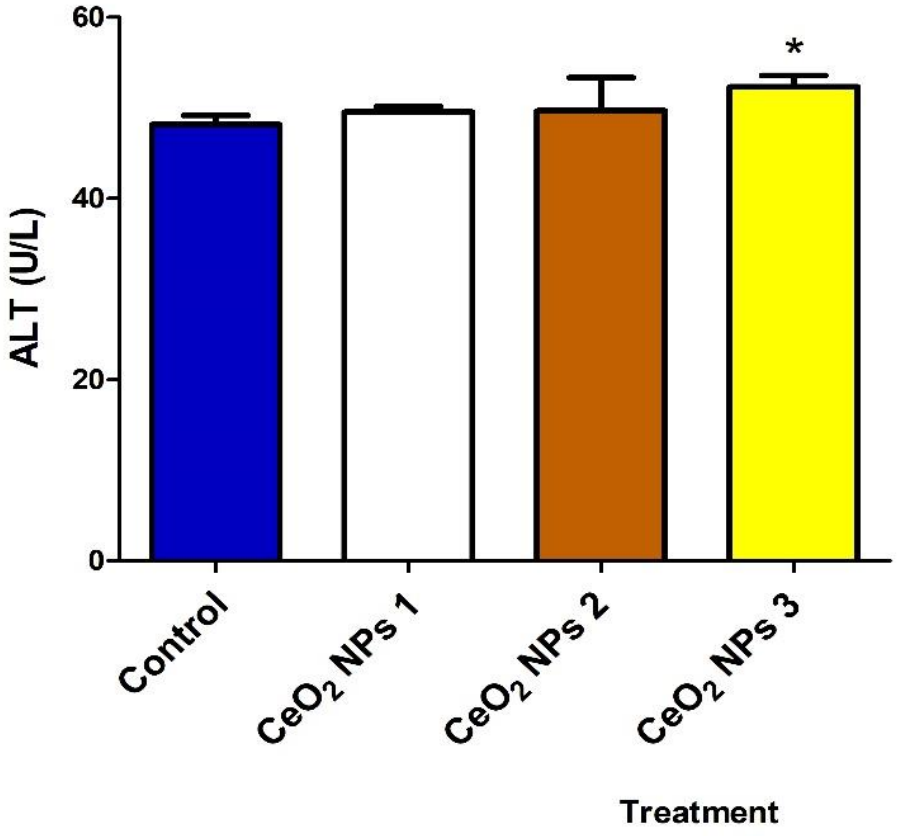

Figure 4.20: Effect of Nanoceria on serum alanine aminotransferase (ALT) activities in adult mice

Values are means ± STDEV of 5 replicates. Control=mice that obtained normal saline, CeO_2 NPs 1, 2 and 3 = Cerium oxide nanoparticles at 100µg/kg bd/wt, 200µg/kg bd/wt and 300µg/kg bd/wt. P value<5% was adjudged significant. *= Significantly different from control

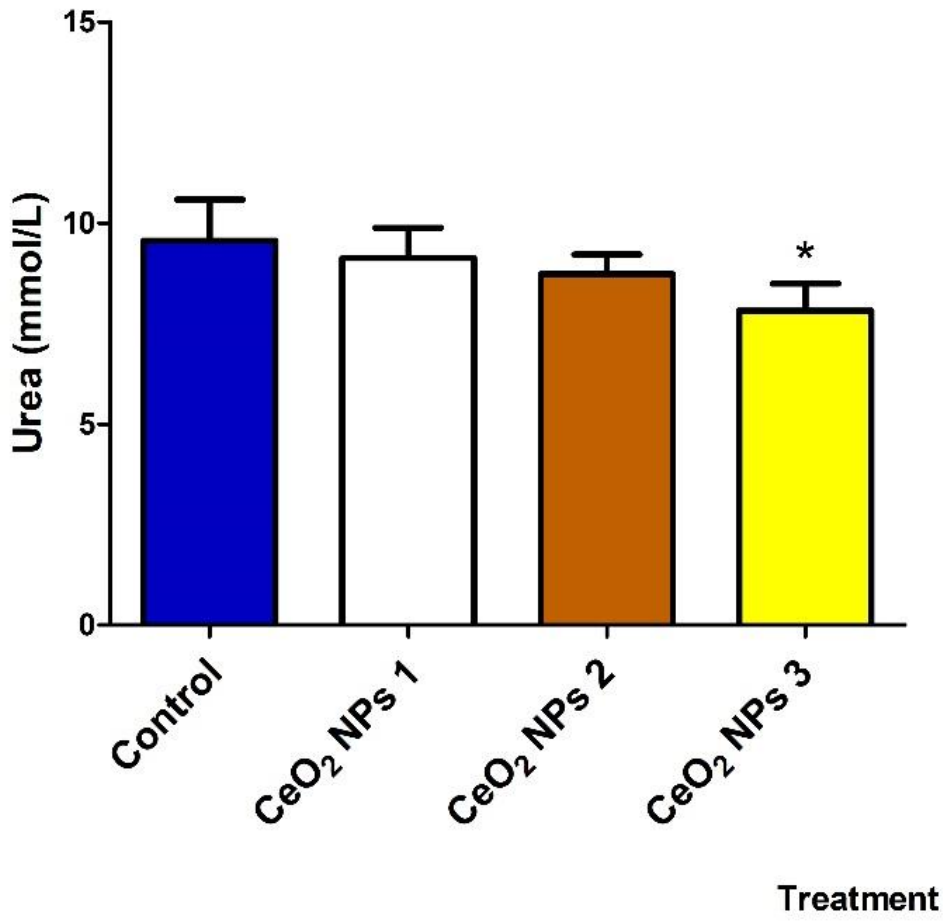

Figure 4.21: Effect of Nanoceria on serum urea level of adult mice

Values are means ± STDEV of 5 replicates. Control=mice that obtained normal saline, CeO_2 NPs 1, 2 and 3 = Cerium oxide nanoparticles at 100µg/kg bd/wt, 200µg/kg bd/wt and 300µg/kg bd/wt. P value<5% was adjudged significant. *= Significantly different from control

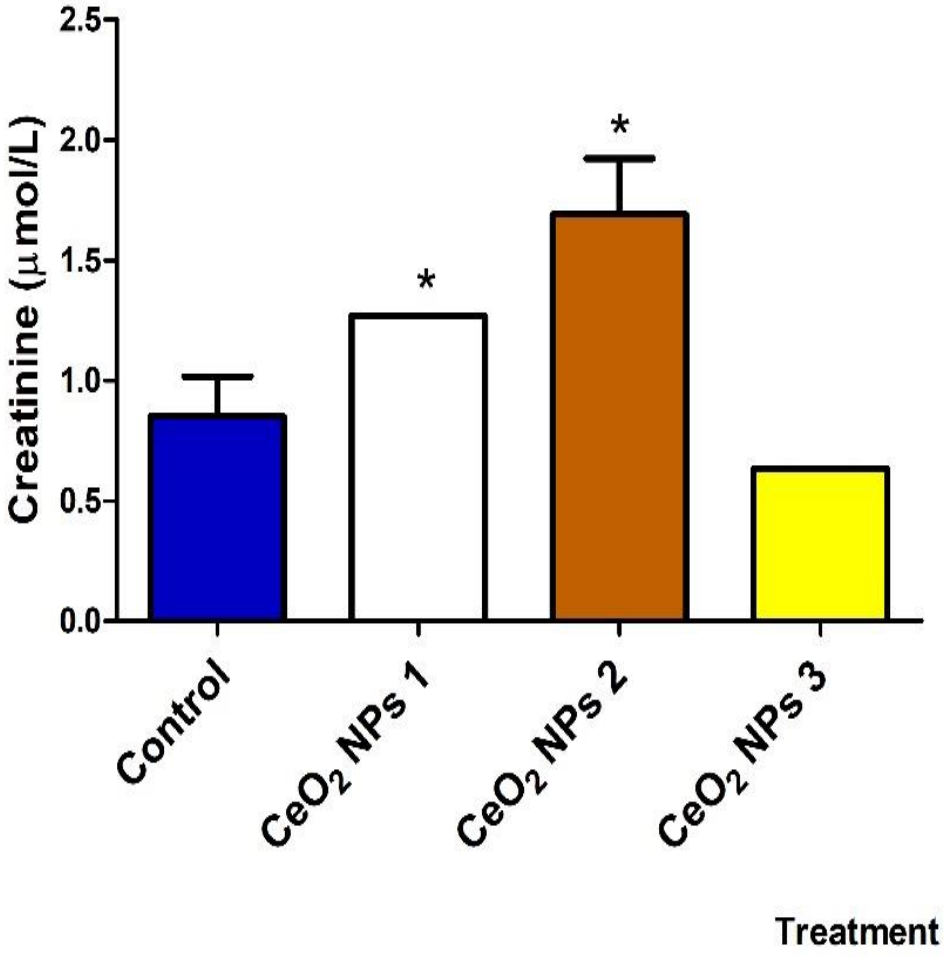

Figure 4.22: Effect of Nanoceria on serum creatinine level in adult mice

Values are means ± STDEV of 5 replicates. Control=mice that obtained normal saline, CeO_2 NPs 1, 2 and 3 = Cerium oxide nanoparticles at 100µg/kg bd/wt, 200µg/kg bd/wt and 300µg/kg bd/wt. P value<5% was adjudged significant. *= Significantly different from control

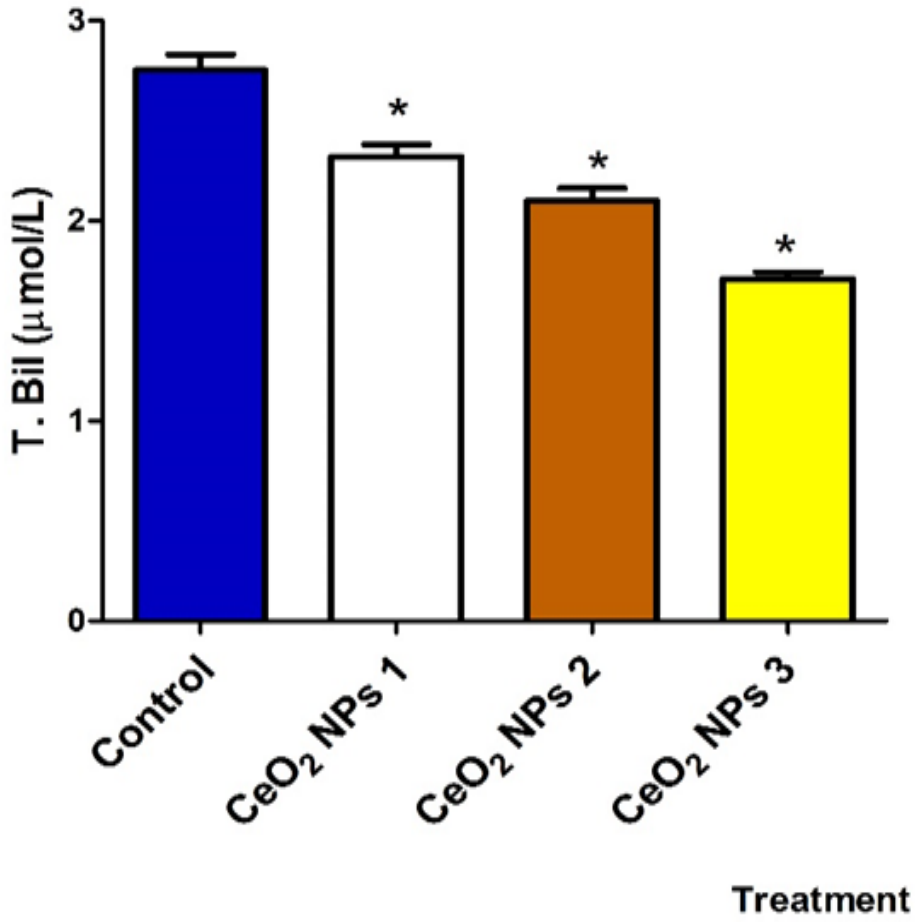

Figure 4.23: Effect of Nanoceria on serum total bilirubin level in adult mice

Values are means ± STDEV of 5 replicates Control=mice that obtained normal saline, CeO_2 NPs 1, 2 and 3 = Cerium oxide nanoparticles at 100µg/kg bd/wt, 200µg/kg bd/wt and 300µg/kg bd/wt. P value<5% was adjudged significant. *= Significantly different from control

Inflammatory indices

Hepatic inflammatory markers, notably nitric oxide (figure 4.24) was significantly ($p<0.05$) increased upon administration of cerium oxide nanoparticles in 100µg/kg, 200µg/kg by 22%, 30% respectively, relative to control. However, the activity of myeloperoxidase (figure 4.25) was not affected by the administration of cerium oxide nanoparticles across the treatment groups, relative to control. Lipid peroxidation (figure 4.26) result showed a dose-dependent decreasing effect across all groups, relative to control. Specifically, LPO increased in the liver of mice exposed to 100, 200 and 300 µg/kg, cerium oxide nanoparticles by 51%, 64% and 79% respectively.

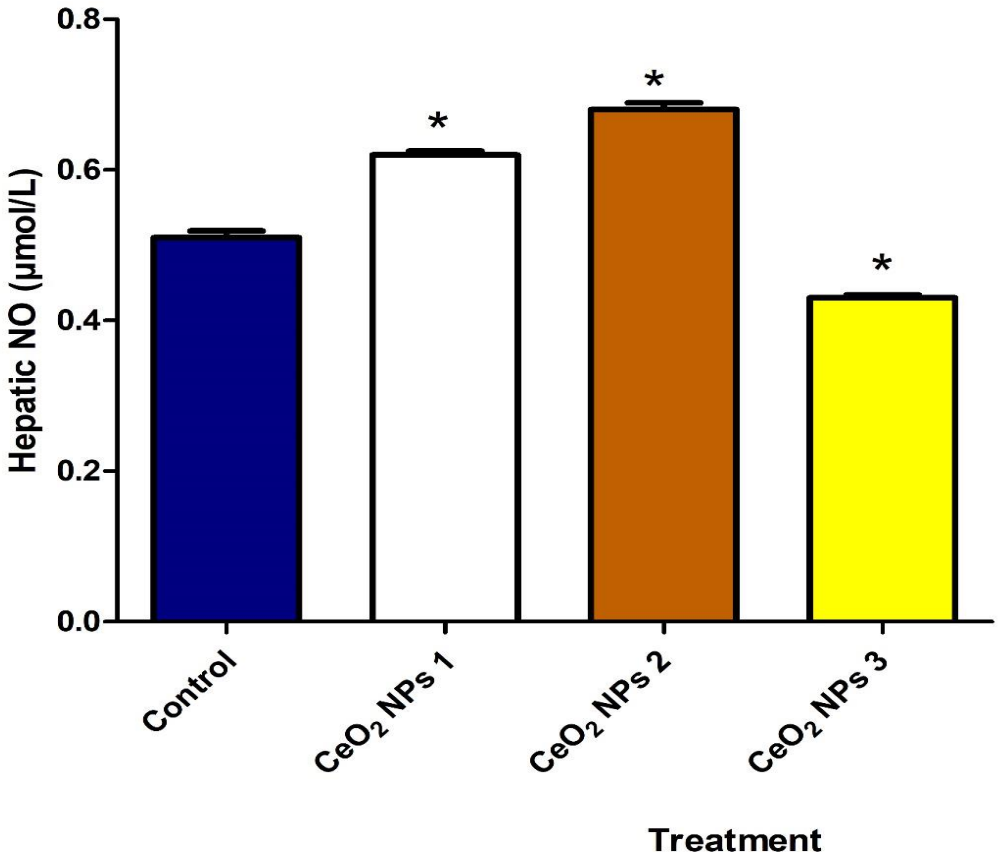

Figure 4.24: Effect of Nanoceria on nitric oxide (NO) level in the liver of adult mice

Values are means ± STDEV of 5 replicates. Control=mice that obtained normal saline, CeO_2 NPs 1, 2 and 3 = Cerium oxide nanoparticles at 100µg/kg bd/wt, 200µg/kg bd/wt and 300µg/kg bd/wt. P value<5% was adjudged significant. *= Significantly different from control

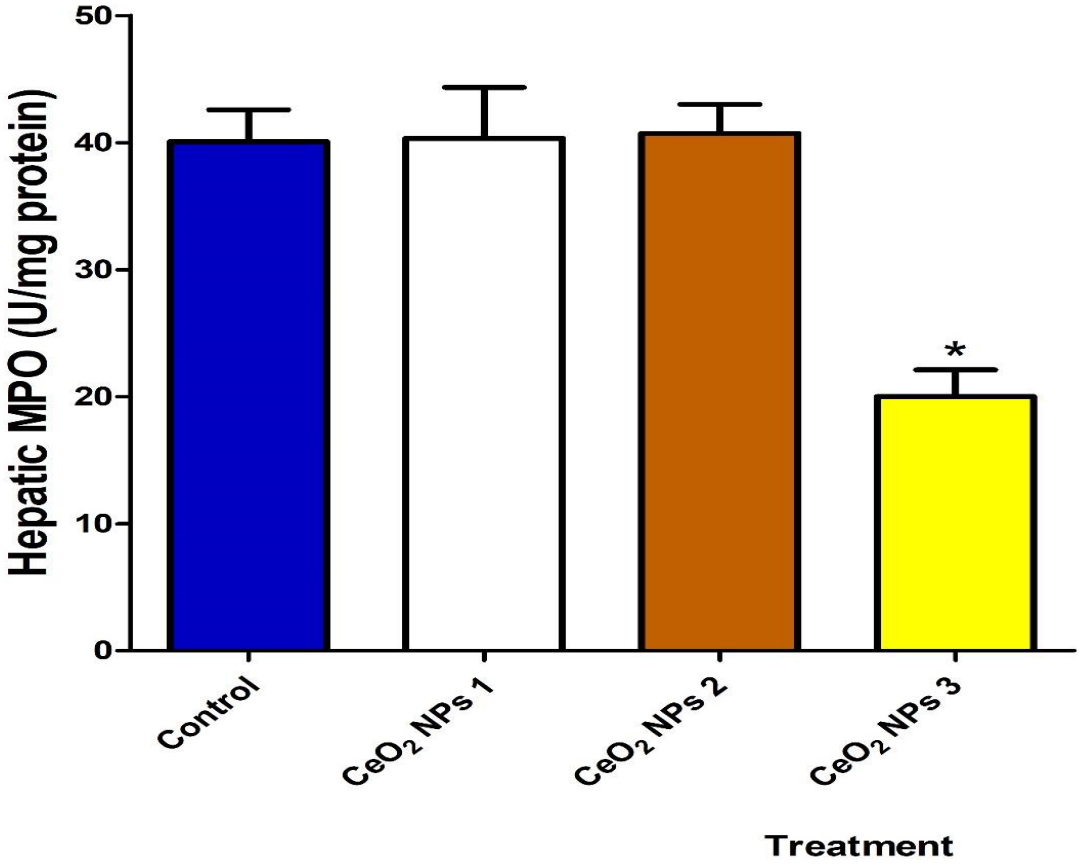

Figure 4.25: Effect of Nanoceria on hepatic myeloperoxidase (MPO) activities in adult mice

Values are means ± STDEV of 5 replicates. Control=mice that obtained normal saline, CeO_2 NPs 1, 2 and 3 = Cerium oxide nanoparticles at 100µg/kg bd/wt, 200µg/kg bd/wt and 300µg/kg bd/wt. P value<5% was adjudged significant. *= Significantly different from control

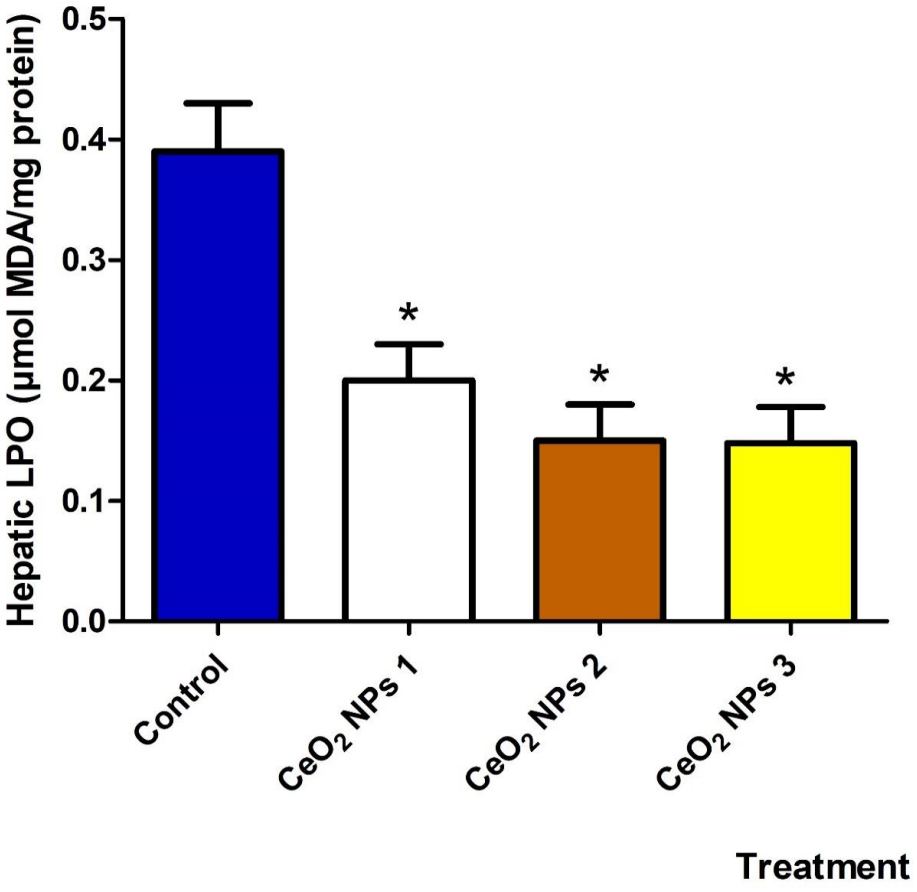

Figure 4.26: Effect of Nanoceria on Malondialdehyde (MDA) level in liver of adult mice.

Values are means ± STDEV of 5 replicates. Control=mice that obtained normal saline, CeO_2 NPs 1, 2 and 3 = Cerium oxide nanoparticles at 100µg/kg bd/wt, 200µg/kg bd/wt and 300µg/kg bd/wt. P value<5% was adjudged significant. *= Significantly different from control

Antioxidant Enzymes and Histology

Administration of nanoceria decreased catalase (figure 4.27) and SOD (4.28) activities across the treatment groups, relative to control. Precisely, activity of SOD reduced in 100, 200 and 300 µg/kg, by 45%, 54% and 66% respectively, while catalase activity of mice administered 100, 200 and 300 µg/b.wt cerium oxide nanoparticles decreased by 40%, 45%, and 64% respectively. Figure 4.29 showed that cerium oxide nanoparticles significantly ($p<0.05$) decreased hepatic glutathione-s-transferase in all the test groups, with 57%, 41% and 45% decrease for 100, 200 and 300 µg/kg, respectively. In figure 4.30 glutathione peroxidase activity decreased by 32%, 57.8% and 55% in 100, 200 and 300 µg/kg respectively. Also, there was significant decrease of reduced GSH (figure 4.31) in all treated groups, relative to control. Precisely, GSH level decreased by 57%, 41% and 54% in 100, 200 and 300 µg/kg respectively. Histopathological examination of stained liver sections (plate 4.2) revealed closely packed hepatocytes in the control. However, in the 100, 200 µg/kg exposed groups, there were random foci of single-cell hepatocellular necrosis. $P^{53}$was moderately expressed across the treatment group relative to control (plate 4.3)

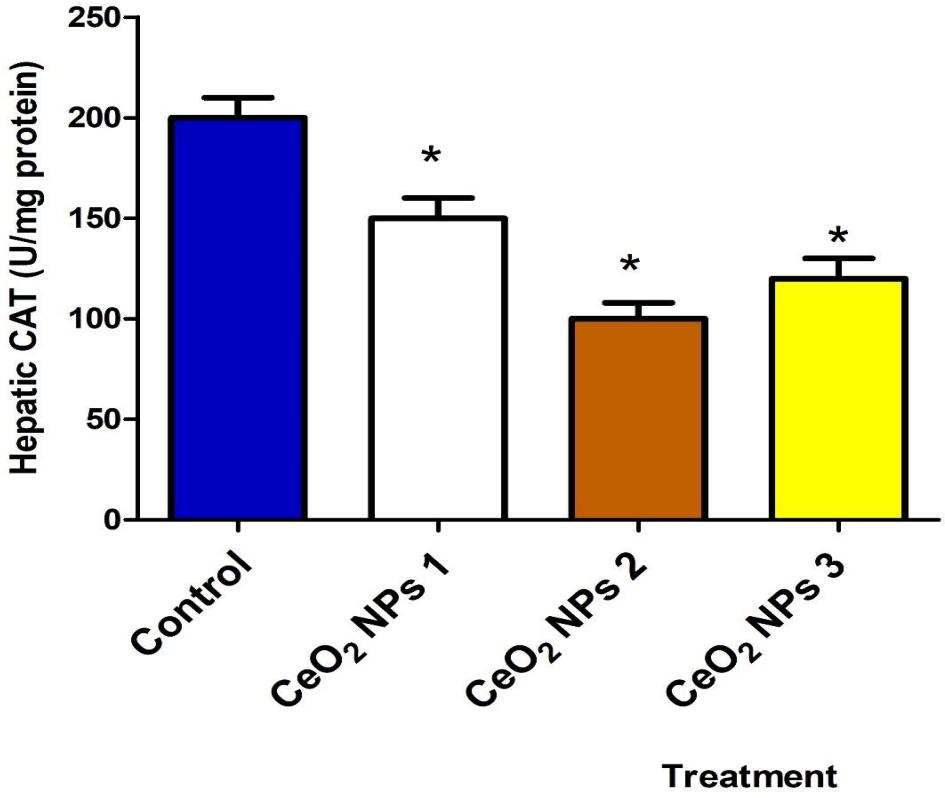

Figure 4.27: Effect of Nanoceria on hepatic catalase (CAT) activity of adult mice

Values are means ± STDEV of 5 replicates. Control=mice that obtained normal saline, CeO_2 NPs 1, 2 and 3 = Cerium oxide nanoparticles at 100µg/kg bd/wt, 200µg/kg bd/wt and 300µg/kg bd/wt. P value<5% was adjudged significant. *= Significantly different from control

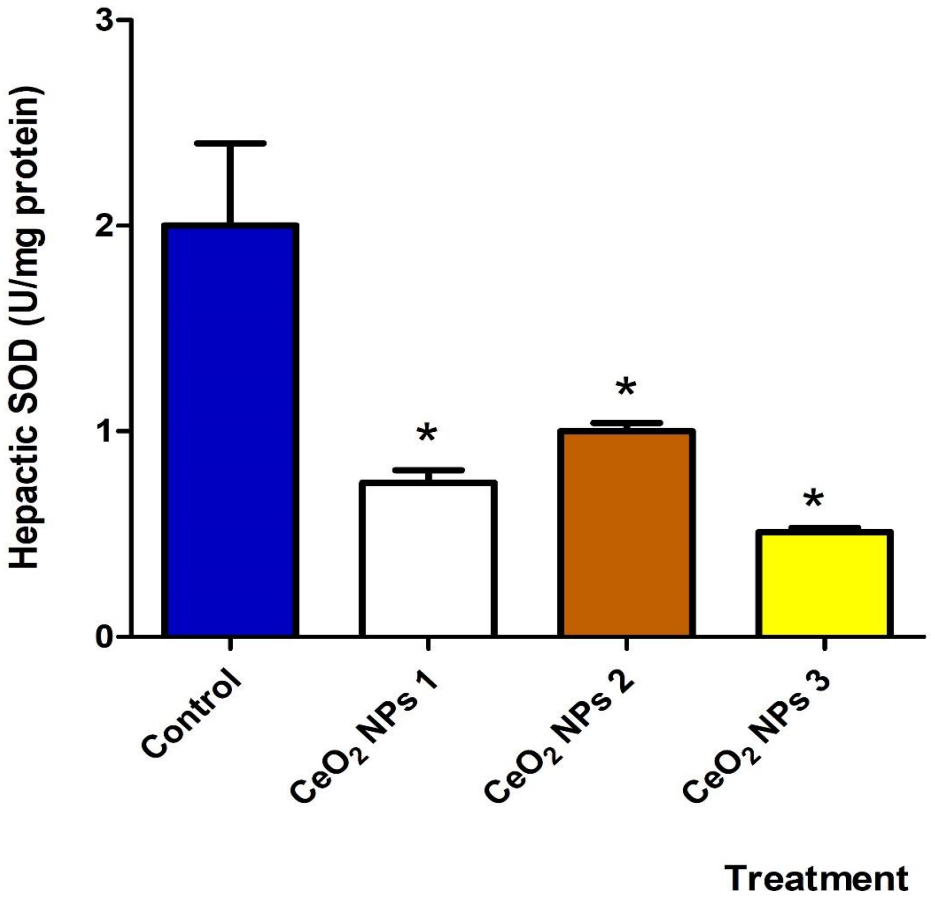

Figure 4.28: Effect of Nanoceria on activities of hepatic superoxide dismutase (SOD) in adult mice

Values are means ± STDEV of 5 replicates. Control=mice that obtained normal saline, CeO_2 NPs 1, 2 and 3 = Cerium oxide nanoparticles at 100µg/kg bd/wt, 200µg/kg bd/wt and 300µg/kg bd/wt. P value<5% was adjudged significant. *= Significantly different from control

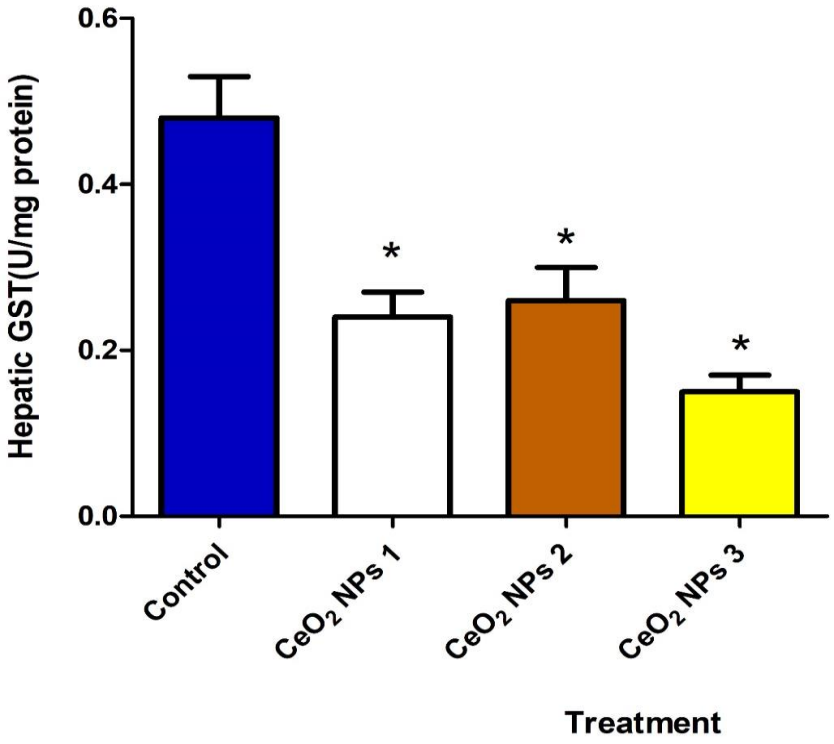

Figure 4.29: Glutathione- s -transferase activity in adult mouse following exposure to cerium oxide nanoparticles

Values are means ± STDEV of 5 replicates. Control=mice that obtained normal saline, CeO_2 NPs 1, 2 and 3 = Cerium oxide nanoparticles at 100µg/kg bd/wt, 200µg/kg bd/wt and 300µg/kg bd/wt. P value<5% was adjudged significant. *= Significantly different from control

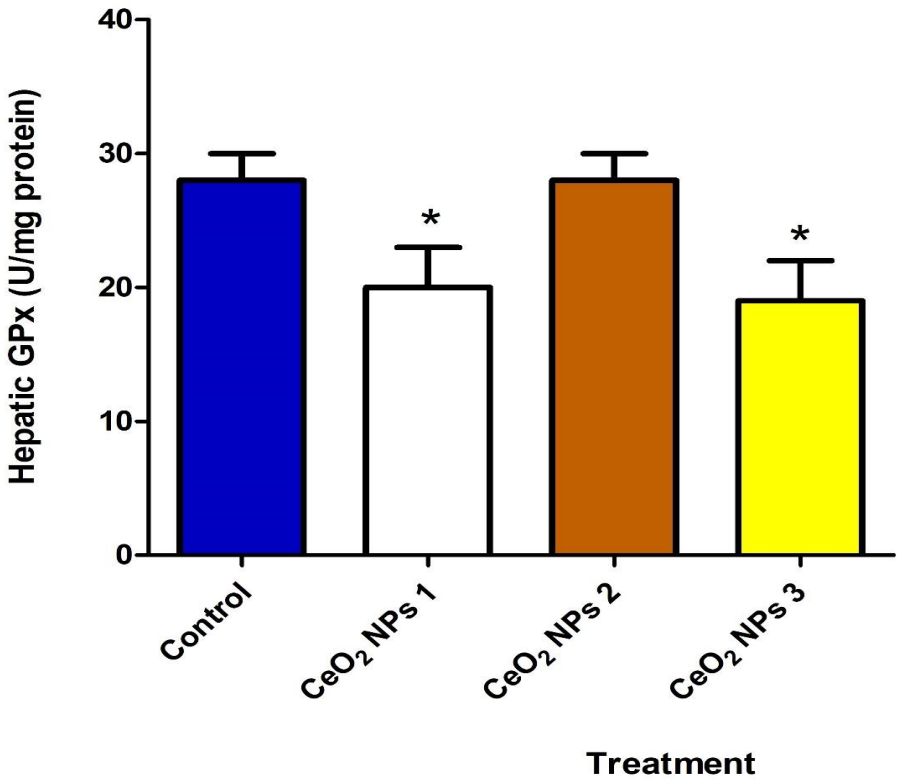

Figure 4.30: Glutathione peroxidase activity in adult mouse following exposure to cerium oxide nanoparticles

Values are means ± STDEV of 5 replicates. Control=mice that obtained normal saline, CeO_2 NPs 1, 2 and 3 = Cerium oxide nanoparticles at 100µg/kg bd/wt, 200µg/kg bd/wt and 300µg/kg bd/wt. P value<5% was adjudged significant. *= Significantly different from control

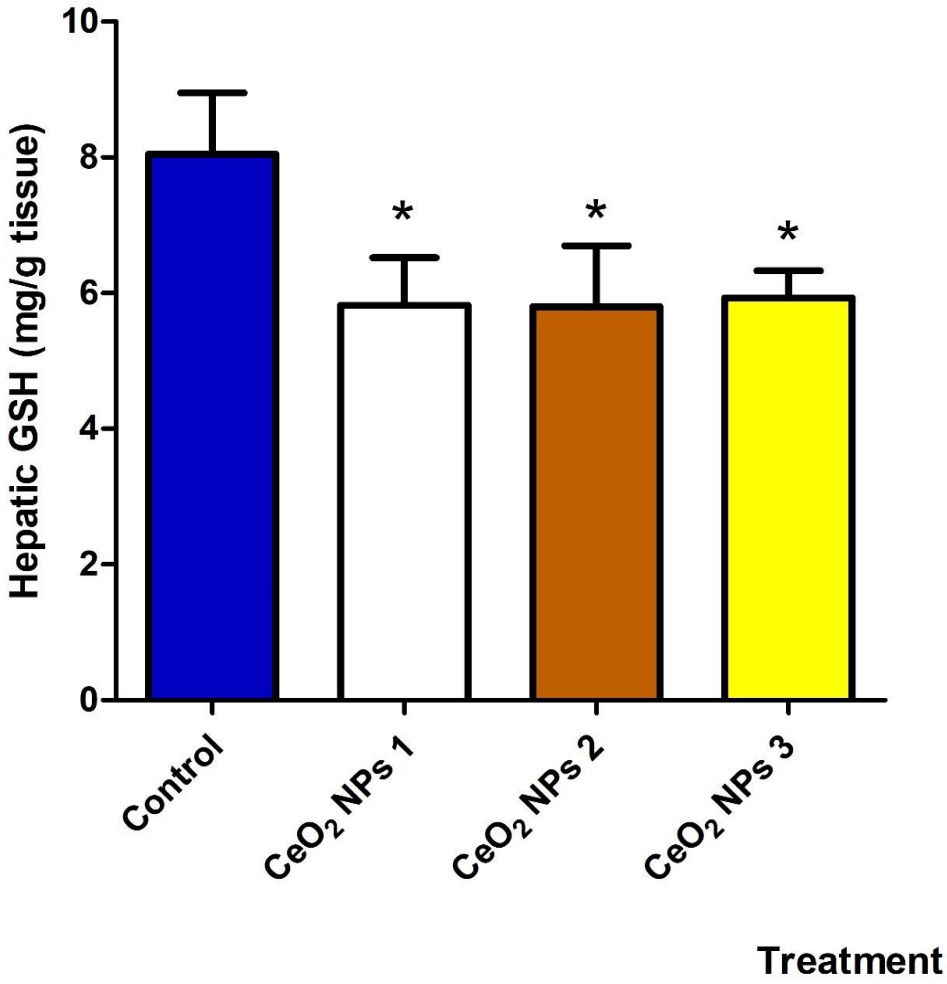

Figure 4.31: Reduced glutathione level in adult mouse exposed to cerium oxide nanoparticles

Values are means ± STDEV of 5 replicates. Control=mice that obtained normal saline, CeO_2 NPs 1, 2 and 3 = Cerium oxide nanoparticles at 100µg/kg bd/wt, 200µg/kg bd/wt and 300µg/kg bd/wt. P value<5% was adjudged significant. *= Significantly different from control

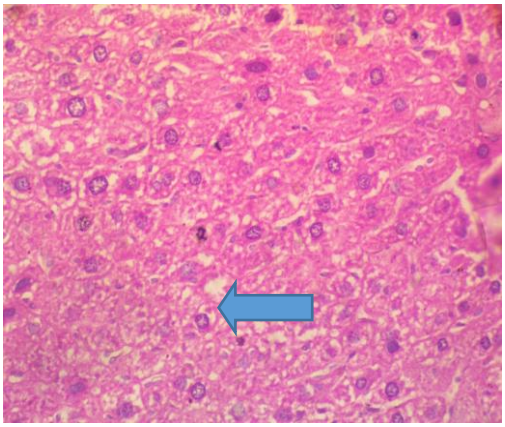

Control

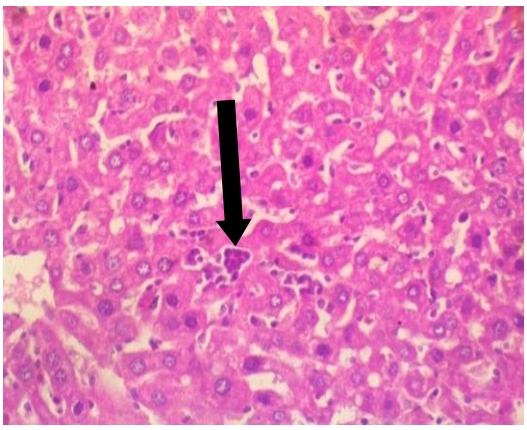

CeO_2 NPs 1

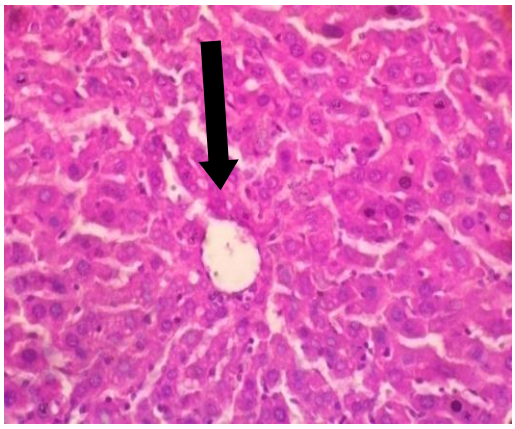

CeO_2 NPs 2

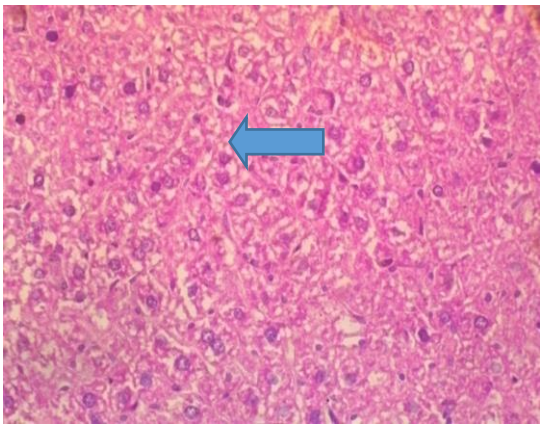

CeO_2 NPs 3

Plate 4.2: Representative photomicrographs of liver from mice treated with nanoceria at different doses. (M x 400)

Values shown here were displayed by way of mean ± STDEV of 5 mouse per grouping. Control=mice that obtained normal saline, CeO_2 NPs 1, 2 and 3 = Cerium oxide nanoparticles at 100µg/k, 200µg/kg and 300µg/kg. In the control, the cytoarchitecture remain intact. Moderate presence of inflammatory cells of CeO_2NPs treated mice, especially at 100µg/kg bd/wt and 200µg/kg body weight.

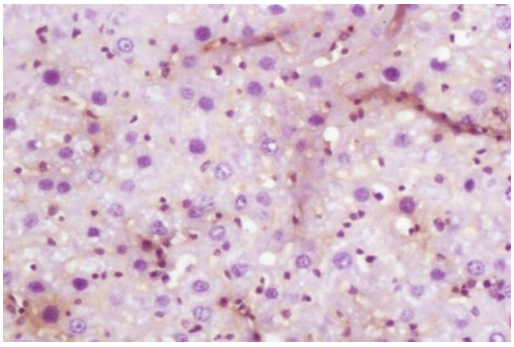

Control

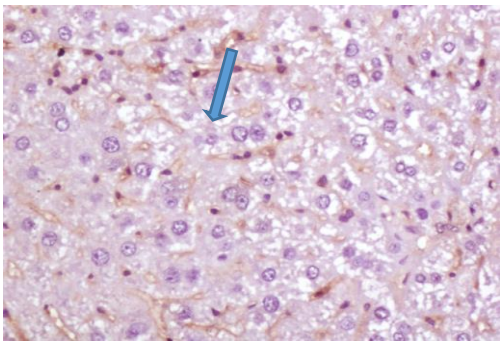

CeO_2 NPs 1

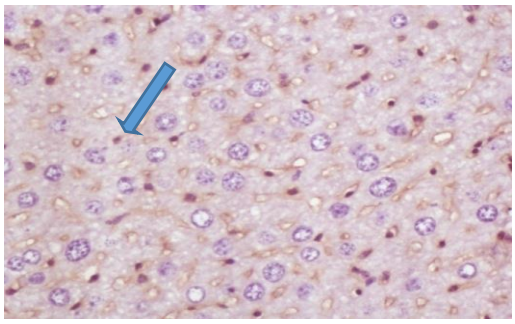

CeO_2 NPs 2

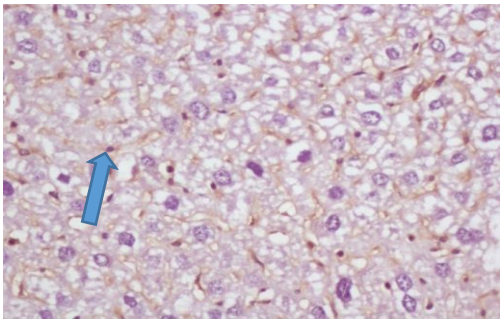

CeO_2 NPs 3

.

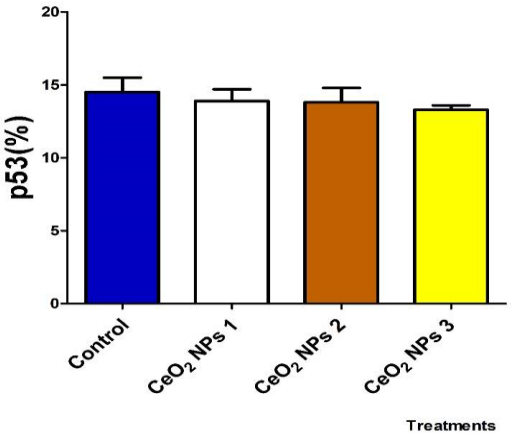

Plate 4.3: p53 expression in the liver of following exposure to cerium oxide nanoparticles. (M=X400).

4.3: Ameliorative potential of nanoceria following induction of hepatotoxicity via injection of diethylnitrosamine (DEN) on adult mouse

Result

Weight and serum indices

Table 4.3.1 showed that exposure of animals to DEN had no significant effect on the weight of animals as all exposed groups had no significant changes in the weight difference. Also, the liver and its organosomatic revealed no difference in their weights in DEN exposed groups relative to control. However, administration of nanoceria showed a 67% hepatic weight increase, relative to DEN exposed animals. Exposure of animals to DEN caused increased ALT activities (figure 4.32) and AST (figure 4.33) by 45% and 48%, relative to control. Pre-treatment with cerium oxide nanoparticles, at both doses decreased activity of these enzymes relative to DEN. Specifically, alanine amino aminotransferase and aspartate amino aminotransferase increased at 100µg/kg CeO_2NPs by 45% and 118% and in 200µg/kg of CeO_2NPs by 46% and 62% respectively.

Table 4.4: Body and liver weights of adult mice following diethylnitrosamine induction and post treatment with cerium oxide nanoparticles

Groupings	Initial.	Final	Diff	Liver	Organo Somatic
Control.	24.05±2.75	26.85±4.74	2.8±0.037	1.21±0.06	6.123±0.70
DEN.	30.33±0.87	28.6±2.71	1.93±0.026*	1.33±0.0.16	4.68±0.61
CeO_2NPs 1 + DEN	31.85±2.08	28.62±1.17	3.23±0.027	1.48±0.15	5 .707±0.65
CeO_2NPs 2 + DEN	30.23±2.05	28.73±3.71	1.50±0.035	1.50±0.15	5.244±0.40
CeO_2NPs 1	27.08±0.71	26.75±1.44	0.33±0.03**	1.28±0.12	5.810±0.58
CeO_2NPs 2	28.56±1.69	27.97±2.92	0.60±0.03**	1.32±0.22	5.189±0.54

Values shown here were displayed by way of mean ± STDEV of 5 mouse per grouping. Control=mice that received normal saline, CeO_2 NPs 1, 2 and 3 = Cerium oxide nanoparticles at 100µg/k, 200µg/kg and 300µg/kg. DEN= Diethylnitrosamine *P and **P values<5% was adjudged significant upon comparison to control and DEN.

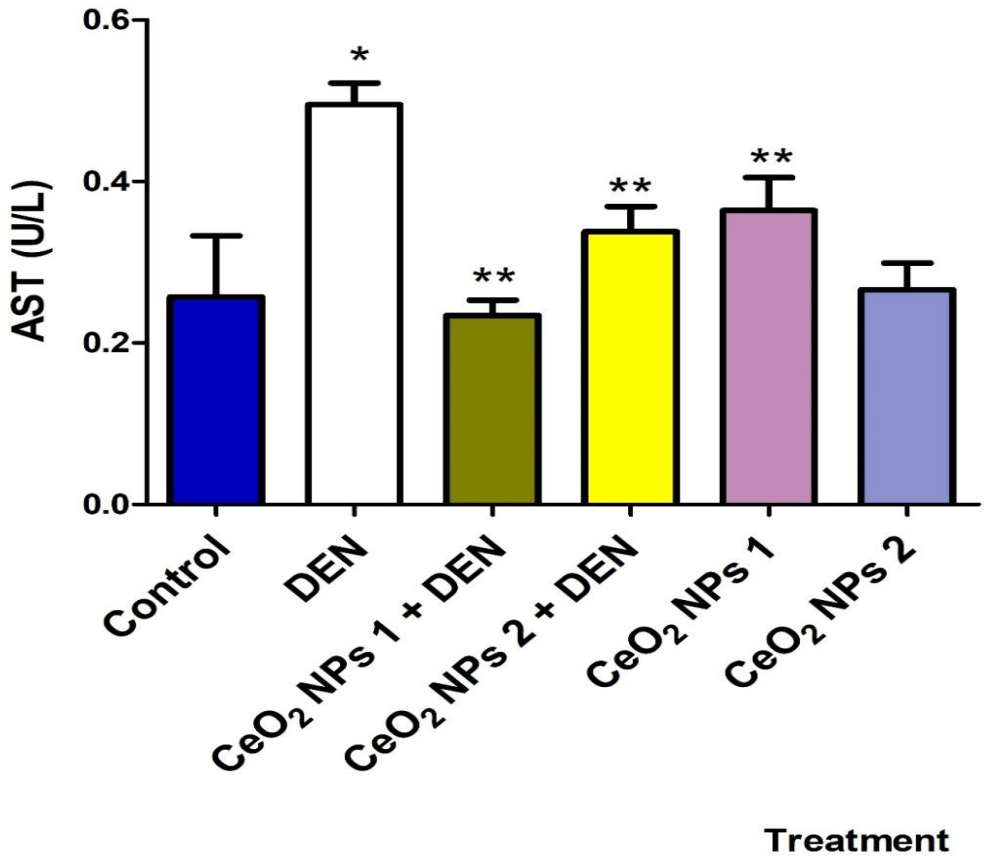

Figure 4.32: Effect of Nanoceria on serum aspartate aminotransferase (AST) activities of adult mice exposed to diethylnitrosamine.

Values are means ± STDEV of 5 replicates. Control=mice that received normal saline, CeO_2 NPs 1, 2 and 3 = Cerium oxide nanoparticles at 100µg/k, 200µg/kg and 300µg/kg. DEN= Diethylnitrosamine *P and **P values<5% was adjudged significant upon comparison to control and DEN.

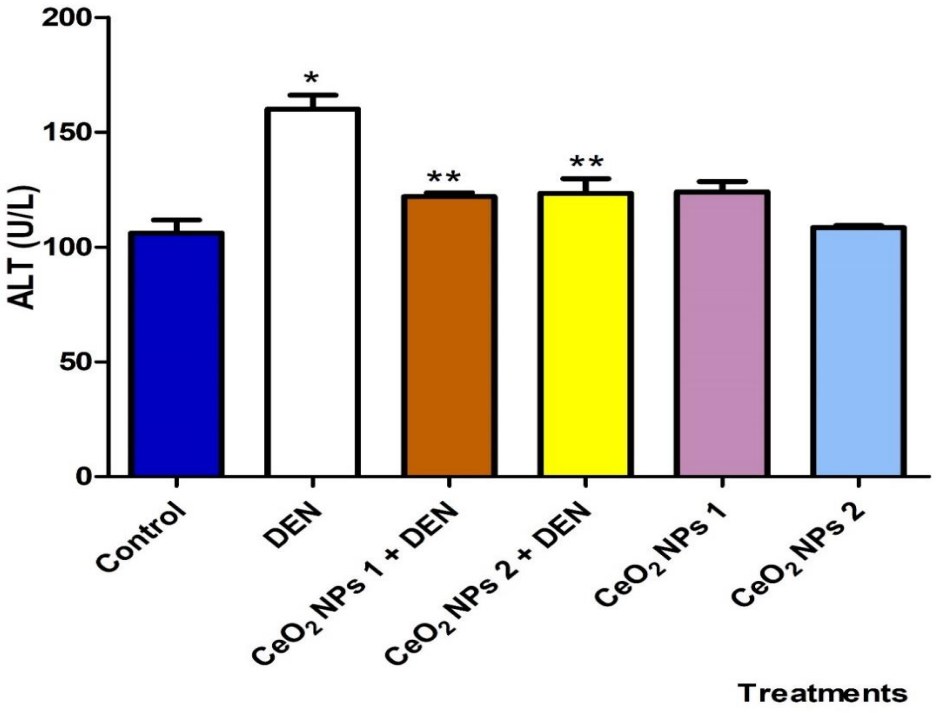

Figure 4.33: Effect of Nanoceria on serum alanine aminotransferase (ALT) activities of adult mice exposed to diethylnitrosamine.

Values are means ± STDEV of 5 replicates. Control=mice that received normal saline, CeO_2 NPs 1, 2 and 3 = Cerium oxide nanoparticles at 100µg/k, 200µg/kg and 300µg/kg. DEN= Diethylnitrosamine *P and **P values<5% was adjudged significant upon comparison to control and DEN.

.

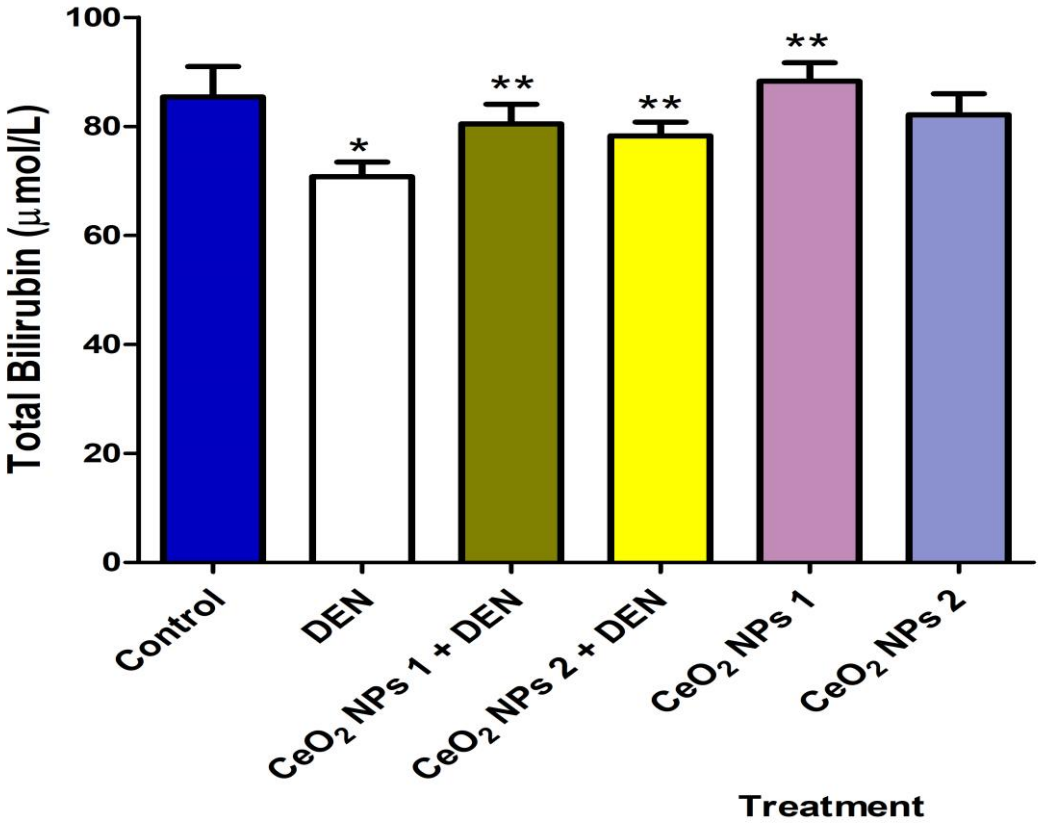

Figure 4.34: Effect of Nanoceria on serum total bilirubin level of adult mice exposed to diethylnitrosamine.

Values are means ± STDEV of 5 replicates. Control=mice that received normal saline, CeO_2 NPs 1, 2 and 3 = Cerium oxide nanoparticles at 100µg/k, 200µg/kg and 300µg/kg. DEN= Diethylnitrosamine *P and **P values<5% was adjudged significant upon comparison to control and DEN.

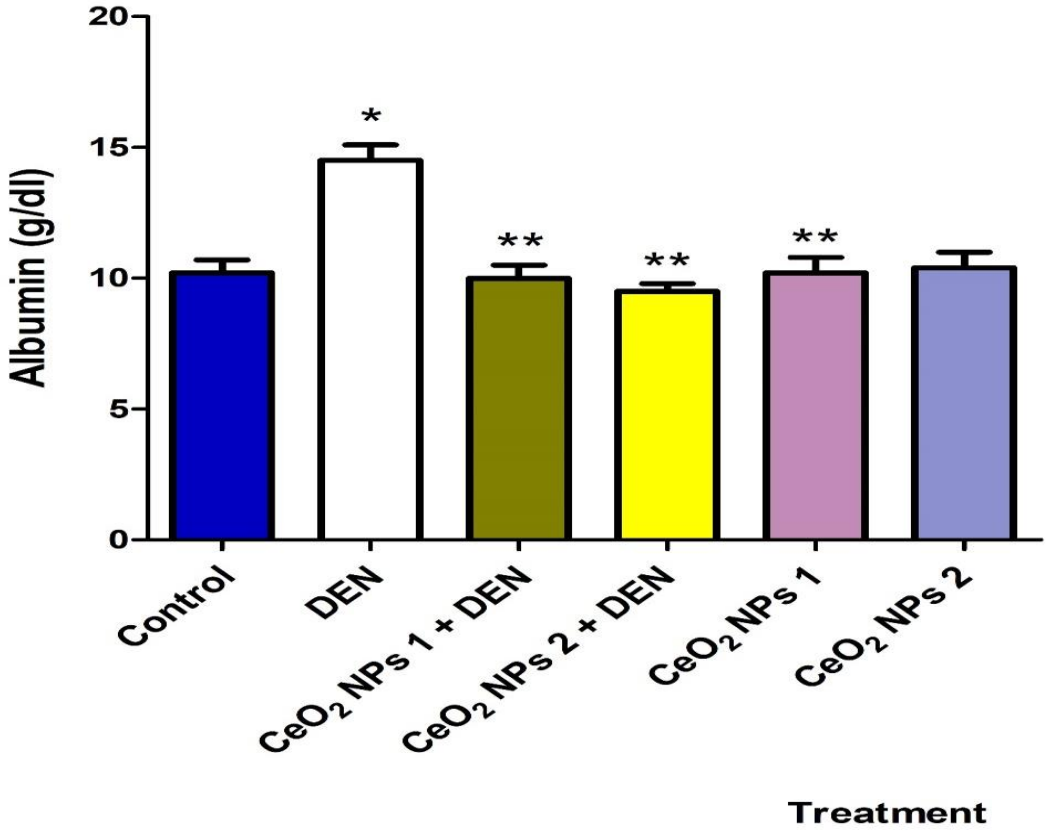

Figure 4.35: Effect of Nanoceria on serum albumin level of adult mice exposed to diethylnitrosamine.

Values are means ± STDEV of 5 replicates. Control=mice that received normal saline, CeO_2 NPs 1, 2 and 3 = Cerium oxide nanoparticles at 100µg/k, 200µg/kg and 300µg/kg. DEN= Diethylnitrosamine *P and **P values<5% was adjudged significant upon comparison to control and DEN.

Inflammatory Markers

DEN caused increased in MPO (figure 4.36) as well as NO (figure 4.37) level, relative to control, with 385 and 18% increase respectively. Pre-treatment with 100µg/kg and 200µg/kg of CeO_2NPs caused a decrease in hepatic myeloperoxidase by 32% and 31% and nitric oxide by 20% and 36% respectively. Also, administration of diethylnitrosamine increase lipid peroxidation (figure 4.38) in animals. Precisely, LPO increased by 81% when compared to the control.

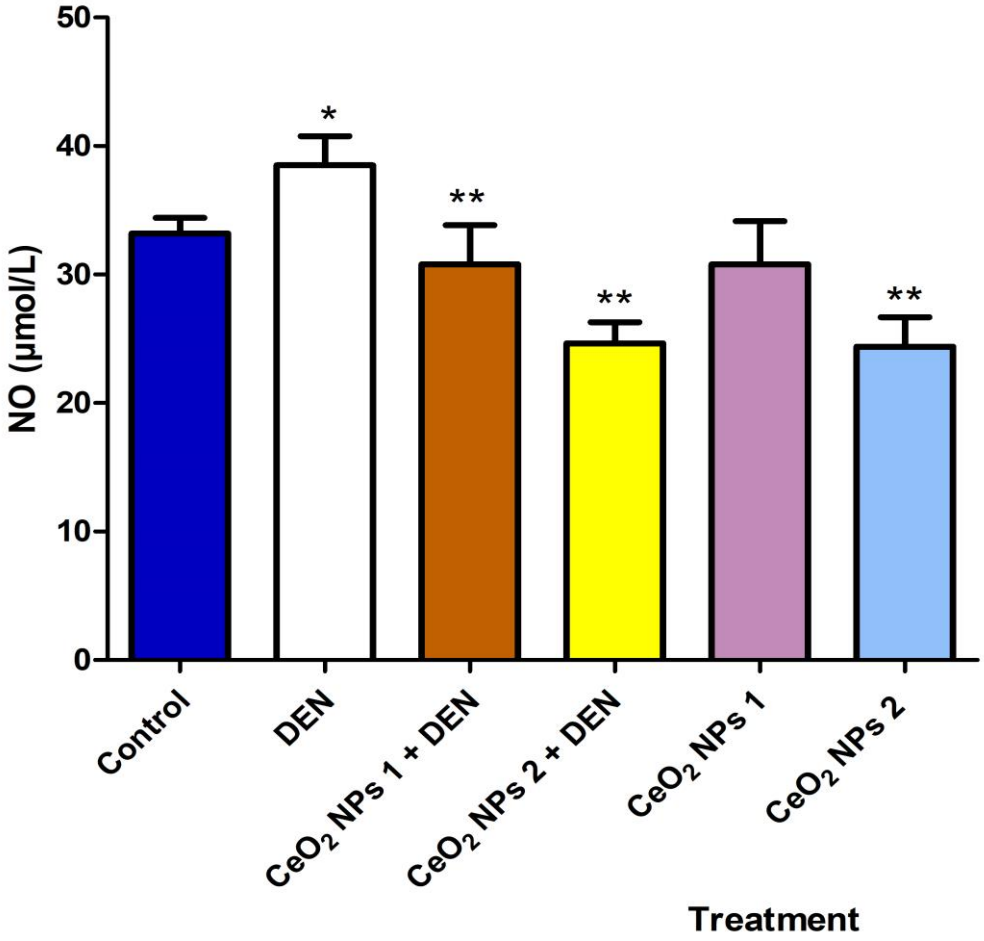

Figure 4.36: Effect of Nanoceria on hepatic nitric oxide (NO) level of adult mice exposed to diethylnitrosamine.

Values are means ± STDEV of 5 replicates. Control=mice that received normal saline, CeO_2 NPs 1, 2 and 3 = Cerium oxide nanoparticles at 100µg/k, 200µg/kg and 300µg/kg. DEN= Diethylnitrosamine *P and **P values<5% was adjudged significant upon comparison to control and DEN.

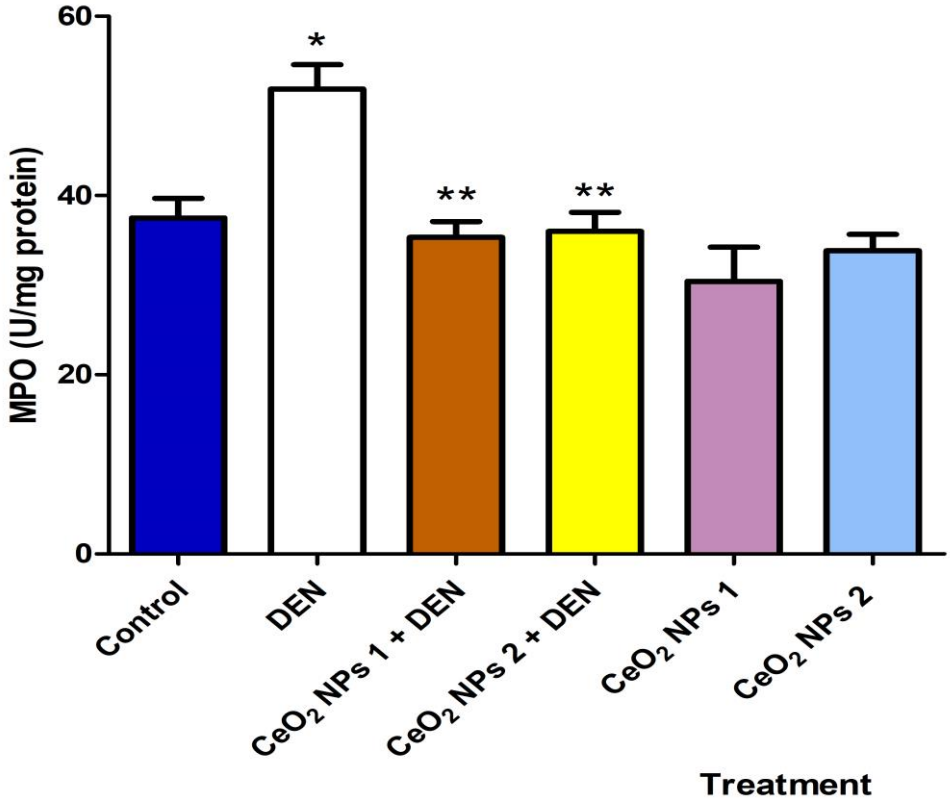

Figure 4.37 Effect of Nanoceria on hepatic myeloperoxidase activities of adult mice exposed to diethylnitrosamine.

Values are means ± STDEV of 5 replicates. Control=mice that received normal saline, CeO_2 NPs 1, 2 and 3 = Cerium oxide nanoparticles at 100µg/k, 200µg/kg and 300µg/kg. DEN= Diethylnitrosamine *P and **P values<5% was adjudged significant upon comparison to control and DEN.

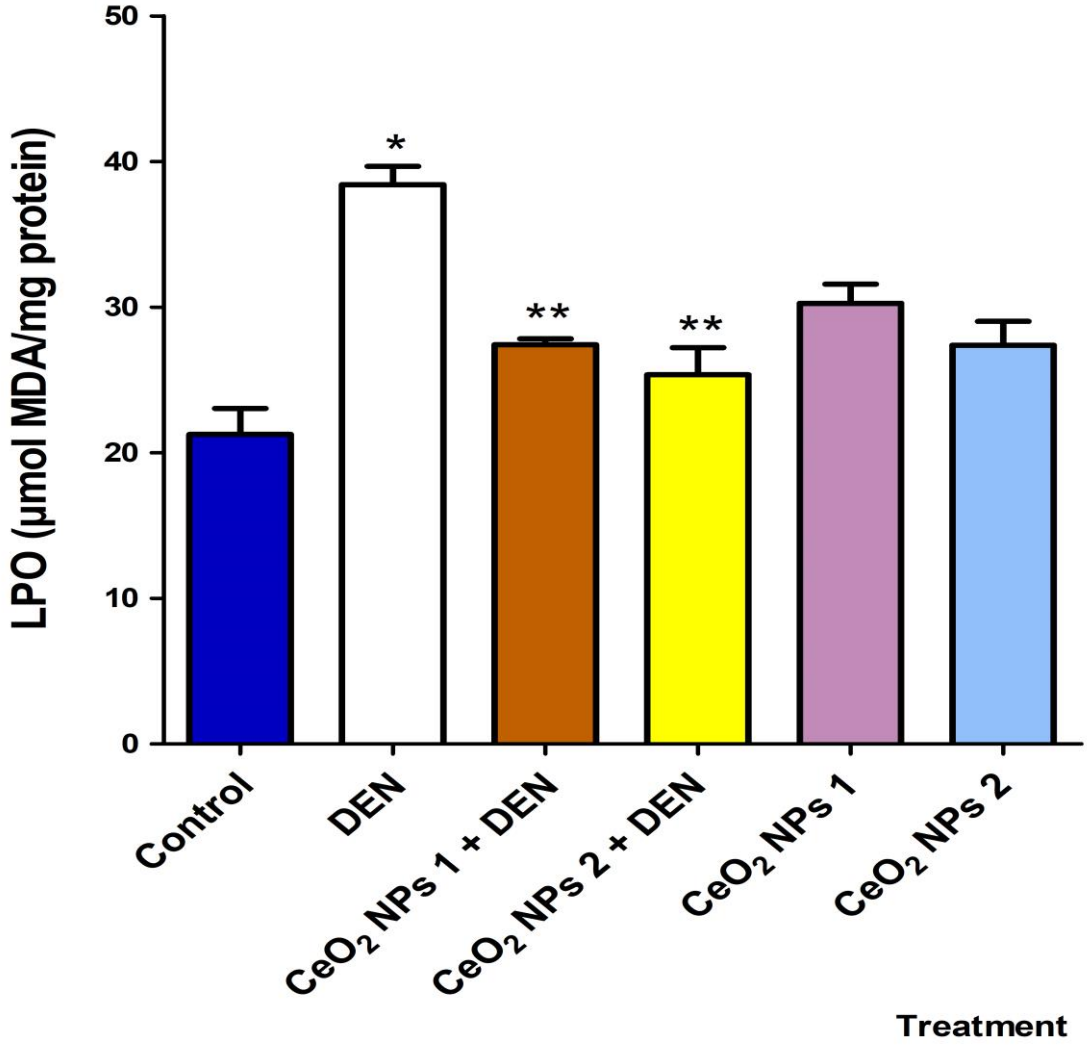

Figure 4.38: Effect of Nanoceria on hepatic malonaldehyde (MDA) level of adult mice exposed to diethylnitrosamine.

Values are means ± STDEV of 5 replicates. Control=mice that received normal saline, CeO_2 NPs 1, 2 and 3 = Cerium oxide nanoparticles at 100µg/k, 200µg/kg and 300µg/kg. DEN= Diethylnitrosamine *P and **P values<5% was adjudged significant upon comparison to control and DEN.

Oxidative stress and antioxidant enzymes

Increased Lipid peroxidation in animals administered DEN was accompanied with a resultant decrease in antioxidant enzyme activities. Particularly, catalase (figure 4.40) as well SOD (figure 4.39) activities were significantly ($p<0.05$) decrease by 27% and 56% respectively in groups pre-treated with 200 µg/kg CeO_2NPs. Also, administration of DEN to animals caused a significant ($p<0.05$) decrease in activities of GST (43%) (figure 4.43), GSH (81%) (figure 4.42) and GPx (49%) (figure 4.41) level relative to the control. However, when pre-treated with cerium oxide nanoparticles at single and double doses, MDA was significantly ($P<0.05$) decreased by 28% and 35% in 100 and 200 µg/kg group, while CeO_2NPs pre-treatment significantly increased significantly ($p<0.05$) the activities of antioxidant defence enzymes.

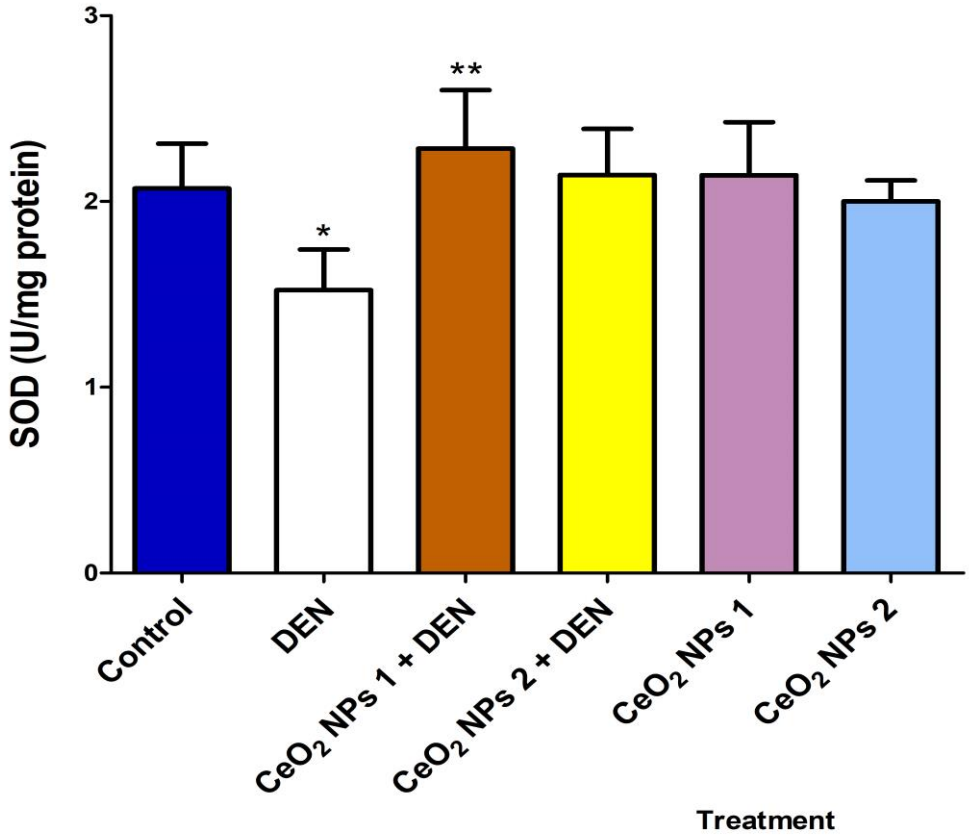

Figure 4.39: Effect of Nanoceria on hepatic superoxide dismutase activity of adult mice exposed to diethylnitrosamine.

Values are means ± STDEV of 5 replicates. Control=mice that received normal saline, CeO_2 NPs 1, 2 and 3 = Cerium oxide nanoparticles at 100µg/k, 200µg/kg and 300µg/kg. DEN= Diethylnitrosamine *P and **P values<5% was adjudged significant upon comparison to control and DEN.

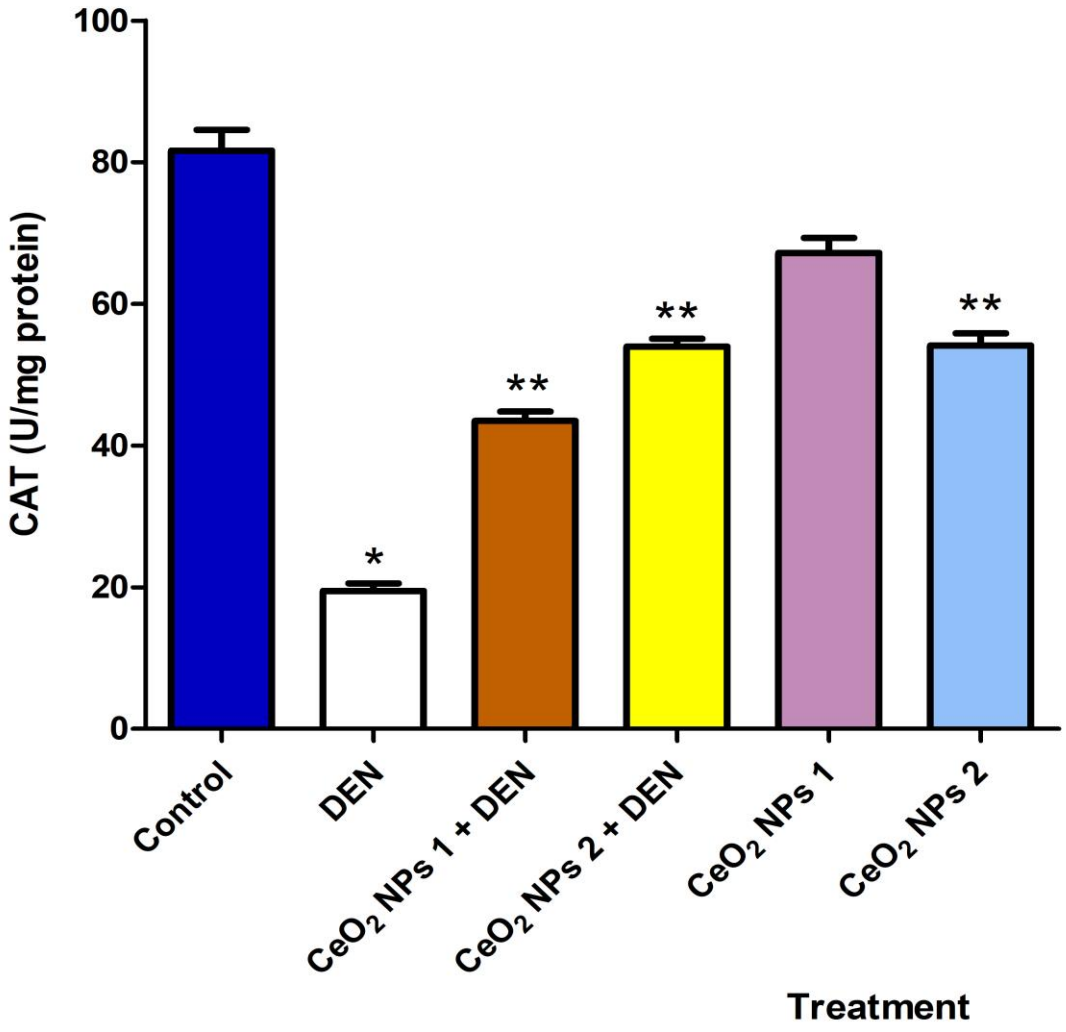

Figure 4.40: Effect of Nanoceria on hepatic catalase activity of adult mice exposed to diethylnitrosamine.

Values are means ± STDEV of 5 replicates. Control=mice that received normal saline, CeO_2 NPs 1, 2 and 3 = Cerium oxide nanoparticles at 100µg/k, 200µg/kg and 300µg/kg. DEN= Diethylnitrosamine *P and **P values<5% was adjudged significant upon comparison to control and DEN.

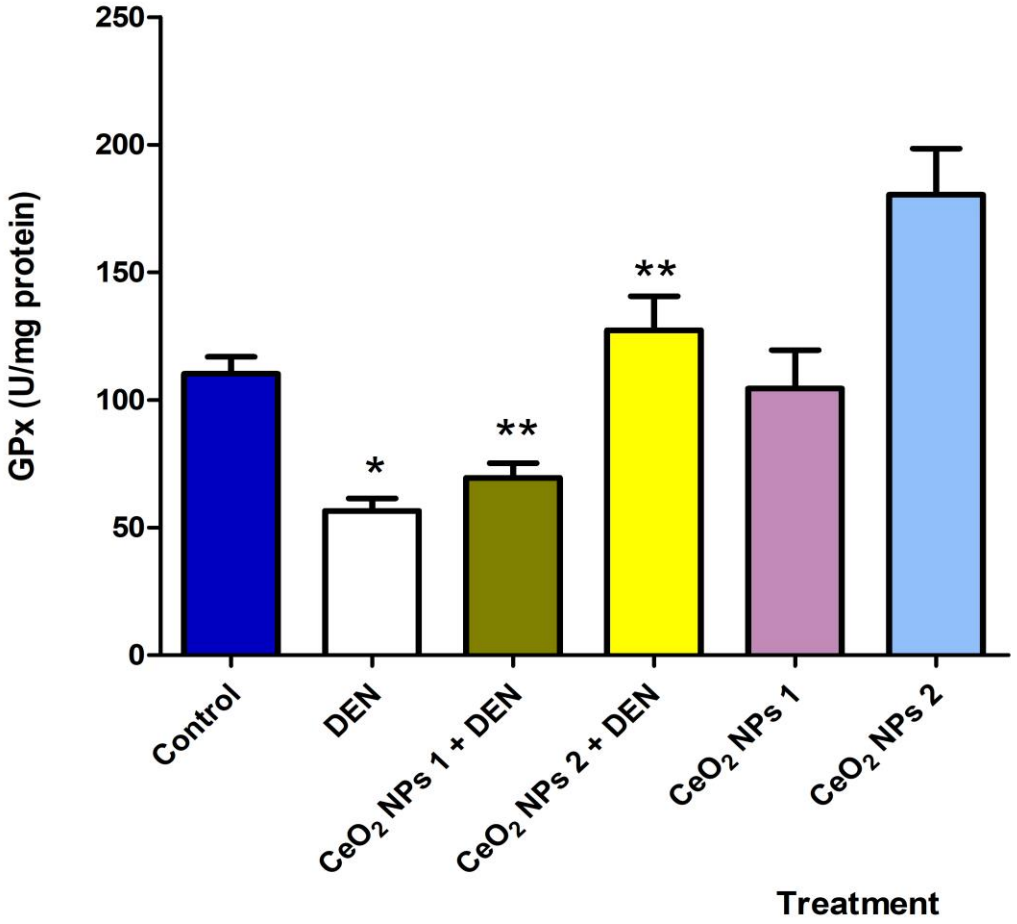

Figure 4.41 Effect of Nanoceria on hepatic glutathione peroxidase activity of adult mice exposed to diethylnitrosamine.

Values are means ± STDEV of 5 replicates. Control=mice that received normal saline, CeO_2 NPs 1, 2 and 3 = Cerium oxide nanoparticles at 100µg/k, 200µg/kg and 300µg/kg. DEN= Diethylnitrosamine *P and **P values<5% was adjudged significant upon comparison to control and DEN.

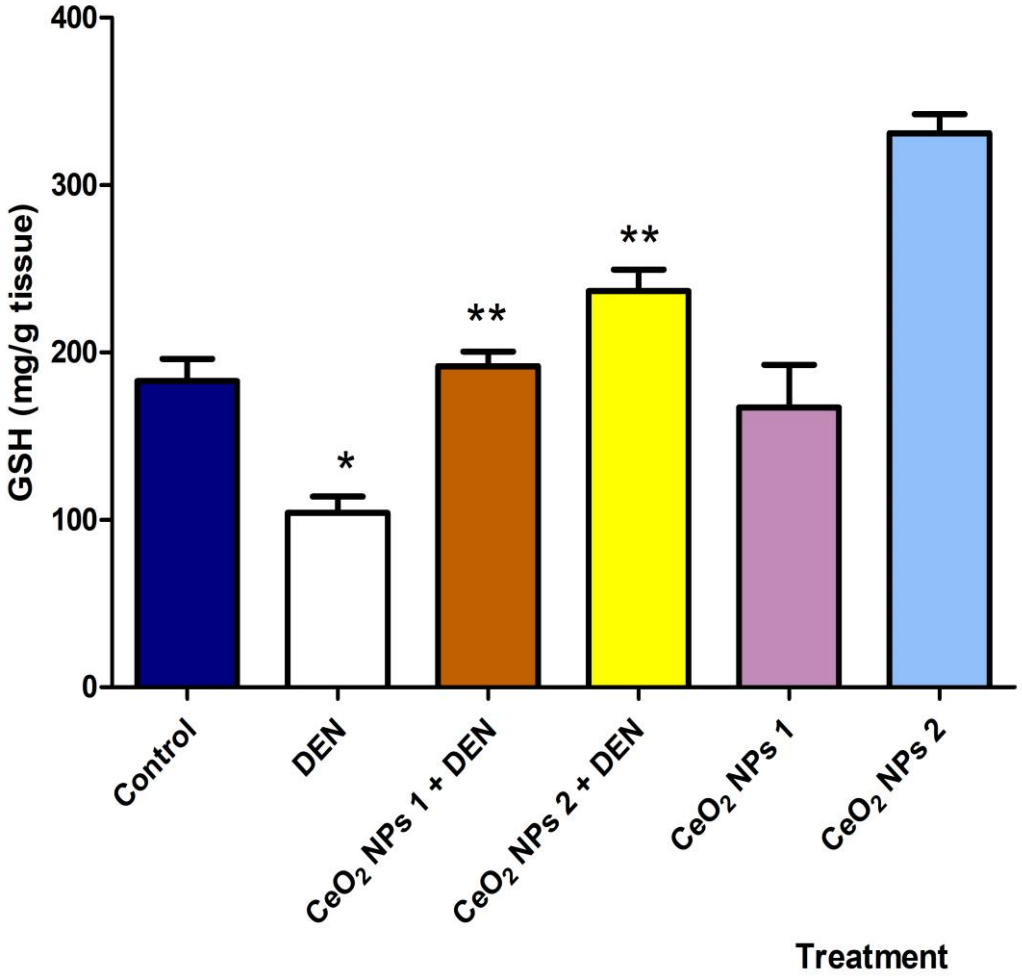

Figure 4.42: Effect of Nanoceria on hepatic reduced glutathione level of adult mice exposed to diethylnitrosamine.

Values are means ± STDEV of 5 replicates. Control=mice that received normal saline, CeO_2 NPs 1, 2 and 3 = Cerium oxide nanoparticles at 100µg/k, 200µg/kg and 300µg/kg. DEN= Diethylnitrosamine *P and **P values<5% was adjudged significant upon comparison to control and DEN.

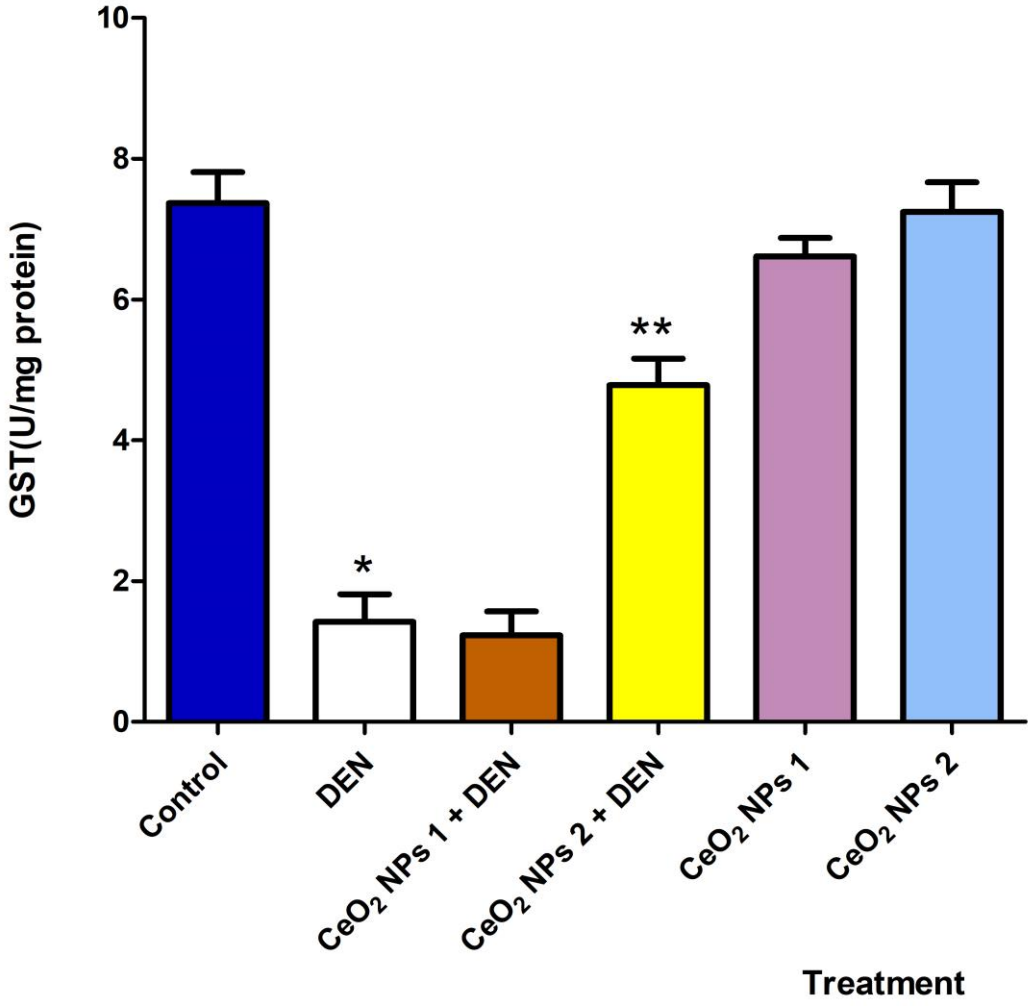

Figure 4.43: Effect of Nanoceria on hepatic glutathione-s-transferase of adult mice exposed to diethylnitrosamine.

Values are means ± STDEV of 5 replicates. Control=mice that received normal saline, CeO_2 NPs 1, 2 and 3 = Cerium oxide nanoparticles at 100µg/k, 200µg/kg and 300µg/kg. DEN= Diethylnitrosamine *P and **P values<5% was adjudged significant upon comparison to control and DEN.

Histology and Immunohistochemistry

Histopathological examination of liver sections showed presence of inflammatory cells in animals exposed to DEN, relative to control which revealed no visible lesions in the hepatocytes. However, pre-treatment, at single and double doses revealed hepatocytes with normal morphology, accompanied with slight presence of inflammatory cells (plate 4.4). Immunochemical staining of the liver revealed that pre-treatment with 100µg/kg and 200µg/kg CeO_2NPs mitigated high iNOS (plate 4.5), cox- 2 (plate 4.6) as well as Bcl_2 (plate 4.7) expression in animals exposed to DEN and attendant mild p53 (plate 4.8) expression relative to DEN-treated animals.

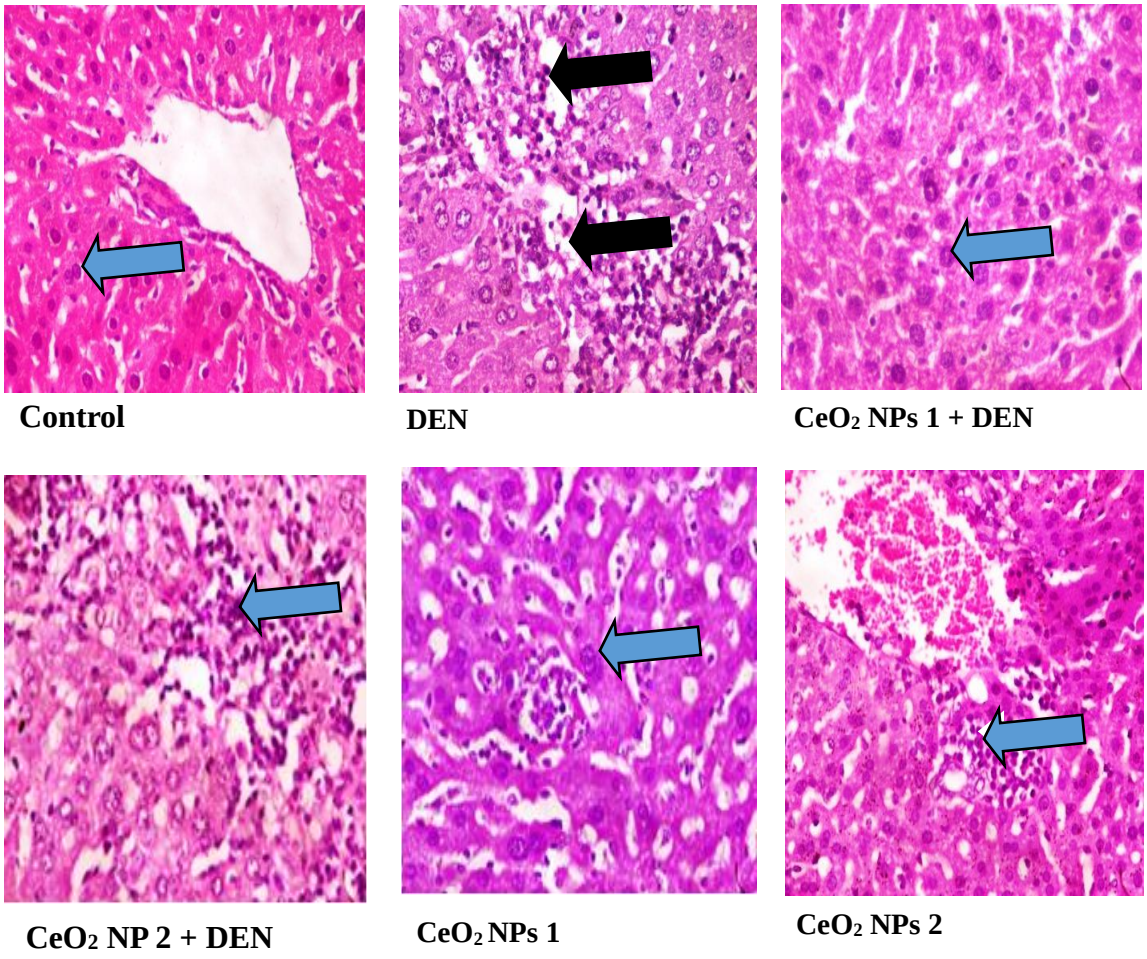

Plate 4.4: Representative photomicrographs of the liver of adult mouse following pre-treatment with cerium oxide nanoparticles and exposed to DEN (M x 400). Control revealed usual architecture. In DEN group, there was presence of severe inflammation. DEN + CeO_2NPs (100µg/kg) revealed normal architecture. In DEN+CeO_2NPs (200µg/kg), there was shows normal architecture alongside minor inflammation. In CeO_2NPs at single (100µg/kg) and double doses (200µg/kg) both revealed normal architecture

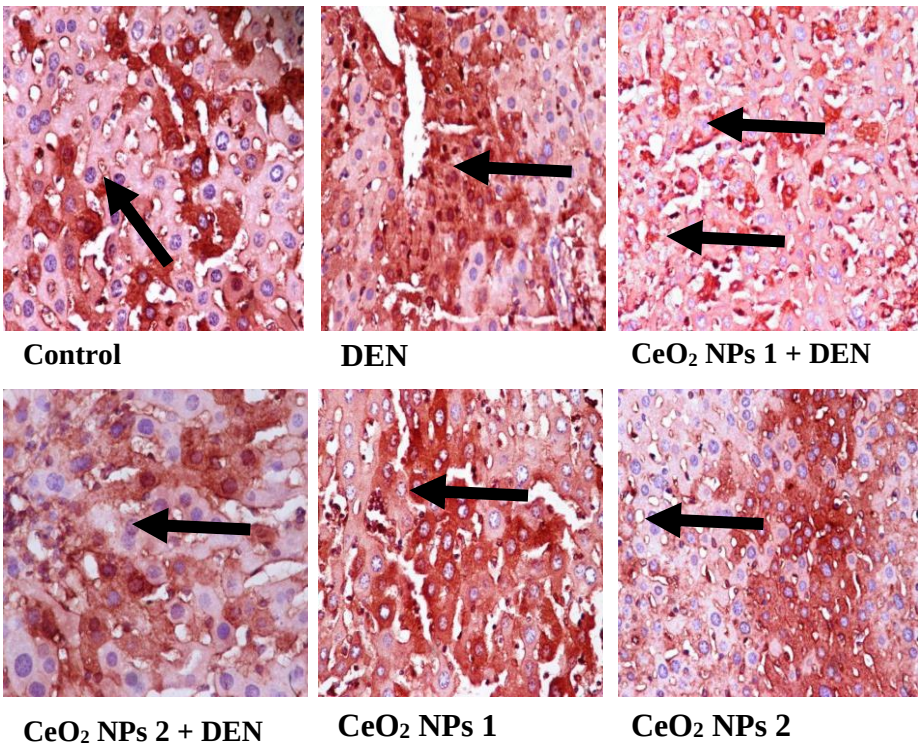

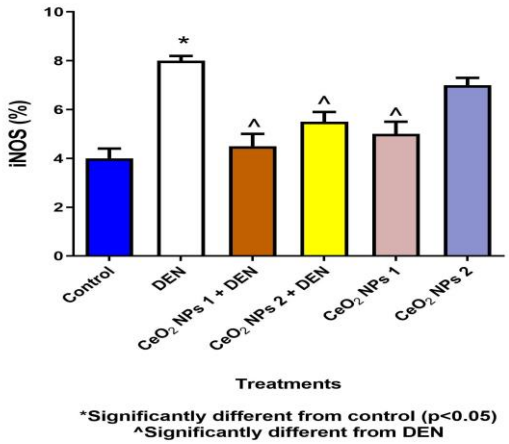

Plate 4.5: iNOS expression in the liver of adult mouse following pre-treatment with cerium oxide nanoparticles and exposure to diethylnitrosamine. (M=X400).

Values are means ± STDEV of 5 replicates. Control=mice that received normal saline, CeO_2 NPs 1, 2 and 3 = Cerium oxide nanoparticles at 100µg/k, 200µg/kg and 300µg/kg. DEN= Diethylnitrosamine *P and **P values<5% was adjudged significant upon comparison to control and DEN.

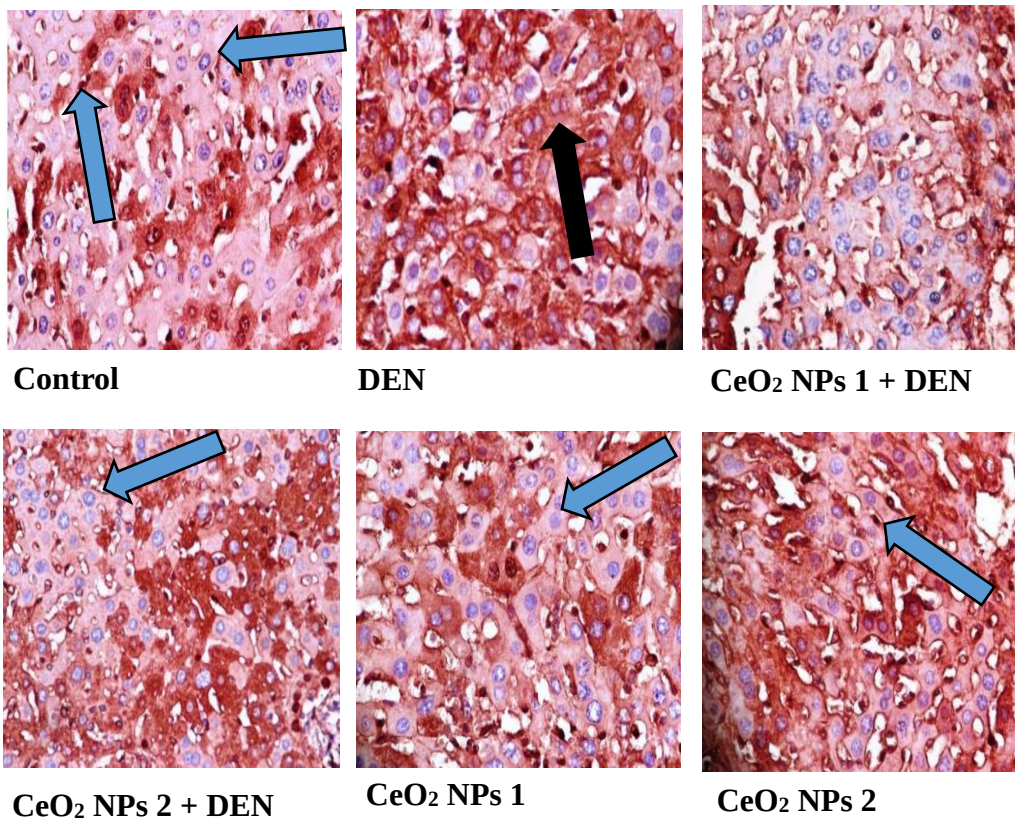

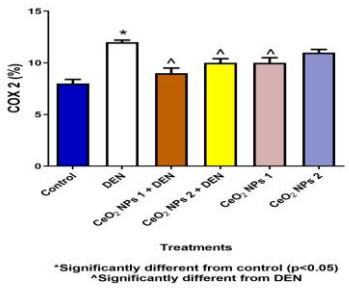

Plate 4.6: COX-2 level by immunohistochemical staining of the liver of adult mouse following pre-treatment with cerium oxide nanoparticles and exposure to diethylnitrosamine.

Values are means ± STDEV of 5 replicates. Control=mice that received normal saline, CeO_2 NPs 1, 2 and 3 = Cerium oxide nanoparticles at 100µg/k, 200µg/kg and 300µg/kg. DEN= Diethylnitrosamine *P and **P values<5% was adjudged significant upon comparison to control and DEN.

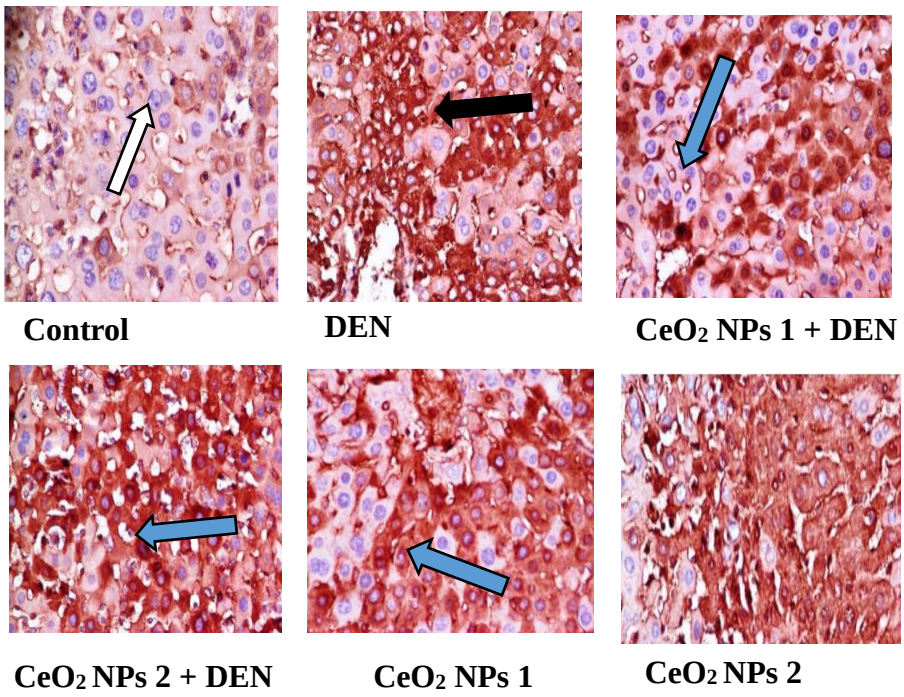

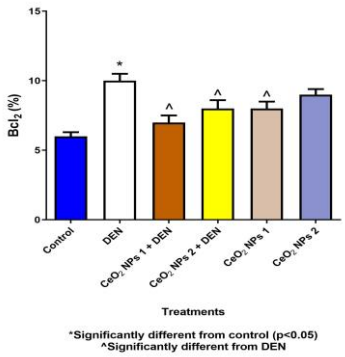

Plate 4.7: Bcl_2 level by immunohistochemical staining of the liver of adult mouse following pre-treatment with cerium oxide nanoparticles and exposed to diethylnitrosamine.

Values are means ± STDEV of 5 replicates. Control=mice that received normal saline, CeO_2 NPs 1, 2 and 3 = Cerium oxide nanoparticles at 100µg/k, 200µg/kg and 300µg/kg. DEN= Diethylnitrosamine *P and **P values<5% was adjudged significant upon comparison to control and DEN.

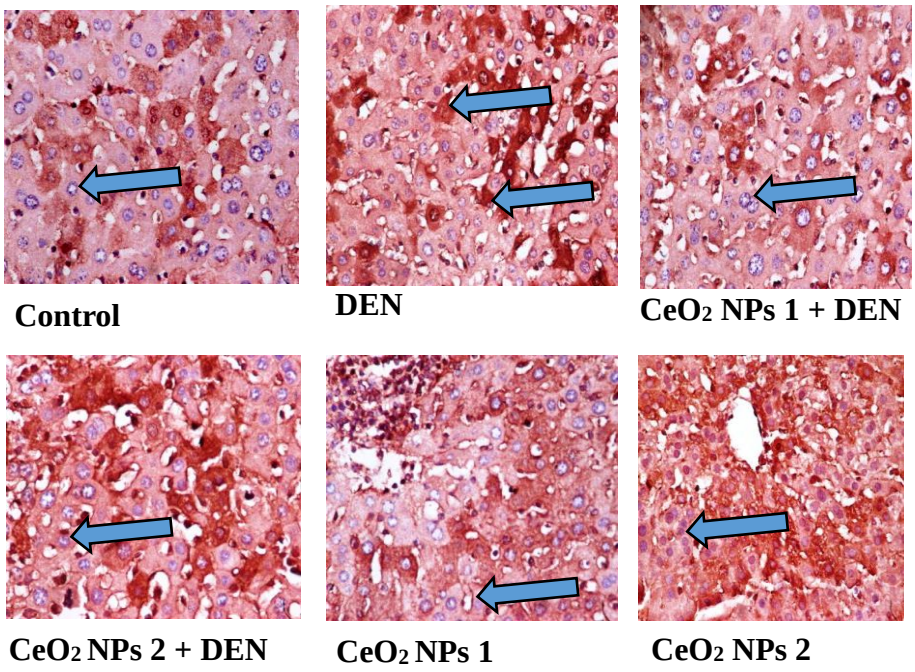

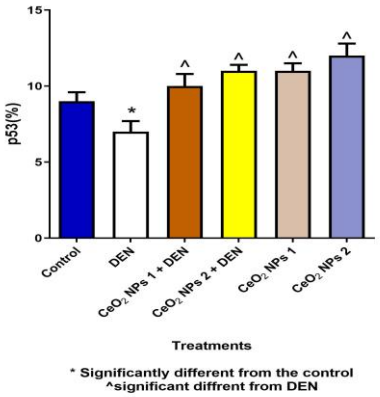

Plate 4.8: p53 level by immunohistochemical staining of the liver of adult mouse following pre-treatment with cerium oxide nanoparticles and exposed to diethylnitrosamine.

Values are means ± STDEV of 5 replicates. Control=mice that received normal saline, CeO_2 NPs 1, 2 and 3 = Cerium oxide nanoparticles at 100µg/k, 200µg/kg and 300µg/kg. DEN= Diethylnitrosamine *P and **P values<5% was adjudged significant upon comparison to control and DEN.

4.4 Ameliorative potential of cerium oxide nanoparticles following induction of mammary toxicity in female via injection of Benz[a]pyrene and N-Nitroso-N-methylurea to adult female rats.

Results

Weight and Serum indices

Result of this experiment revealed that exposure of female rats to NMU + BaP caused loss in the weight of the animals by 12% while organosomatic weight, mammary tissue weight, increased by 84%, 36% relative to the control group (table 4.6). However, administration of cerium oxide nanoparticles significantly restored organosomatic weight, mammary tissue weight by 67%, 54% and animal weight 47% relative to animals treated with NMU + BaP alone. Also, NMU and BaP administration produced decreased ALT activity (figure 4.45) relative to control. On the other hand, nanoceria ameliorated it to control level. In addition, exposure of NMU + BaP to animals significantly increased the MPO (figure 4.48) and NO level (figure 4.47) in mammary tissue by 20% and 25% respectively. Administration of nanoceria however decreased MPO and NO level significantly with 38% and 24% correspondingly relative to animals exposed to NMU + BaP alone.

Table 4.5: Weight indices of animals exposed to Benz[a]pyrene and N-Nitroso-N-methylurea and thereafter treated with nanoceria

Grouping	Initial (g)	Final (g)	Diff. (g)	Mammary Wt. (g)	Organo-somatic
Control.	60.3±4.92	149±5.2	89.8±5.7	0.36±0.07	0.24±0.05
NMU + BaP	85.7±2.23	159±6.8	73.35±3.1	1.46±0.40*	0.92±0.04*
NMU +BaP+CeO_2NPs	74.5±2.53	174±8.7	99.50±6.8	1.00±0.21	0.55±0.07**
NMU + BaP + Vin	56.4±6.28	179±1.5	122.60±3.4	1.22±0.37	0.68±0.03**

Values shown here were displayed by way of mean ± STDEV of 5 mouse per grouping. Control=mice that received normal saline, BaP = Benz[a]pyrene, NMU= N-Nitroso-N-methylurea, CeO_2 NPs=Cerium oxide nanoparticles. Vin=Vincristine. *P and **P values<5% was adjudged significant upon comparison to control and NMU + BaP.

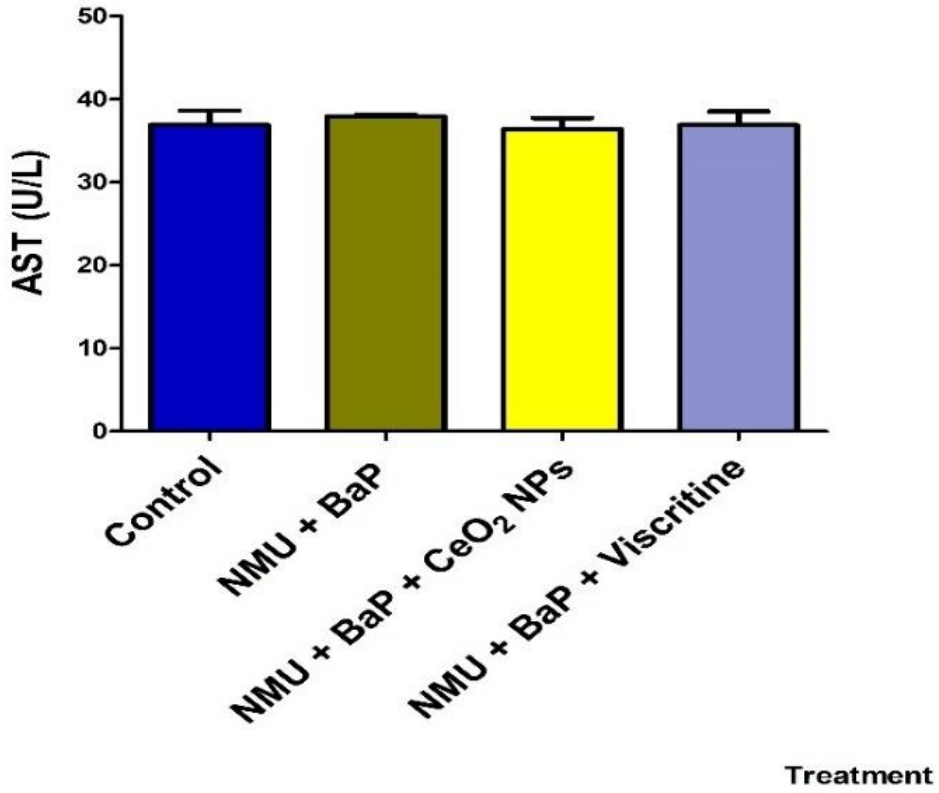

Figure 4.44: Effect of nanoceria on serum aspartate aminotransferase (AST) activities in adult rats exposed to NMU and BaP an

Values shown here were displayed by way of mean ± STDEV of 5 mouse per grouping. Control=mice that received normal saline, BaP = Benz[a]pyrene, NMU=N - N-Nitroso-N-methylurea, CeO_2 NPs=Cerium oxide nanoparticles. Vin=Vincristine. *P and **P values<5% was adjudged significant upon comparison to control and NMU + BaP.

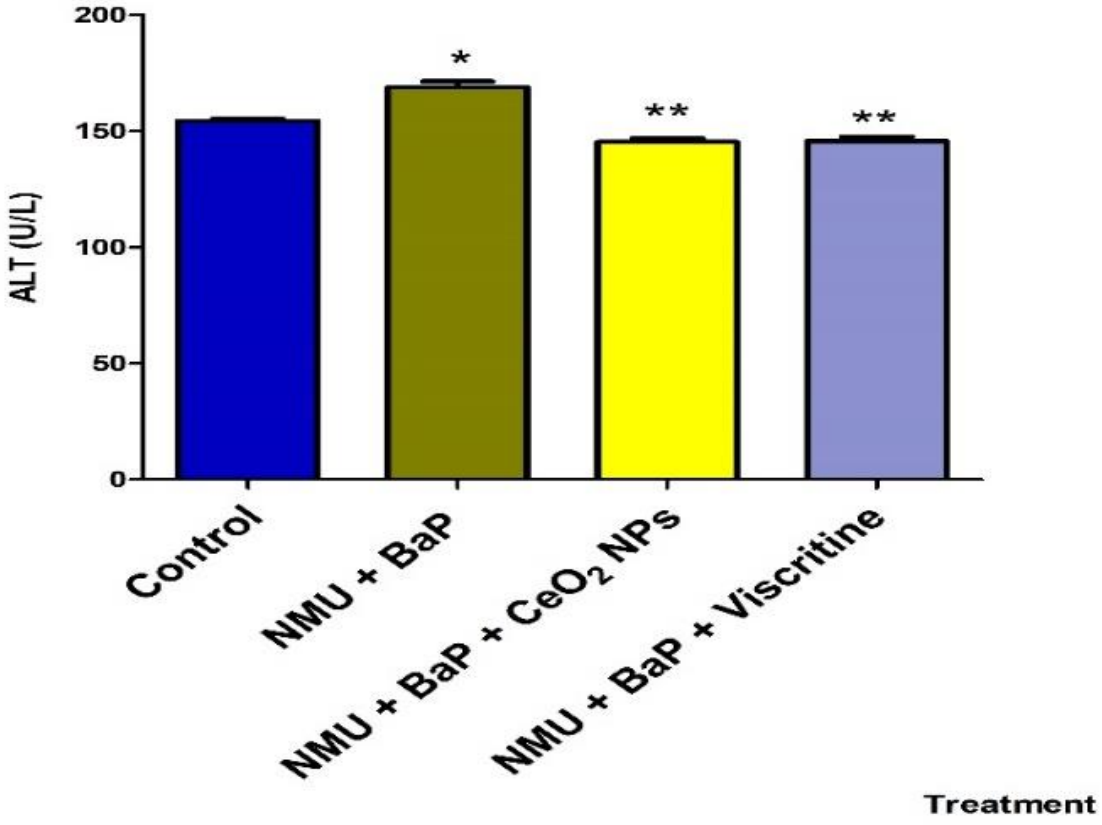

Figure 4.45: Effect of nanoceria on serum alanine aminotransferase (ALT) activities in adult rats exposed to NMU and BaP

Values shown here were displayed by way of mean ± STDEV of 5 mouse per grouping. Control=mice that received normal saline, BaP = Benz[a]pyrene, NMU= N-Nitroso-N-methylurea, CeO_2 NPs=Cerium oxide nanoparticles. Vin=Vincristine. *P and **P values<5% was adjudged significant upon comparison to control and NMU + BaP.

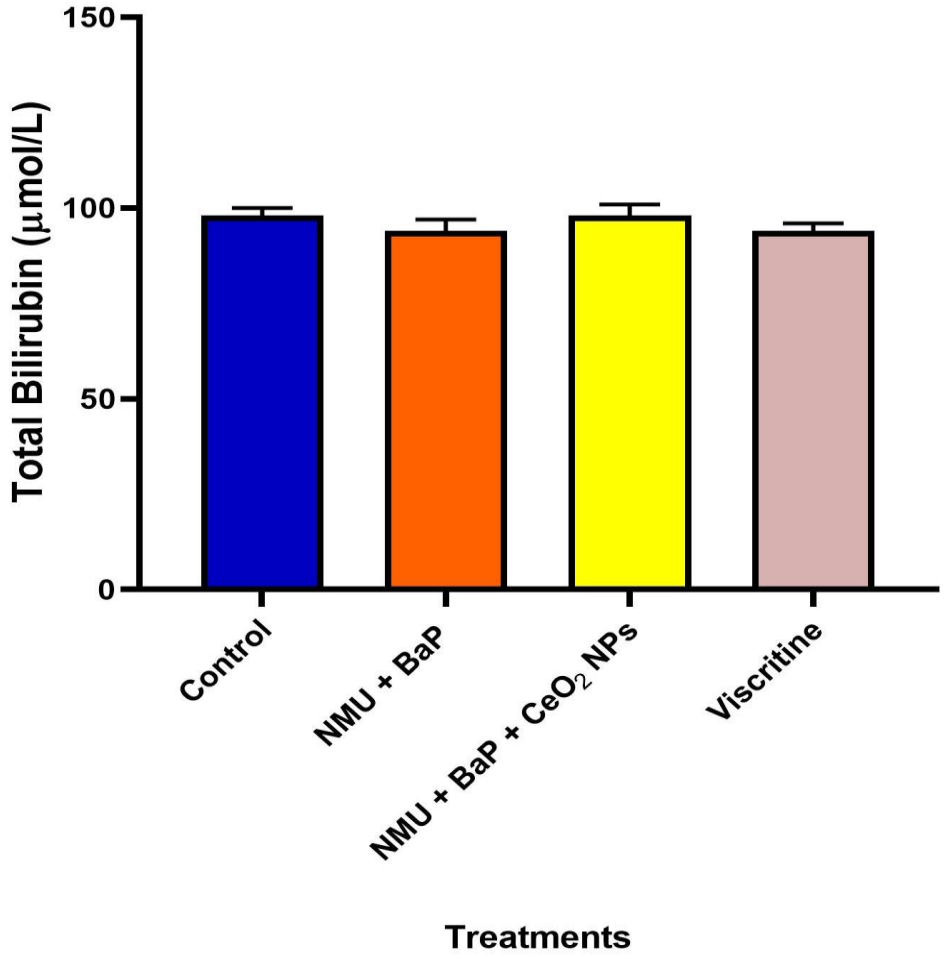

Figure 4.46: Effect of nanoceria on serum total bilirubin levels in adult rats exposed to NMU and BaP

Values shown here were displayed by way of mean ± STDEV of 5 mouse per grouping. Control=mice that received normal saline, BaP = Benzo[a]pyrene, NMU= N-Nitroso-N-methylurea, CeO_2 NPs=Cerium oxide nanoparticles. Vin=Vincristine. *P and **P values<5% was adjudged significant upon comparison to control and NMU + BaP.

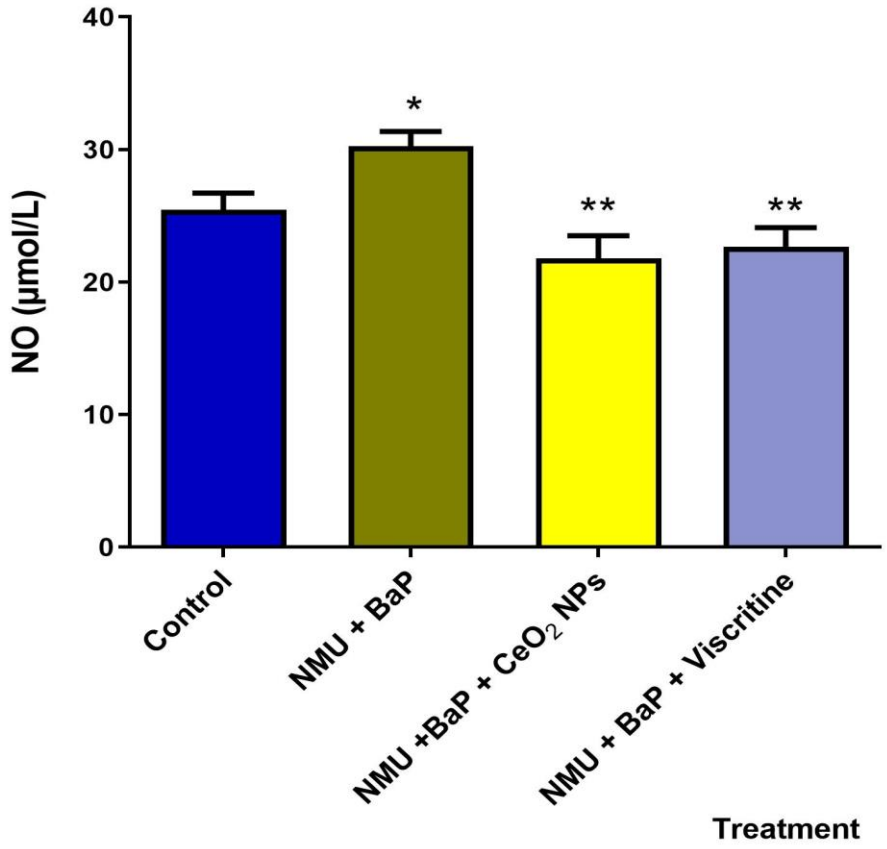

Figure 4.47: Effect of nanoceria on serum nitric oxide (NO) levels in mammary tissue of adult rats exposed to NMU and BaP

Values shown here were displayed by way of mean ± STDEV of 5 mouse per grouping. Control=mice that received normal saline, BaP = Benz[a]pyrene, NMU= N-Nitroso-N-methylurea, CeO_2 NPs=Cerium oxide nanoparticles. Vin=Vincristine. *P and **P values<5% was adjudged significant upon comparison to control and NMU + BaP.

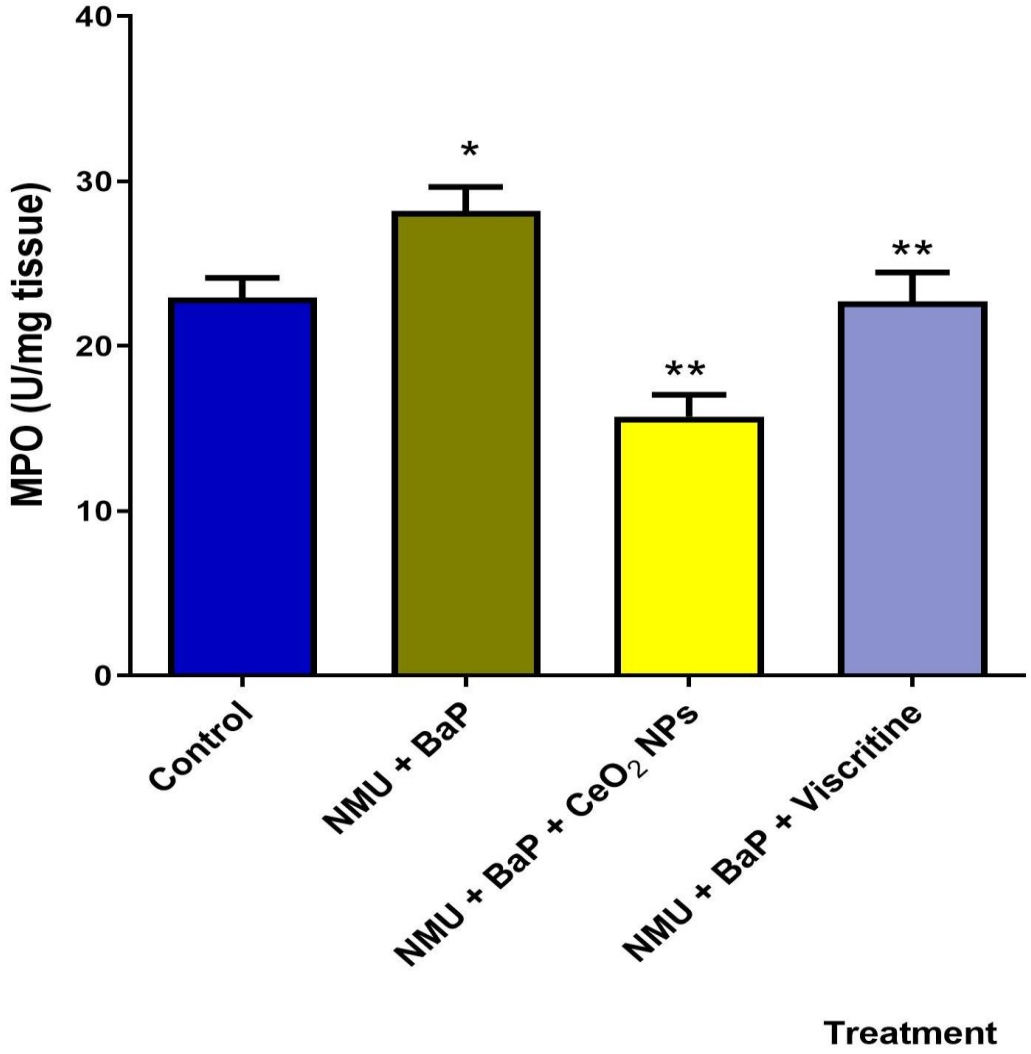

Figure 4.48: Effect of nanoceria on serum myeloperoxidase (MPO) activities in mammary tissues of adult rats exposed to NMU and BaP

Values shown here were displayed by way of mean ± STDEV of 5 mouse per grouping. Control=mice that received normal saline, BaP = Benz[a]pyrene, NMU= N-Nitroso-N-methylurea CeO_2 NPs=Cerium oxide nanoparticles. Vin=Vincristine. *P and **P values<5% was adjudged significant upon comparison to control and NMU + BaP.

Oxidative stress and Antioxidant enzymes

Biochemical analysis of mammary tissue showed the presence of oxidative stress, evidenced by the increased malondialdehyde (figure 4.49) level in animals exposed to NMU + BaP. MDA increased by 23% with respect to the control. Also, NMU + BaP decreased mammary SOD (figure 4.50) and CAT (figure 4.51) by 166% and 139% respectively relative to control. In addition, the mammary total thiol (figure 4.54) and reduced glutathione levels (figure 4.55) as well as GST activity (figure 4.52) were decreased significantly($p<0.05$) by 37% and 36% respectively in animals treated with NMU + BaP. However, upon treatment with nanoceria, the level of MDA decreased, with resultant increase in SOD activities and CAT enzymes. Both enzymes increased by 169% and 115% relative to animals exposed to NMU + BaP alone. In addition, TSH and GST significantly ($p<0.05$) by 30% and 37%.

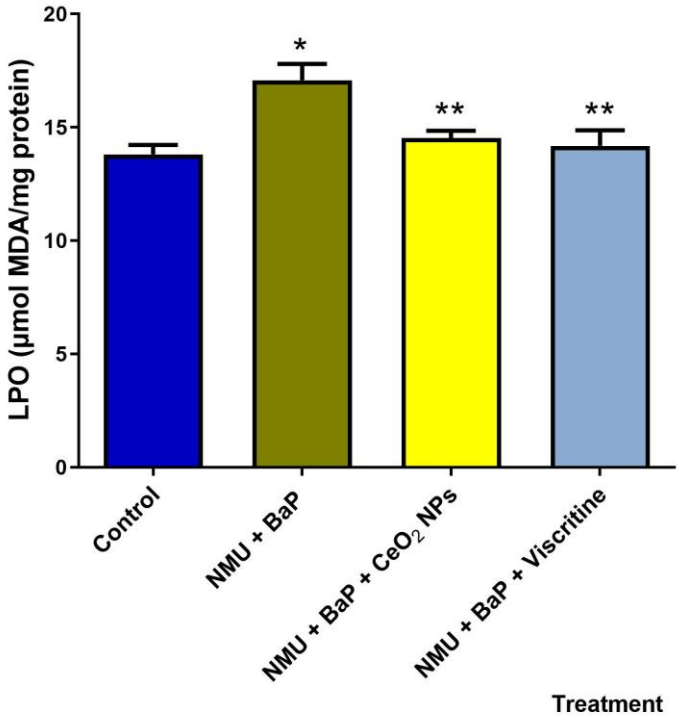

Figure 4.49: Effect of nanoceria on mammary Malondialdehyde (MDA) levels in adult rats exposed to NMU and BaP

Values shown here were displayed by way of mean ± STDEV of 5 mouse per grouping. Control=mice that received normal saline, BaP = Benz[a]pyrene, NMU= N-Nitroso-N-methylurea, CeO_2 NPs=Cerium oxide nanoparticles. Vin=Vincristine. *P and **P values<5% was adjudged significant upon comparison to control and NMU + BaP.

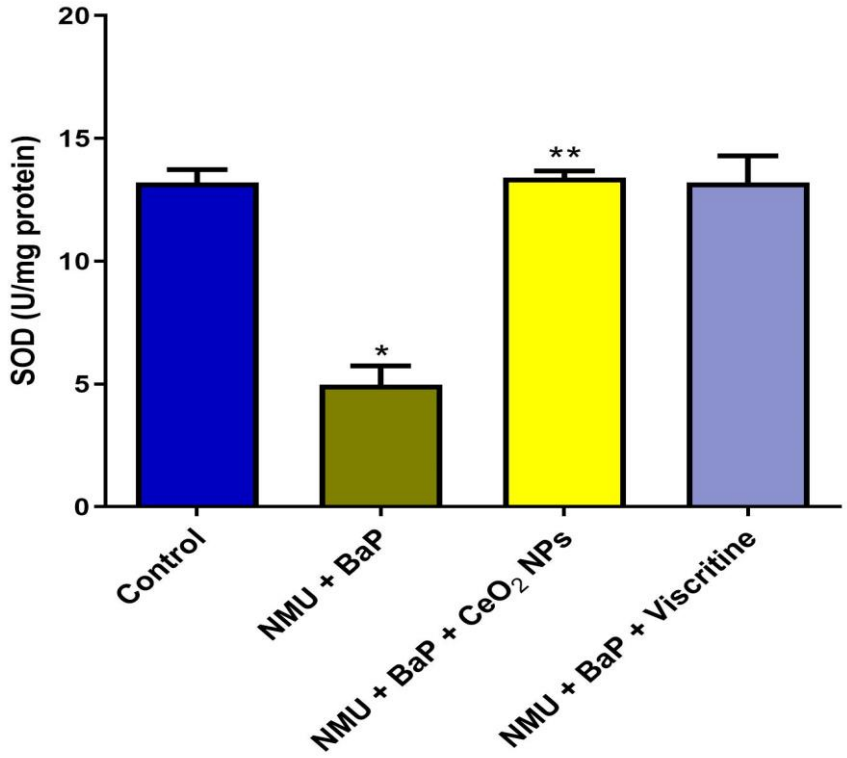

Figure 4.50: Effect of nanoceria on mammary superoxide dismutase (SOD) activities in adult rats exposed to NMU and BaP

Values shown here were displayed by way of mean ± STDEV of 5 mouse per grouping. Control=mice that received normal saline, BaP = Benz[a]pyrene, NMU= N-Nitroso-N-methylurea, CeO_2 NPs=Cerium oxide nanoparticles. Vin=Vincristine. *P and **P values<5% was adjudged significant upon comparison to control and NMU + BaP.

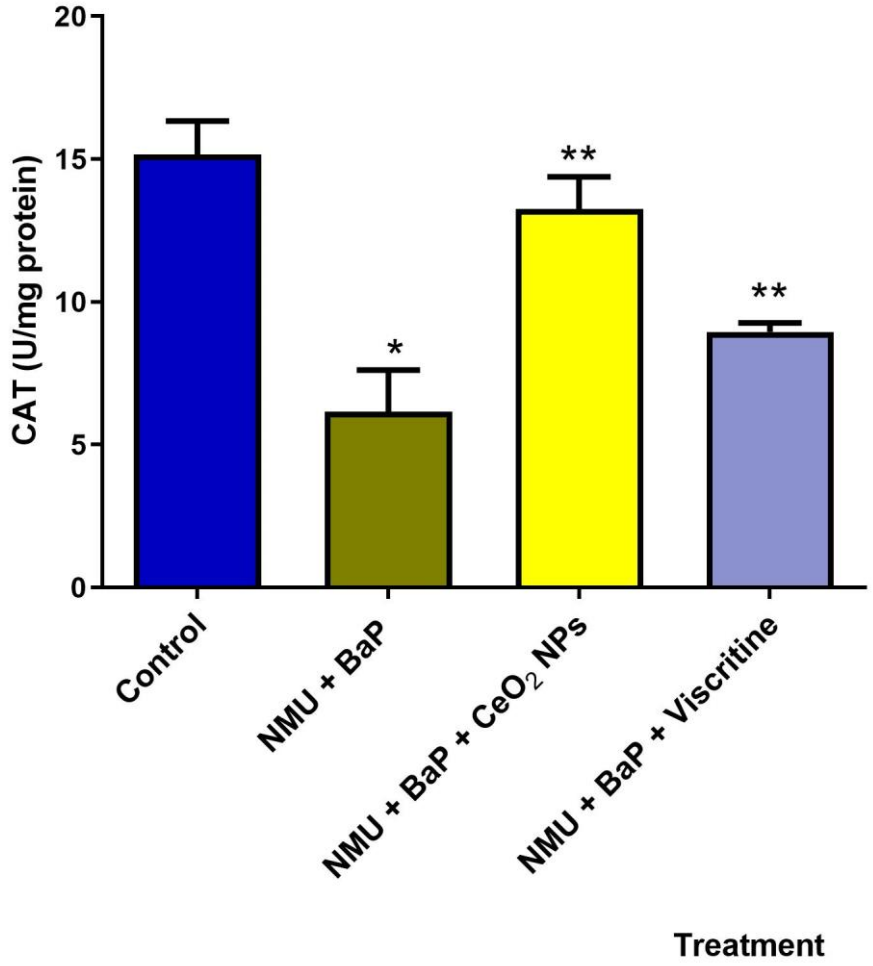

Figure 4.51: Effect of nanoceria on mammary catalase (CAT) activities in adult rats exposed to NMU and BaP

Values shown here were displayed by way of mean ± STDEV of 5 mouse per grouping. Control=mice that received normal saline, BaP = Benz[a]pyrene, NMU= N-Nitroso-N-methylurea, CeO_2 NPs=Cerium oxide nanoparticles. Vin=Vincristine. *P and **P values<5% was adjudged significant upon comparison to control and NMU + BaP.

.

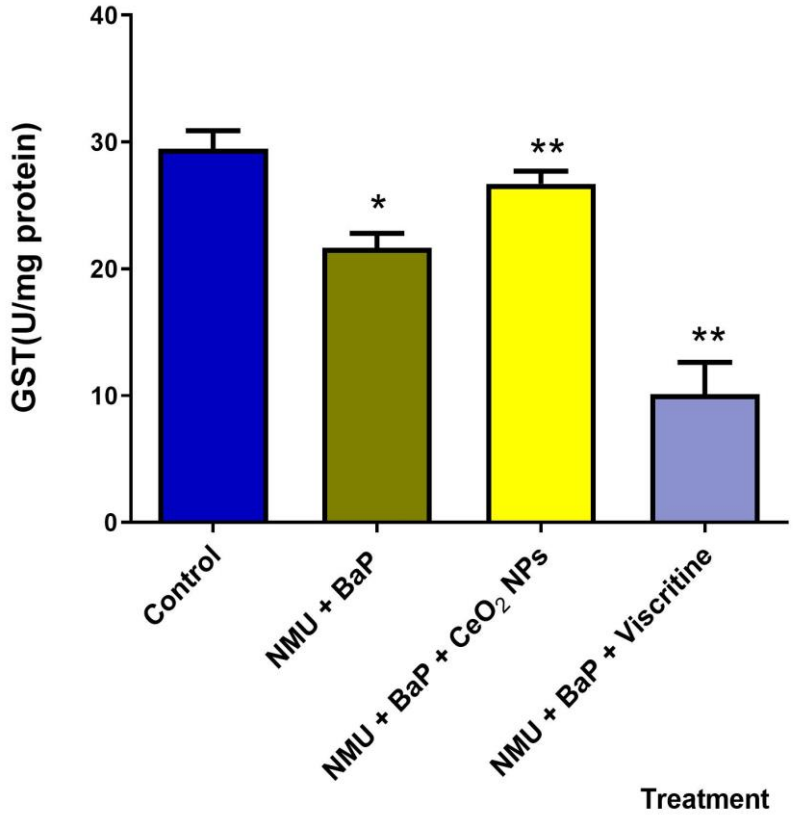

Figure 4.52: Effect of nanoceria on mammary glutathione-s-transferase (GST) activities in adult rats exposed to NMU and BaP

Values shown here were displayed by way of mean ± STDEV of 5 mouse per grouping. Control=mice that received normal saline, BaP = Benz[a]pyrene, NMU= N-Nitroso-N-methylurea, CeO_2 NPs=Cerium oxide nanoparticles. Vin=Vincristine. *P and **P values<5% was adjudged significant upon comparison to control and NMU + BaP.

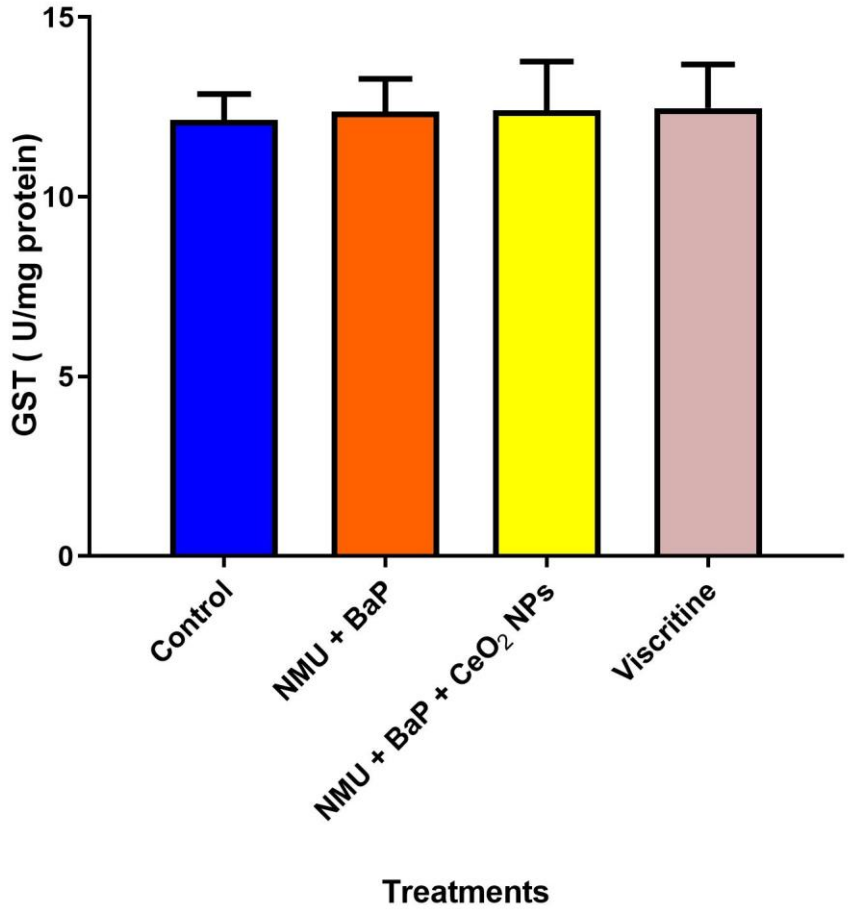

Figure 4.53: Effect of nanoceria on mammary glutathione peroxidase (GPx) activities in adult rats exposed to NMU and BaP.

Values shown here were displayed by way of mean ± STDEV of 5 mouse per grouping. Control=mice that received normal saline, BaP = Benz[a]pyrene, NMU= N-Nitroso-N-methylurea, CeO_2 NPs=Cerium oxide nanoparticles. Vin=Vincristine. *P and **P values<5% was adjudged significant upon comparison to control and NMU + BaP.

.

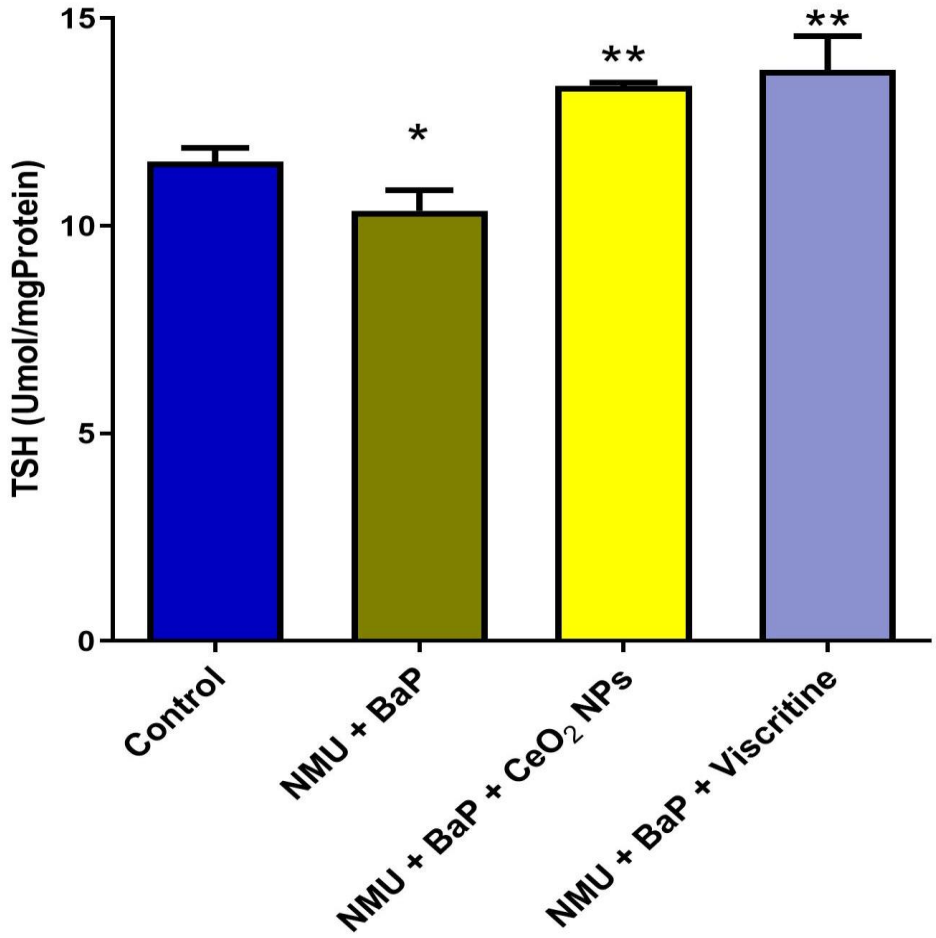

Figure 4.54: Effect of nanoceria on mammary total thiol (TSH) levels in adult rats exposed to NMU and BaP.

Values shown here were presented as mean ± STDEV of five mice in each group. Control=mice administered normal saline, NMU= N-Nitroso-N-methylurea, BaP= Benz(a)pyrene, CeO_2 NPs=Cerium oxide nanoparticles. Vin=Vincristine. *P and **P values<5% was adjudged significant upon comparison to control and NMU + BaP.

Antioxidant continuation

In figure 4.55, NMU and BaP significantly reduced GSH levels by 25% relative to the control. Also, mammary NO (figure 4.56) and MPO (Figure 4.57) increased by 25% and 75% respectively upon administration of NMU + BaP to animals. Treatment with nanoceria caused NO and MPO to decrease by 50% and 35% respectively, while GSH increased significantly by 48% relative to the test group.

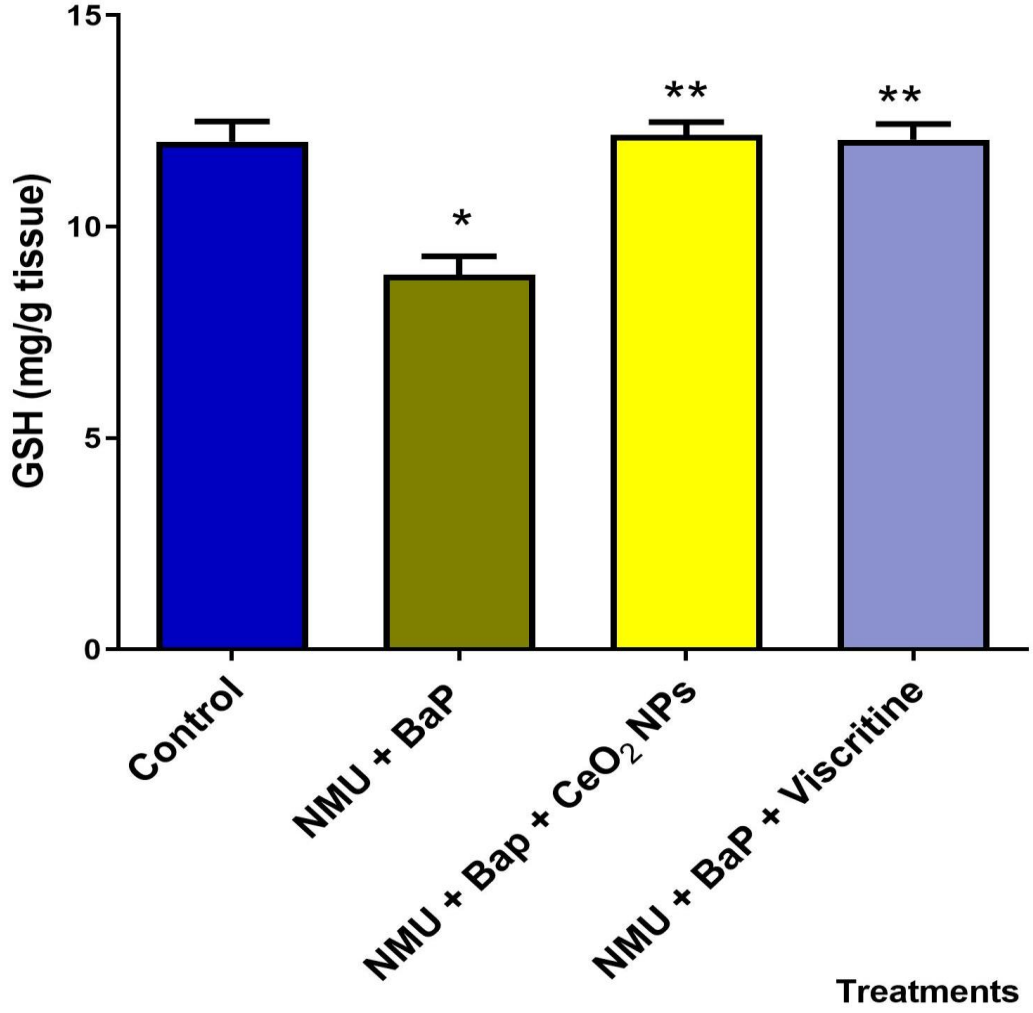

Figure 4.55: Effect of nanoceria on mammary reduced glutathione (GSH) levels in adult rats exposed to NMU and BaP

Values shown here were displayed by way of mean ± STDEV of 5 mouse per grouping. Control=mice that received normal saline, BaP = Benz[a]pyrene, NMU= N-Nitroso-N-methylurea, CeO_2 NPs=Cerium oxide nanoparticles. Vin=Vincristine. In comparison to control and NMU+BaP groups,*P and **P values<5% is adjudged significant.

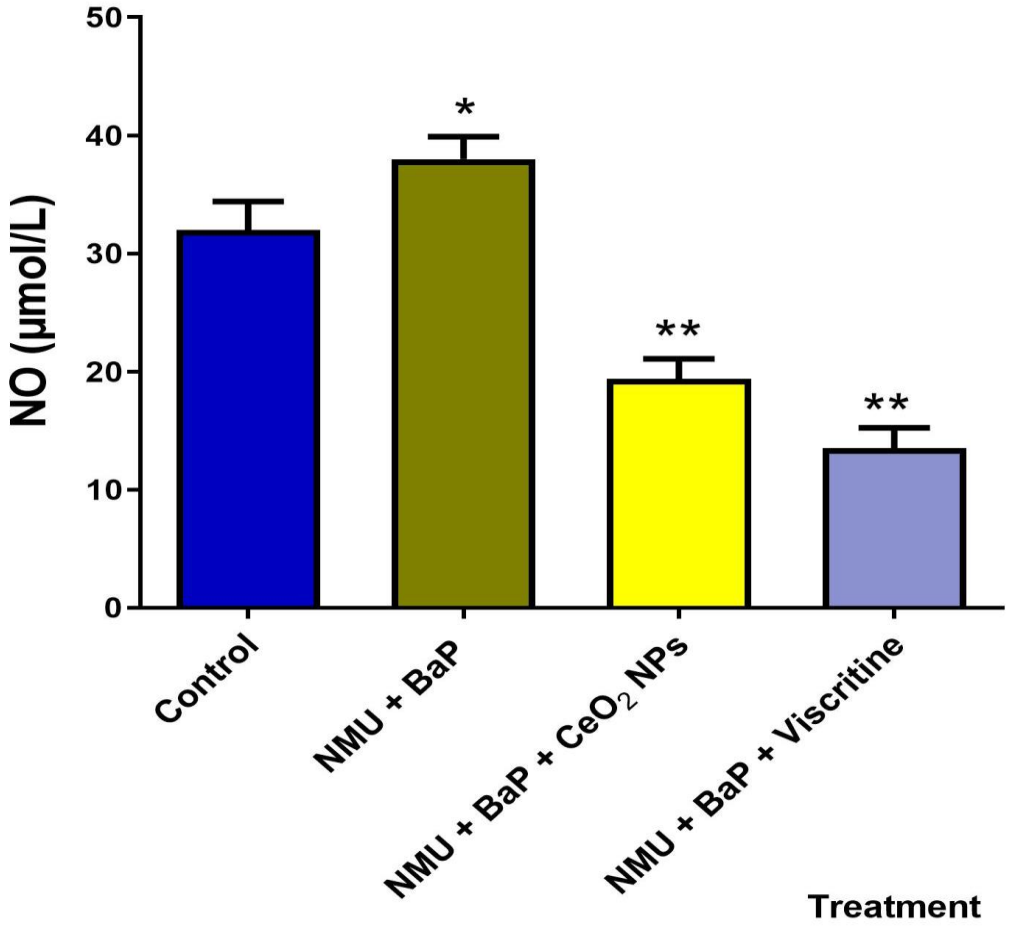

Figure 4.56: Effect of nanoceria on mammary nitric oxide (NO) levels in adult rats exposed to NMU and BaP

Values shown here were displayed by way of mean ± STDEV of 5 mouse per grouping. Control=mice that received normal saline, BaP = Benz[a]pyrene, NMU= N-Nitroso-N-methylurea, CeO_2 NPs=Cerium oxide nanoparticles. Vin=Vincristine. *P and **P values<5% was adjudged significant upon comparison to control and NMU + BaP.

.

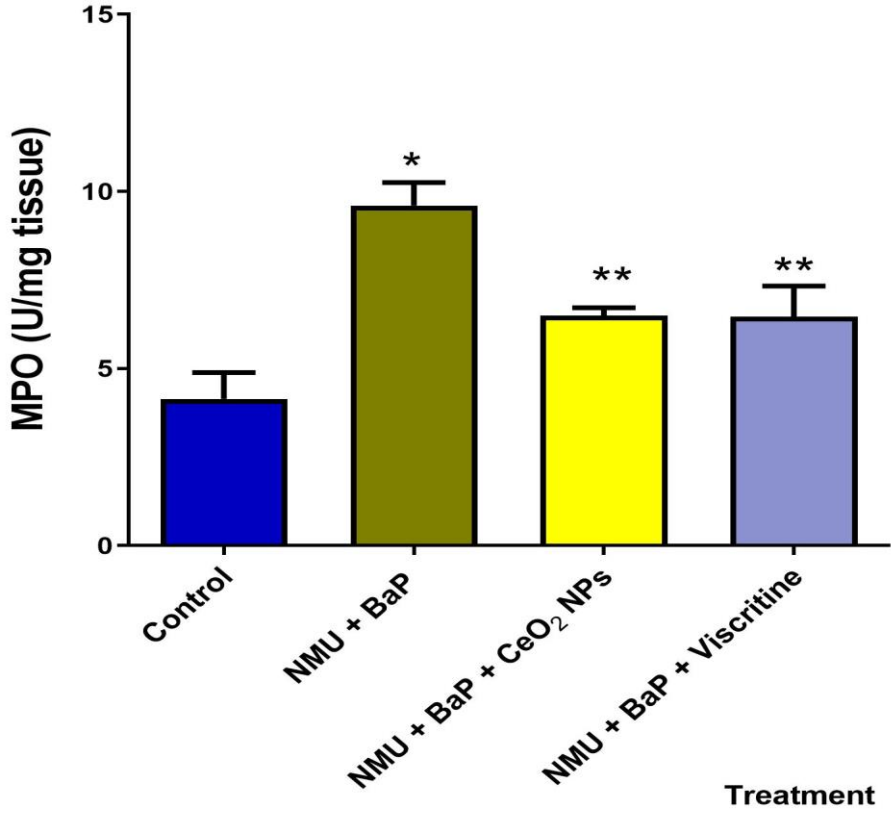

Figure 4.57: Effect of nanoceria on mammary myeloperoxidase activity in adult rats exposed to NMU and BaP

Values shown here were displayed by way of mean ± STDEV of 5 mouse per grouping. Control=mice that received normal saline, BaP = Benz[a]pyrene, NMU= N-Nitroso-N-methylurea, CeO_2 NPs=Cerium oxide nanoparticles. Vin=Vincristine. *P and **P values<5% was adjudged significant upon comparison to control and NMU + BaP.

Histology and immunohistochemistry

Histological examination (plate 4.9) revealed moderate hyperplasia of the epithelia cells covering the mammary tissue and mild haemorrhage in NMU + BaP exposed animals, relative to control which revealed normal connective tissues of the mammary gland tissue. Also, further immunohistochemical examination revealed Bax (plate 4.10), p53 (plate 4.11) and Caspase 3 (plate 4.12) activity in tissue samples of animals exposed to NMU + BaP in contrast to control which revealed severe expression of BAX. Conversely, administration of cerium oxide nanoparticles revealed severe BAX, p53 and caspase 3 expression relative to animals exposed to NMU + BaP animals.

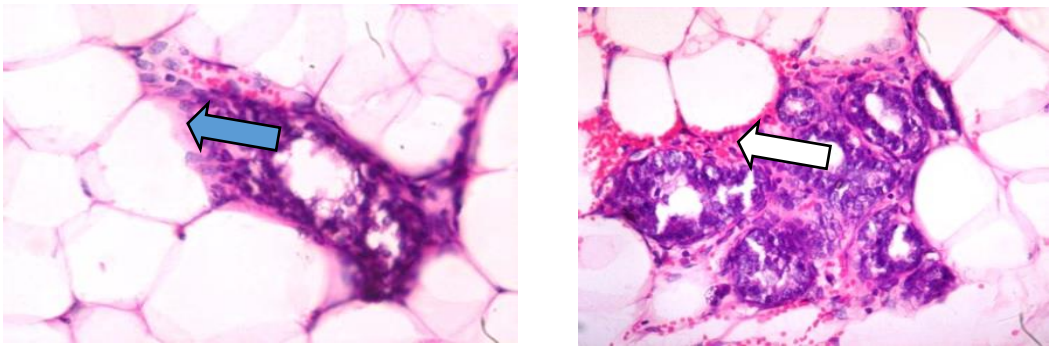

Control **NMU + BaP**

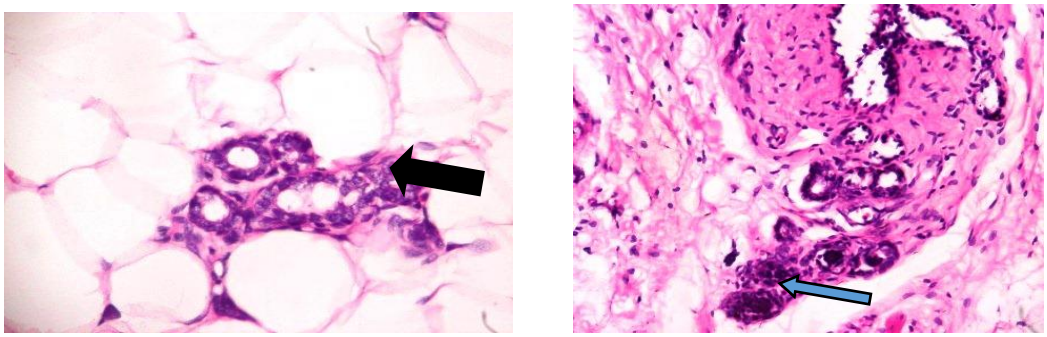

NMU + BaP + CeO_2 NPs **NMU + BaP + Vincristine**

Plate 4.9: Representative photomicrographs showing mammary tissue in adult rats exposed to N-Nitroso-N-methylurea (NMU) and Benz[a]pyrene (BaP) and treated with cerium oxide nanoparticle. Control revealed normal architecture. In NMU + BaP there was severe hyperplasia of the membrane lining the mammary tissues. The NMU + BaP + CeO_2 NPs group revealed mild hyperplasia lining the tissue while the NMU + BaP + Vincristine group revealed moderate haemorrhage

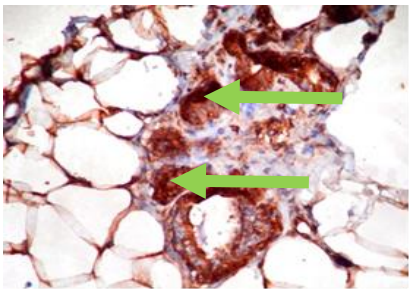

Control

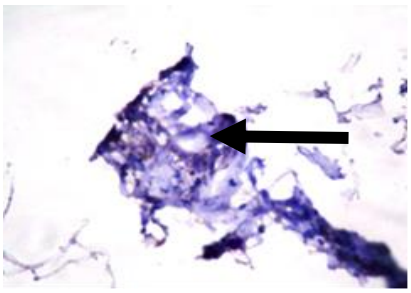

NMU + BaP

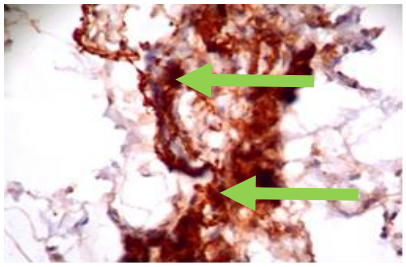

NMU + BaP + CeO_2 NPs

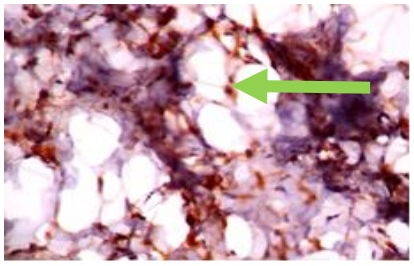

NMU + BaP + Vincristine

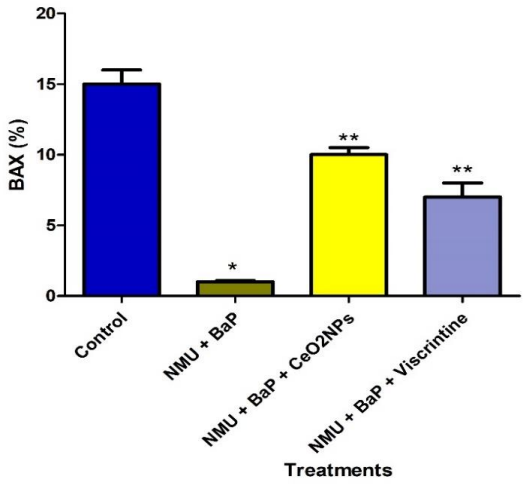

*** Significantly different from control**
****Significantly different from NMU + BaP**

Plate 4.10: BAX expression of the mammary tissue in adult rats exposed to Benz[a]pyrene and N-Nitroso-N-methylurea and treated with cerium oxide nanoparticle. Control group revealed increase BAX activity while NMU + BaP group showed absence of BAX activity. NMU + BaP + CeO_2 NPs revealed increased activity of BAX while NMU + BaP + CeO_2 NPs and NMU + BaP + Vincristine revealed moderate BAX activity.

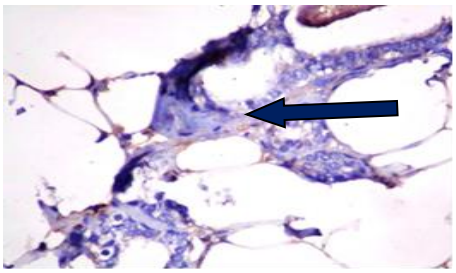

Control

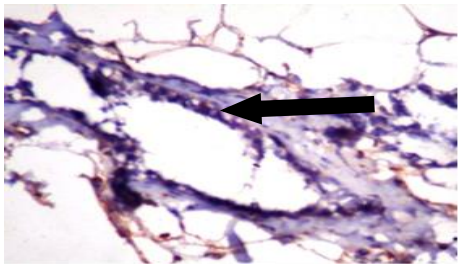

NMU + BaP

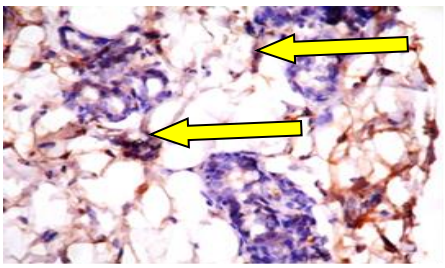

NMU + BaP + CeO_2 NPs

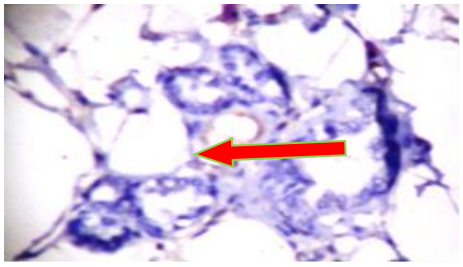

NMU + BaP + Vincristine

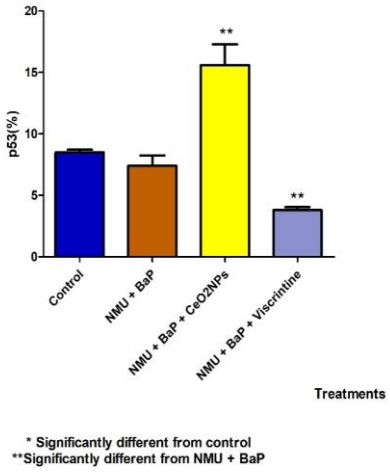

Plate 4.11: p53 expression of the mammary tissue in adult rats exposed to Benz[a]pyrene and N-Nitroso-N-methylurea and treated with cerium oxide nanoparticle. The control shows decreased activity of p53 while moderate activity of p53 was observed in NMU + BaP group. In NMU + BaP + CeO_2 NPs group, increased activity of p53 was observed while decreased p53 activity was observed in NMU + BaP + Vincristine

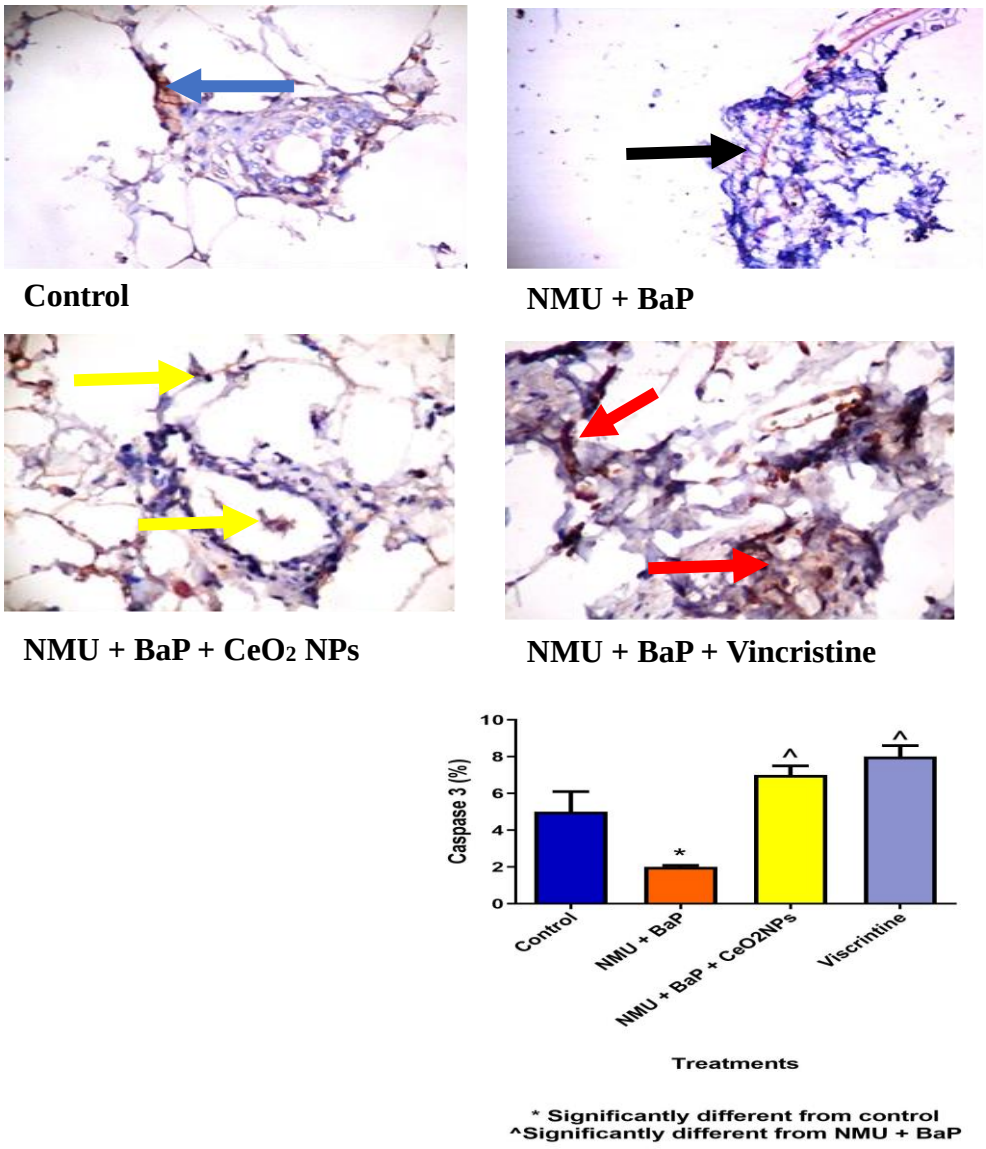

Plate 4.12: Caspase 3 expression of the mammary tissue in adult rats exposed Benz[a]pyrene and N-Nitroso-N-methylurea and treated with cerium oxide nanoparticles. The control group shows mild activity of caspase 3 while caspases 3 was absent in NMU + BaP group. In the NMU + BaP + CeO_2 NPs and NMU + BaP + Vincristine groups, there was mild activity of caspases 3

Control.

NMU + BaP

NMU + BaP + CeO_2 NPs

NMU + BaP + Vincristine

Plate 4.13: Pictorial representative of neck tumor in adult rats exposed to Benz[a]pyrene and N-Nitroso-N-methylurea and treated with cerium oxide nanoparticle.

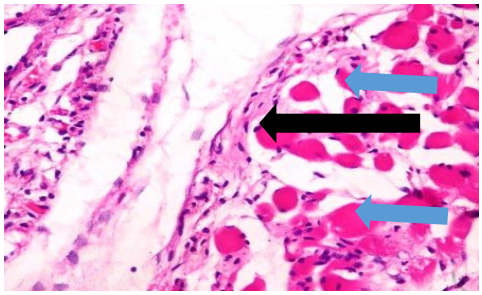

Control

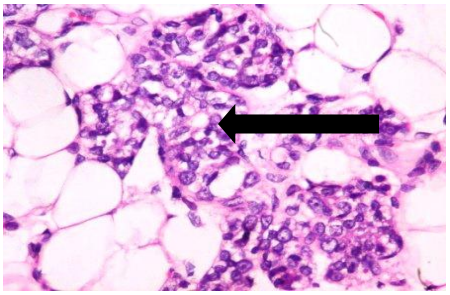

NMU + BaP

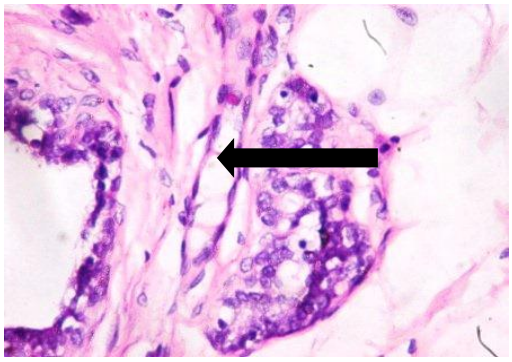

NMU + BaP + CeO_2 NPs

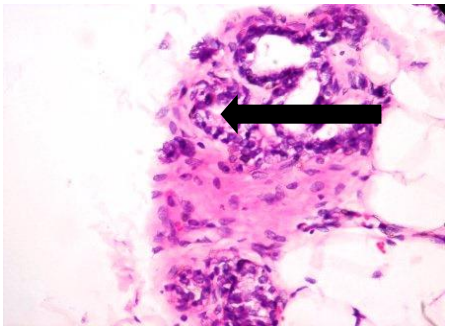

NMU + BaP + Vincristine

Plate 4.14: Representative photomicrographs of neck tumor in adult rats exposed to Benz[a]pyrene and N-Nitroso-N-methylurea and treated with cerium oxide nanoparticle. M= X400. Shows normal architecture of the mammary tissue in the control group while in NMU + BaP group showed sever presence of malignant breast tissue. Treatment with nanoceria and Vincristine showed moderate presence of malignant mammary tissue.

CHAPTER FIVE

DISCUSSION

Acute exposure to diesel exhaust particles (DEP) has remained a potent inducer of tumour development *in vivo* (Kim *et al.,* 2022). Such introduction also causes the induction of inflammatory responses in the lung, activating the macrophages as well as immune response modification of the lungs to environmental toxicants and infections; (Moldoveanu *et al*., 2009; Chaplain, 2010; Hiraiwa *et al.,* 2013). The potential health implications arising from the exposure to cerium oxide nanoparticles from diesel engines has not been fully elucidated, a phenomenon which is consistent with other studies, casting doubts on effects of artificial biomaterials on the environment and general health (Casee *et al,* 2011). Cerium is reported to promote the induction of pneumoconiosis, caused by ingestion and subsequent build-up of nanoceria in epithelial cells of the lungs following prolonged workplace exposure to nanoceria and additional forms of earth-based metals (Guo *et al.,* 2019).

Effect of nanoceria on male reproductive and hepatic function in adult mice

Administration of nanoceria experimental animals at 200 µg/kg and 300 µg/kg slightly decreased the weight of animals. This can be due to the reduction in appetite or digestive disorders and malabsorption; it however cannot be used as justification for the toxic effect of this particle since the body weight is also dependent on the organ weight (Camilleri *et al.,* 2017). Nanoceria's effect was not manifested in the weight of the testis and testicular organo-somatic weight as there was no difference in weights. Exposure of mice to 200µg/kg and 300µg/kg body weight nanoceria caused insignificant ($p>0.05$) increase in both organo-somatic weight and weight of the liver. The liver, being the main organ for drug biotransformation and xenobiotic detoxification can be a major target for chemicals and drugs. This observation suggests that cerium oxide nanoparticles at graded doses could cause hypertrophy (increase in size) of the liver.

In other to determine the effect of cerium oxide nanoparticles on the blood, some haematological indices were assessed and results showed that nanoceria significantly reduced PCV, HB, RBC levels across the treatment groups. Increased PCV is an indication of increased number of red blood cells, a condition which may arise due to physiological response to external stimuli (Premont et al, 2021). However, low PCV levels are normally associated with chronic anaemia, which result to abnormal synthesis of haemoglobin during erythropoiesis (Premont et al, 2021). Cerium oxide nanoparticle can therefore be suggested to cause anaemia due to low PCV and RBC levels. Decreased haematocrit levels could indicate life-threatening diseases such as leukaemia (Zubieta-Calleja *et al.*, 2007). The red blood cells transport oxygenated blood, which are attached to the haemoglobin, and therefore, a reduced levels of haemoglobin in the red cells relates to decrease in oxygen transport by blood.

In the course of this study, there was no loss of any of the animals exposed to cerium oxide nanoparticles during this research. In the liver, the animals were treated with graded doses of nanoceria and results showed that nanoceria did not alter serum ALT and AST activities across exposed animals, excluding 300 µg/kg group in which substantial elevation in activities of these two kidney enzymes were observed. Similarly, serum urea levels and creatinine levels was not affected by cerium oxide nanoparticle in test animals, suggesting that at a higher concentration, the nanoparticle can be detrimental to hepatic function. To evaluate nanoceria's effect on male reproductive system, sperm qualities such as motility and count, sperm abnormalities, sperm volume and live:dead ratio were estimated, and a decline in sperm count and motility was observed across groups. This was verified following elevation in total sperm abnormality in exposed animals. This study correlates with Tokeda 2009 who reported that introduction of experimental pregnant rats to titanium dioxide resulted in conformational changes at the seminiferous tubules, resulting tin reduction in daily sperm production and epidermal sperm count (Tokeda *et al.*, 2009). In this study, cerium oxide nanoparticles resulted in decline in luteinizing hormone, prolactin (only in 300 µg/kg) and follicle stimulating hormone levels in 200 µg/kg and 300 µg/kg cerium oxide nanoparticles exposed animals. LH and FSH are referred to as gonadotropins because of their stimulating activity in the testis and ovary of males and females respectively. (Ramaswamy and Weinbauer, 2015). LH promotes the secretion of sex steroids from the gonads. In the testis, it stimulates the production of

testosterone where it binds to specific receptor on Leydig cells. The significant decrease in LH levels also lead to declined levels of the hormone, testosterone in 100 µg/kg and 200 µg/kg nanoceria exposed mice. Prolactin is a polypeptide molecule synthesized via lactotrophic cells of the frontal pituitary secretor. (Majumdar and Mangal, 2013). Result obtained from this study therefore justifies the earlier report of this particle causing disruption of the male reproductive function.

Lipid Peroxidation involves a chain of events whereby oxidants such as ROS attacks lipid containing double bonds in their carbon, which are mainly polyunsaturated fatty acids (Anthonio *et al*., 2014). This study monitored MDA generation, a key product of lipid peroxidation, testicular and hepatic antioxidative enzymes. As shown in results, cerium oxide nanoparticles potentiated a decreasing effect on hepatic MDA level in exposed animals, whereas there was marked elevated MDA in the testis of all the treated animals, an indication of the peroxidation of testicular membrane lipids by cerium oxide nanoparticle. This increase in lipid peroxidation suggests the capability of nanoceria to cause perturbation of the membrane and leaching of the cellular components and a resultant loss of membrane function.

The opioid-rich nature of some cellular membranes makes them highly susceptible to peroxidation which ultimately alters the structure and functions while activating varying forms of cell death. In addition, studies have shown that MDA is a potent mutagen and a carcinogen which can interact with DNA molecule, forming adducts, which finally results into DNA impairment (Bartsch and Nair, 2006), signifying the ability of cerium oxide nanoparticles to trigger cell death. A decrease in liver and testis GSH levels of animals exposed to nanoceria was observed. The reduced glutathione (GSH) plays substantial function in eliminating ROS generated within tissues of the body (Kennedy *et al.,* 2020). Also, there are abundant amount of testicular GSH in mammals (Calvin and Turner, 1982), playing a significant function during spermatogenesis (Knapen *et al.,* 1999). The decreased GSH level and attendant increase in the amount of testicular MDA mirrors the extent of oxidative damage to the testis.

The exact mechanism of oxidative attack of cerium oxide nanoparticles in biological systems has not been fully explained in recent studies. It can however be associated

with the characteristic two oxidation states (Ce^{3+} or Ce^{4+}) of the element, as outlined by Lin *et al.*, (2006) and Szymansk *et al.*, (2015). Catalase as well as superoxide dismutase are two endogenous first line antioxidant enzymes. While catalase mop up reactive oxygen species by converting it to H_20_2 to H_20 and 0_2 (Ransy *et al.*, 2020), SOD dismutase superoxide radical into less toxic compounds (Younus, 2018). In this study, there was remarkable decrease in both hepatic and testicular CAT and SOD in all animals exposed to cerium oxide nanoparticles. However, MDA was not increased in the liver. The observed decrease may be explained as the ability the nanoparticles to induce the generation of free radicals which consumes antioxidant enzymes. This study also investigated the effect cerium oxide nanoparticles on glutathione-s-transferase (GST), an enzyme that catalyses the reaction of several obnoxious chemicals with reduced glutathione (Amin *et al.*, 2011) and it was observed that GST activities was decreased in the testis and liver of animals exposed to nanoceria.

One of the suggested mechanisms of GST to reduce the toxicity of carcinogens is via inhibiting the activity of ASK1, leading to an increase in communications between cellular DNA and ultimate carcinogenic metabolic products (McIlwain *et al.*, 2006). To assess the influence of inflammation upon cerium oxide nanoparticles exposure, we investigated nitric oxide generation and myeloperoxidase activity and results showed increased nitric oxide in the liver at 100µg/kg and 200µg/kg exposed animals. Likewise, myeloperoxidase activity was significantly increased in the testis of 100µg/kg, 200µg/kg and 300µg/kg exposed animals, demonstrating the induction of inflammation in the testis by cerium oxide nanoparticles. There has been growing evidence of induction of proinflammatory responses in the lung by transition metals which are in association with different particles. (Hetland *et al.*, 2005; Valavanidis *et al.*, 2013). Moreover, it has been established that nanoparticles phagocytised by Alveolar macrophages (AMs) activates the induction and release of proinflammatory proteins including interleukin-6, interleukin-1 and the tumour necrosis factor alpha which activates eosinophils and neutrophils to induce inflammation of the pulmonary. (Teruel *et al.*, 2008; Hiraiwa et al., 2013). The study further assessed cerium oxide nanoparticle effect on apoptotic indices, where percentage fragmented DNA and expression of p53 was determined. Results revealed cerium oxide nanoparticles induced apoptosis via elevated fragmented testicular DNA in the liver and testis of animals.

A well-established role of p53 is induction of internal and external apoptotic pathways where it acts as a tumor suppressor. P53-mediated apoptosis primarily utilizes the intrinsic pathway, while the extrinsic pathway compliments the apoptotic response. (Shen and White, 2001) In the study, p53 was moderately expressed in all the exposed animals. Sialic acid acts as a potent hydrogen peroxide scavenger by converting it into water and nontoxic carboxylic acid, thereby imparting defence against oxidative damage (Iijima *et al.,* 2004). Results from the experiment showed decreasing sialic acid in testis in all the exposed animals. This demonstrates that cerium oxide nanoparticle suppressed the ability of sialic acid to mop up hydroperoxide from the testis which also confirms its ability to induce oxidative damage. Result from histological examination showed minimal damage to hepatocytes while the testis was severely damaged, evidenced by the necrosis of spermatogenic cells of the germinal epithelium.

Ameliorative potential of Nanoceria in Diethylnitrosamine (DEN)-induced hepatotoxicity in male wistar rats

Studies have found that inhaling CeO_2NPs can alter general circulation, causing aggregation in major organs such as liver (Snow *et al.,* 2014). Mice that had been pre-treated with nanoceria and then administered diethylnitrosamine all survived throughout the period of experimental setup. Mice exposed to DEN alone and those pre-treated with CeO_2NPs both lost weights, although insignificantly. Diethylnitrosamine has been reported to cause reduced craving for food (Anoopraj *et al.,* 2014), this therefore can explain the reason behind the observed weight loss. The presence of elevated level of liver biomarker enzymes in the serum of DEN treated mice, mainly ALT and AST indicates the onset of hepato-cellular damage. These enzymes are predominantly localized in the intracellular compartment and during cellular injury they leak into the extracellular matrix (Salie *et al.,* 1999).

Circulating levels of ALT in the serum were found to be considerably higher in rats exposed to DEN, among the hepatic biomarkers studied in this study. Notably, pre-treatment with CeO_2NPs revealed hepato-protection via attenuation of increased liver biomarkers. Oxidative injury to cells, tissue and organs arises due to disturbances in redox equilibrium between free radical generation and antioxidative enzymes, brought

about by the excessive synthesis of ROS and concomitant depletion in activities of antioxidants (Nita *et al.,* 2016). Liver parenchymal are mostly vulnerable to oxidative injury by free radicals (Sha Li *et al.,* 2015). This is because of the ability of certain organelles (peroxisomes, microsomes and mitochondria) within the liver parenchymal cells to produced reactive oxygen species that can induced fatty acids oxidation), thereby rendering the liver as the most susceptible to ROS attack (Su *et al.,* 2019).

Aside ROS, some proinflammatory proteins like the TNF-α which is primarily produced in *kuffer* cells have been shown to play vital function in inducing oxidative damage, a condition that can increase apoptosis and inflammation (Sha Li *et al.,* 2015). Result from this study revealed that diethylnitrosamine induced oxidative stress, evidenced by increased lipid peroxidation generation in the liver. DEN can induce oxidative stress via oxidation of membrane lipids, fatty acids and proteins (Allen and Tresini 2000). The increased MDA elicited by DEN led to attendant decreasing antioxidant enzymes. Glutathione is an important non-enzymic antioxidants which function in getting rid of endo and exogenous radicals synthesised from various organelles of the cell. It primarily induces immune functions, regulates cytokine production and serves as co-factor for glutathione-s-transferase (Wang *et al.,* 2013), therefore playing a vital part in liver function. Results from this study showed that cerium oxide nanoparticles restored GSH level in DEN-treated animals, therefore suggesting that nanoceria can halt oxidative stress via prevention of bio membrane peroxidation by ROS formed at the time DEN has been metabolised.

Despite that the precise mechanism of hepato-protection of cerium oxide nanoparticles has not been fully explained, it has however been proposed that notable ability of this nanoparticle to store up oxygen in its vacant lattice, coupled with it antioxidative potential might be connected to its capacity in scavenging reactive oxygen species (Dowding *et al.,* 2013). Superoxide dismutase and catalase belongs to the primary cellular antioxidant enzymes in cells. While SOD acts on superoxide radical converting it to hydrogen peroxide (H_2O_2), catalase converts H_2O2 to water and oxygen, thereby conferring protection against ROS (Fukai 2011). The study showed that pre-treatment of mice using nanoceria restored the activities of both antioxidant enzymes. GST, an enzyme that helps in the detoxification of xenobiotic molecules by conjugating them with reduced glutathione, was restored upon pre-treatment with

cerium oxide nanoparticles. Similar result was also obtained for glutathione peroxidase.

Myeloperoxidase (MPO) is hydrolytic enzyme found primarily in basophils, eosinophils and neutrophils that catalyses the oxidative reaction of a number of compounds, using H_20_2 synthesised from neutrophils in order to produce substrate to enhance the activity of most bacteria (Klebanoff *et al.,* 2013). The capability of nanoceria to decrease the elevated MPO activity occasioned by DEN is indicative of it acting as an inhibitor of inflammation in chemically induced hepatic damage. In addition, nitric oxide which serve as a biological messenger is produced from the conversion of arginine to citrulline, catalysed by iNOS (Palmer *et al.,* 1987). It was observed in the study that DEN induced inflammatory process in the liver via increase in NO level. However, the anti-inflammatory activity of nanoceria restored the condition, though earlier research has revealed that transition metals that possess that ability to undergo redox cycling, when present in a particular form can induce allergic reactions and inflammation in the epithelial cells of the lungs (Zhao *et al.,* 2021).

In contrast, findings of this research revealed that pre-treatment of animals with cerium oxide nanoparticles at test concentrations significantly supressed the expression of hepatic cyclooxygenase 2 and iNOS among mice treated with CeO_2NPs compared to DEN treated animals. In normal physiological processes, cyclooxygenase 2 is expressed in relatively small amount, but its induction is highly enhanced during attack by obnoxious agents which include hypoxia, ROS, and inflammatory cytokines (Wieczfinska *et al.,* 2019). As a tumor suppressor, p53 has a well-defined role in triggering both intracellular and extracellular routes of apoptosis. DEN caused weak p53 expression, it can inhibit p53 expression. However, pre-treatment with CeO_2NPs at both doses resulted in substantial p53 expression. This shows that the cerium oxide nanoparticles may protect the cell from oxidative damage by inducing p53.

Bcl_2, a member of anti-apoptotic protein family highly expressed in the liver of DEN exposed animals was decreased in animals pre-treated with both doses of cerium oxide nanoparticles. This study therefore suggests that mechanistically, DEN induced liver damage via suppression of pro-apoptotic proteins while promoting the induction of anti-apoptotic proteins. Liver histology revealed a distorted architecture of the liver, characterised by presence of inflammatory cells in animals exposed to DEN, however

in animals pre-treated with cerium oxide nanoparticles, the architecture of the liver appears normal with few inflammatory cells.

Ameliorative Potential of Nanoceria following induction of mammary toxicity via injection of Benz[a]pyrene and N-Nitroso-N-methylurea to adult female rats.

Proteolytic breakdown, angiogenesis and migration through the extracellular matrix are all important interrelated events in cancer metastasis. The current treatment regimen for cancer seeks to inhibit tumor invasion and angiogenesis by reducing ROS or free radicals and induction of apoptosis. Interestingly, some natural substances have been shown to target these events in cancer chemoprevention. The study demonstrated that nanoceria, due to their anti-oxidative, anti-neoplastic and anti-inflammatory abilities mitigated damage to mammary gland in female wistar rats. Redox reaction is one major mechanism by which cerium oxide nanoparticles exert their effect on biological entity. A report by Pagliari *et al,* (2012) showed that cerium oxide nanoparticle confers protection on progenitor cells of the cardiac tissue against oxidative stress (Pagliari *et al.,* 2012). Such activity has been traced to its free radical scavenging properties of the nanoparticle (Rubio *et al.*, 2016).

Rapidly dividing cancer cells are reported to experience oxidative stress, especially at early metastasis stage when recently created cellular bodies are yet to attain stability. (Liou and Storz *et al.,* 2010). High ROS levels causes peroxidation of the membrane, subsequently reducing it to very active electrophilic lipid peroxide (Su *et al.,* 2019). In the course of the study, nanoceria's ability in attenuating oxidative stress on mammary gland tissue was investigated by monitoring the amount of malondialdehyde produced as well as antioxidant enzyme activities. It was observed that administration of NMU and BaP induced oxidative stress via increased LPO process, an observation consistent with Adedoyin *et al* (2018) who reported oxidative stress incidence in the mammary gland of experimental animals treated with NMU. One major consequence of ROS effect on structure and function of membranes is the extent of lipid peroxidation. (Stark, 2005).

Administration of cerium oxide nanoparticle however ameliorated this increase. Despite the fact that the exact antioxidative mechanism of superoxide dismutase in cancer treatment/management has not been fully explained, it has been shown that this enzyme confers protection against most chemically induced organ damage (Fernández-

Varo et al., 2020). Recent studies have shown that SOD and catalase relieve cells of oxidative damage by interacting with ROS and converting them to forms that are less toxic (Fukai 2011). Mammary toxicity induced by administering NMU and BaP was confirmed by significant reduction in enzymes of GST, Catalase, CAT and GSH. This therefore suggests that suppression of antioxidant defense is probably one out of the various mechanisms by which toxic chemicals induce their damaging effect.

In several studies, nanoceria is suggested as possible alternative chemotherapy against different forms of cancer such as colorectal cancer (Pesic *et al.,* 2015), pancreatic cancer, (Wasson *et al.,* 2014) as well as melanoma (Raju *et al.,* 2022). Also. nanoceria can confer protection on epithelial cells of the colon from damage arising from radiation via lowering ROS production (Colon *et al.,* 2010). Inflammation's role in mammary gland tumor was assessed in the course of this study. Myeloperoxidase plays essential role, in a variety of pathological complications, which include neurodegenerative, cardiovascular, and inflammatory-mediated diseases (Lazarevic-Pasti *et al.,* 2015 and Frangie 2022). MPO catalyses the oxidation of several compounds by making use of hydrogen peroxide synthesised by neutrophils to produced radicals that serves as substrate for bacterial activity (Amjad *et al.,* 2018).

Induction of mammary gland tumor in this study induced inflammation, evidenced by the significant increase in MPO activity. Similarly, the mammary nitric oxide (NO) which plays a vital role in signal transduction increased after exposure to NMU and BaP. Administration of cerium oxide nanoparticles ameliorated this inflammation in mammary gland of the animals, bringing to the fore, the anti-inflammatory activity of nanoceria. Research has confirmed the involvement of ROS in apoptosis by disrupting activities that lead to the opening of the mitochondrial membrane (Pizzino *et al.,* 2017). Several Bcl_2 protein families, specifically pro-apoptotic protein (BAX) as well as anti-apoptotic protein (Bcl_2) are major proteins involved in regulating intrinsic apoptotic pathway (Xu *et al.,* 2007). The study established BAX and Caspase 3 suppression in NMU and BaP-induced mammary gland tumor. Conversely, treatment with cerium oxide nanoparticles induced apoptosis by directing the synthesis of these proteins to initiate the apoptotic process.

CHAPTER SIX

Summary, Conclusion and Recommendations

6.1 Summary

Cerium oxide nanoparticles possess a detrimental effect on the male reproductive system. Though the liver antioxidants enzymes were decreased when challenged with the nanoparticle, its cytoarchitecture was kept intact, showing that the particle possesses less adverse effect on it. In this research, DEN induces hepatoxicity with increased inflammation and oxidative stress while cerium oxide nanoparticles attenuated these effects. Also, the last experiment showed that cerium oxide can protect mammary tissue from NMU and BaP induced mammary toxicity in experimental rats.

6.2 Conclusion

This research further confirms the biomedical importance of CeO_2 NPs in ameliorating disease conditions in animals. Administration of CeO_2 NPs caused testicular dysfunction in experimental rats, evidenced by decreased sperm count and sperm motility. CeO_2 NPs exerts minimal damaging effect on the liver as it relieved hepatocytes from oxidative stress. This study has been able to show that CeO_2 NPs produced promising anti-inflammatory, antioxidative and pro-apoptotic effect against liver injury. Significantly, CeO_2 NPs provided antioxidant buffer, induced apoptosis and improved mammary cyto-architecture in experimental mammary gland toxicity.

6.3 Recommendations

I hereby recommend from these findings that:

1. Occupational exposure to cerium oxide nanoparticles should be monitored as it possess as an adverse effect on male reproductive system
2. Research into the exact oxidation state of cerium oxide nanoparticles (+3 or +4) that confers protection should be looked into

3. The ability of nanoceria to cross blood brain barrier (BBB) should be researched on, this will allow or promote research into its protective effect against neurological disorders.
4. Potential of this nanoceria as an anticancer agent against BCA can be explored.

5..4 Contributions to knowledge

The study on the toxicological profiling and nanoceria's protection has contributed to the body of knowledge in nanomedicine in the following ways:

1. Cerium oxide nanoparticles exerted male reproductive toxicity by disrupting hormonal balance and inducing testicular oxidative stress in adult male mice.
2. Cerium oxide nanoparticles showed protection against diethylnitrosamine-induced hepatic damage via anti-inflammatory and apoptotic properties.
3. Cerium oxide nanoparticles play a protective role on the liver of diethylnitrosamine-induced hepatoxicity in rats via induction of anti-oxidative enzymes and apoptosis.
4. For the first time, cerium oxide nanoparticles have shown to preserve the cytoarchitecture of the mammary gland against chemically induced mammary tumorigenesis.
5. Relying on its antioxidant, anti-inflammatory and pro apoptotic properties, cerium oxide nanoparticles ameliorated mammary gland toxicity from NMU and BaP induced mammary tumorigenesis.

\

REFERENCES

Abdel-Salam, M. Omran, B., Whitehetad, K., and Baek, K. H. 2020. Superior Properties and Biomedical Applications of Microorganism-Derived Fluorescent Quantum Dots. *Molecules* 25.19: 44-86.

Aebi, H. Ed 1974. Catalase. *Methods of enzymatic analysis*. Verlag Chemie/Academic Press Inc., Weinheim, pp 673–680.

Aggarwal, P. Hall, J. B. McLeland, C. B. Dobrovolskaia, M. A. McNeil, S. E. 2000. Nanoparticle interaction with plasma proteins as it relates to particle biodistribution, biocompatibility and therapeutic efficacy. *Adv Drug Deliv Rev.* 61. 6:428-437

Aghebati-Maleki, A. Dolati, S. Ahmadi, M. Baghbanzhadeh, A. Asadi, M. Fotouhi, A. Yousefi, M. Aghebati-Maleki. L, 2020. Nanoparticles and cancer therapy: Perspectives for application of nanoparticles in the treatment of cancers. *J Cell Physiol* 235. 3:1962-1972.

Aitken, R. J. Buckingham, D. Harkiss, D. 1993. Use of a xanthine oxidase free radical generating system to investigate the cytotoxic effects of reactive oxygen species on human spermatozoa. *J Reprod Fertil* 97. 2:441-450

Akerman, M.E. Chan, W. C. Laakkonen, P. Bhatia. S. N. Ruoslahti, E. 2002. Nanocrystal targeting in vivo. *Proc Natl Acad Sci* 99 20:12617–12621.

Ali, H. S. Mahdi, A. Parveen, I. and Azam, A. 2018. Optical properties of cerium oxide (CeO_2) nanoparticles synthesized by hydroxide mediated method. AIP Conf. *Proc* 15. 21:374-389

Alili, L. Sack, M. Karakoti, A. S. Teuber, S. Puschmann, K. Hirst, S. M. Reilly, C. M. Zanger, K. Stahl. W. Das, S. Seal, S. Brenneisen, P. 2011. Combined cytotoxic and anti-invasive properties of redox-active nanoparticles in tumor-stroma interactions. *Biomaterials* 32. 11:2918-2929.

Allen, R. G. Tresini, M. 2000. Oxidative stress and gene regulation. *Free Radical Biol Med* 28. 3: 463-499.

Amin, K. A. Hassan, M. S. Awadel, S. T. Hashem, K. S. 2011. The protective effects of cerium oxide nanoparticles against hepatic oxidative damage induced by monocrotaline. *Int J Nanomedicine* 17. 6:143-149.

Aminoff, D. 1961. Methods for the quantitative estimation of N-acetylneuraminic acid and their application to hydrolysates of sialomucoids. *The Biochemical Journal* 10. 81: 384–392.

Amjad, A. Khan, Mohammed, A. Alsahli, Arshad, H. Rahmani. 2018. Myeloperoxidase as an Active Disease Biomarker: Recent Biochemical and Pathological Perspectives. *Med Sci* 6. 2: 33.

Anderson, N. L. Anderson, N. G. 2003. The human plasma proteome: history, character, and diagnostic prospects. *Mol Cell Proteomics* 1. 11:845-867.

Anoopraj, R. Hemalatha, S. Balachandra, C. 2014. A preliminary study on serum liver function indices of diethylnitrosamine induced hepatotocarcinogenesis and chemoprotective potential of Eclipta alba in male Wistar rats. *Vet World* 7. 6:439–442

Anthonio, A. Mario, F. Munoz, S. 2014. Lipid Peroxidation; Production, Metabolism and Signalling Mechanisms of Malondialdehyde and 4-Hydroxy-2- Nonenal. *Oxidative Medicine and Cellular Longevity* 5. 18: 15.

Apel, K. Hirt, H. 2004. Reactive oxygen species: metabolism, oxidative stress, and signal transduction. *Annu Rev Plant Biol* 4. 55: 373-399.

Ariga, K. Nishikawa, M. Mori, T. Takeya, J. Shrestha, L. K. Hill J. P. 2019. Self-assembly as a key player for materials nanoarchitectonics. *Sci Technol Adv Mater* 31. 20:51-95

Asim, A. Hilal, A. Tabassum, P, Akil, A. Mohammad, O. Iqbal, M. Huda, A. Khalid, U. Mohama, N. 2020. Recent advances in metals decorated nanomaterials and their various biological applications. *Front. Chem* 28. 10: 341-353.

Attia, Y. A. Samer, M. Mohamed, M. S. 2020. Nanocoating of microbial fuel cell electrodes for enhancing bioelectricity generation from wastewater. *Biomass Conv. Bioref* 39. 6:382-398

Badwal, S. P. Giddey, S.S. Munnings, C. Bhatt, A. I. Hollenkamp, A. F. 2014. Emerging electrochemical energy conversion and storage technologies. *Front Chem* 24. 2: 355-379.

Bailey, Z. Nilson, E. Bates, J. Oyalowo, A. Hockey, K. 2022. Cerium Oxide Nanoparticles Improve Outcome after *In Vitro* and *In Vivo* Mild Traumatic Brain Injury. *J Neurotrauma* 37. 12:1452-1462.

Baldim,V. Bedioui, F. Mignet, N. Margaill, I. Berret, J. F. 2018. The enzyme-like catalytic activity of cerium oxide nanoparticles and its dependency on Ce^{3+} surface area concentration. *Nanoscale* 10. 15:6971-6980.

Balmer, J. Zulliger, R. Roberti, S. and Enzmann, V. 2015. Retinal Cell Death Caused by Sodium Iodate Involves Multiple Caspase-Dependent and Caspase-Independent Cell-Death Pathways. *International journal of molecular sciences* 16. 7:15086–15103.

Barhoum, A. García-Betancourt, M. Jeevanandam, J. Hussien, E. Mekkawy. 2022. Review on Natural, Incidental, Bioinspired, and Engineered Nanomaterials: History, Definitions, Classifications, Synthesis, Properties, Market, Toxicities, Risks, and Regulations. *Nanomaterials* 6. 12:157-177.

Barry, P. Patricia, M. Chris, H. Robert, G. Andrew, W. 2007. Initial in vitro screening approach to investigate the potential health and environmental hazards of Envirox™ – a nanoparticulate cerium oxide diesel fuel additive. *Particle and Fibre Toxicology* 5. 4:121-134.

Batinić-Haberle, I. Rebouças, J. S. Spasojević, I. 2010. Superoxide dismutase mimics: chemistry, pharmacology, and therapeutic potential. *Antioxid Redox Signal* 13. 6:877-918.

Batinić-Haberle, I. Rebouças, J. S. Spasojević, I. 2010. Superoxide dismutase mimics: chemistry, pharmacology, and therapeutic potential. *Antioxid Redox Signal* 13. 6:877-918

Bayda, S. Adeel, M. Tuccinardi, T. Cordani, M. Rizzolio, F. 2019. The History of Nanoscience and Nanotechnology: From Chemical-Physical Applications to Nanomedicine. *Molecules* 25. 1:112.

Beyene, A. M. Moniruzzaman, M. Karthikeyan, A. and Min, T. 2021. Curcumin Nanoformulations with Metal Oxide Nanomaterials for Biomedical Applications. *Nanomaterials,* 11:445-460.

Buege, J. A. Aust, S. D. 1978. Microsomal lipid peroxidation. *Methods Enzymol* 10. 52:302–310.

Burello, E. and Worth, A. 2011. Theoretical framework for predicting the oxidative stress potential of oxide nanoparticles. *Nanotoxicology*. 5. 2:228-235.

Caetano-Lopes, J. Canhão, H. Fonseca, J. E. 2007. Osteoblasts and bone formation. *Acta Reumatol Port* 32. 2:103-110.

Calvin, H. and Tuner, S. 1982. High levels of glutathione attained during postnatal development of rat testis. *Journal of Experimental Zoology* 219. 3:389-393.

Camilleri, M. Malhi, H. Acosta, A. 2017. Gastrointestinal Complications of Obesity. Gastroenterology. 152. 7:1656-1670.

Casals, E. Pfaller, T. Duschl, A. Oostingh, G. Puntes, V. 2011. Hardening of the nanoparticle-protein corona in metal (Au, Ag) and oxide (Fe3O4, CoO, and CeO2) nanoparticles. *Small* 16. 24:3479-3486.

Casals, E. Pfaller, T. Duschl, A. Oostingh, G. J. Puntes, V. 2010. Time evolution of the nanoparticle protein corona. *ACS Nano.* 4. 7:3623-3632.

Casals, G. Perramón, M. Casals, E. Portolés, I. Fernández-Varo. 2021. Cerium Oxide Nanoparticles: A New Therapeutic Tool in Liver Diseases. *Antioxidants 10.* 5 660.

Cassee, F. R. Balen, E. C. Singh, C. Green, D. Muijser, H. Weinstein, J. Dreher, K. 2011. Exposure, health and ecological effects review of engineered nanoscale cerium and cerium oxide associated with its use as a fuel additive. *Crit Rev Toxicol* 12. 41:213–29.

Cedervall, I. Lynch, S. Lindman, T. Berggård, E. Thulin, H. Nilsson, K. A. Dawson and S. Linse, 2007. Proceedings of the National Academy of Sciences, 104, (10) 2050-2055.

Chaplin, D. 2010. Overview of the immune response. *J Allergy Clin Immunol* 125. 2 :13-23.

Chauhan, D. Yadav, A. and Solanki, P. 2021. Carbon cloth-based immunosensor for detection of 25-hydroxy vitamin D_3. *Mikrochimica acta* 188. 4: 145.

Chellagram, C. Murugaboopathi, G. John. A. A. Sivakumar. R. Ganesan, S. Krithika, S. Priya, G. 2014. Significance of Nanotechnology in food industry. *Procedia* 18. 8: 109.113.

Chen, J. Patil, S. Seal, S. McGinnis, J. 2006. Rare earth nanoparticles prevent retinal degeneration induced by intracellular peroxides. *Nat Nanotechnol* 1. 2:142-150.

Chen, S. Hou, Y. Cheng, G. Zhang, C. Wang, S. Zhang, J. 2013. Cerium oxide nanoparticles protect endothelial cells from apoptosis induced by oxidative stress. *Biol Trace Elem Res* 154. 1:156-166.

Chen, W. Zhao, Y. Seefeldt, T. Guan, X. 2008. Determination of thiols and disulfides via HPLC quantification of 5-thio-2-nitrobenzoic acid. *J Pharm Biomed Anal* 48. 5:1375-1380.

Cheng, Z. Li, M. Dey, R. 2021. Nanomaterials for cancer therapy: current progress and perspectives. *J Hematol Oncol* 14. 8:85-106

Choi, H. Liu, W. Misra. P, Tanaka, E. Zimmer, J. 2007. Renal clearance of quantum dots. *Nature biotechnology* 25. 10:1165–1170.

Clarke, B. 2008. Normal bone anatomy and physiology. *Clin J Am Soc Nephrol* Suppl 3. 3:131-139.

Cole, M. F. and Bergeson, L. L. (006. *Regulatory report FDA regulation of food packaging produced using nanotechnology*. Food Safety Magazine.

Coles, R. McDowell, D. and Kirwan, M. J. (Eds.) 2003. *Food Packaging Technology*. Blackwell Publishing, Oxford, UK, p. 346.

Colon, J. Hsieh, N. Ferguson, A. Kupelian, P. 2010. Cerium oxide nanoparticles protect gastrointestinal epithelium from radiation-induced damage by reduction of reactive oxygen species and upregulation of superoxide dismutase 2. *Nanomedicine.* 6. 5:698-705.

Córdoba-Jover, B. Arce-Cerezo, A. Ribera, J. 2019. Cerium oxide nanoparticles improve liver regeneration after acetaminophen-induced liver injury and partial hepatectomy in rats. *J Nanobiotechnol* 17. 10. 100-112.

Corma, P. Atienzar, H. Garc´ıa, Y. and Chane-Ching, J. 2004. Hierarchically mesostructured doped CeO_2 with potential for solarcell use. *Nature Materials* 3. 6:394–397.

Dahle, J. T. Arai Y. 2015. Environmental geochemistry of cerium: applications and toxicology of cerium oxide nanoparticles. *Int J Environ Res Public Health* 12. 2:1253-78.

Daipeng. Z. Lei, W. Qingbin, C. Ryma, I. Yanfei, X. 2020. Repositioning Lidocaine as an Anticancer Drug: The Role Beyond Anesthesia. *Front cell Devl Biol 10.* 8:565-572.

Dale, J. G. Cox, S. S. Vance, M. E. Marr, L. C. Hochella, M. F. Jr. 2017. Transformation of Cerium Oxide Nanoparticles from a Diesel Fuel Additive during Combustion in a Diesel Engine. *Environ Sci Technol* 51. 4:1973-1980.

Das, K. Madhusoodan, A. P. Mili, B. Kumar, A. Saxena, A.C. Kumar, K. Sarkar, M. Singh, P. Srivastava, S. Bag, S. 2017. Functionalized carbon nanotubes as suitable scaffold materials for proliferation and differentiation of canine mesenchymal stem cells. *Int J Nanomedicine* 19. 2:3235-3252.

Datye, A. K. and Votsmeier, M. 2022. Opportunities and challenges in the development of advanced materials for emission control catalysts. *Nat. Mater* 13. 20:1049–1059.

Dowding, J. M. Dosani, T. Kumar, A Seal, S. Self, W. T. 2012. Cerium oxide nanoparticles scavenge nitric oxide radical (˙NO). *Chem Commun* 48. 40:4896–4898.

Duncan, T.V. 2011. Applications of nanotechnology in food packaging and food safety: barrier materials, antimicrobials and sensors. *J Colloid Interface Sci* 1. 1:1-24.

Dutta, D. Mukherjee, R. Patra, M. Banik, M. Dasgupta, R. Mukherjee, M. Basu, T. 2016. Green synthesized cerium oxide nanoparticle: A prospective drug against oxidative harm. *Colloids Surf B Biointerfaces* 1. 147:45-53.

Ebrahim, Abbasi, Vafaei, Naseri, Darini, Masoumeh. 2021. Protective effects of cerium oxide nanoparticles in non-alcoholic fatty liver disease (NAFLD) and carbon tetrachloride-induced liver damage in rats: Study on intestine and liver. *Meabol open* 55. 10: 583-598.

Emerit, J. Edeas, M. Bricaire, F. 2004. Neurodegenerative diseases and oxidative stress. *Biomed Pharmacother* 42. 1:39-46.

Estevez, A.Y. Ganesana, M. Trentini, J. F. 2019. Antioxidant Enzyme-Mimetic Activity and Neuroprotective Effects of Cerium Oxide Nanoparticles Stabilized with Various Ratios of Citric Acid and EDTA. *Biomolecules* 9. 10:562-575

Estrada, L. Moreno, E. Gonzalez-Quiroga, A. Bula, A. Duarte-Forero, J. 2022. Experimental assessment of performance and emissions for hydrogen-diesel dual fuel operation in a low displacement compression ignition engine. *Heliyon* 8. 4:537-549.

Fanelwa, A. Simone, B. Mulisa, N. Nzumbululo, N. Tessia, R. 2022. *Nanoparticles in biosensor development for the detection of pathogenic bacteria in water, Emerging Freshwater Pollutants*. Elsevier, Pages 331-358.

Farias, I. Dos Santos, C. and Sampaio, F. C. 2018. Antimicrobial Activity of Cerium Oxide Nanoparticles on Opportunistic Microorganisms: A Systematic Review. *BioMed Res Intl*, 19. 23:606-619.

Fawcett, J. K. Scott, J. E. 1960. A rapid and precise method for the determination of urea. *J Clin Pathol* 13. 2:156-169.

Felix, C. P. Martin, D. Barbara, T. 2021. Combustion and emissions from cerium oxide nanoparticle dosed diesel fuel in a high-speed diesel research engine under low temperature combustion (LTC) conditions. *Fuel* 288.1:119-129.

Fernández-Varo, G. Perramón, M. Carvajal, S. Oró, D. Casals, E. Boix, L. Oller, L. Macías-Muñoz, L. Marfà, S. Casals, G. Morales-Ruiz, M. Casado, P. Cutillas, P. R. Bruix, J. Navasa, M. Fuster, J. Garcia-Valdecasas, J. C. Pavel, M. C. Puntes, V. Jiménez, W. 2020. Nanoceria: An Effective Treatment in Experimental Hepatocellular Carcinoma. *Hepatology* 72. 4:1267-1282.

Feynma, 1960. Plenty of room at the bottom (reprint from the speech given at the annual meeting of the West Coast section of the American Pysical Society) *Eng Sci* 10. 23:22-36

Fifere, N. Airinei, A. Dobromir, M. Sacarescu, L. Dunca, S. I. 2021. Revealing the Effect of Synthesis Conditions on the Structural, Optical, and Antibacterial Properties of Cerium Oxide Nanoparticles. *Nanomaterials* 11. 10:2596-2606.

Fleischer, U. Kumar, and Payne, C. 2013. Cellular binding of anionic nanoparticles is inhibited by serum proteins independent of nanoparticle composition *Biomater Sci*, 10. 1:975-982.

Foulkes, W. D. 2006. BRCA1 and BRCA2: chemosensitivity, treatment outcomes and prognosis. *Fam Cancer* 5. 2:135-142.

Frangie, C. Daher, J. 2022. Role of myeloperoxidase in inflammation and atherosclerosis (Review). *Biomed Rep.* 16. 6:53-64.

Franken, D. R. Oehninger, S. 2012. Semen analysis and sperm function testing. Asian *J Androl.* 14. 1:6-13.

Fridovich I. 1997. Superoxide anion radical (O_2^-.), superoxide dismutase, and related matters. *J Biol Chem.* 272. 30:18515-18527.

Fukai, T. Ushio-Fukai, M. 2011. Superoxide dismutases: role in redox signalling, vascular function, and diseases. *Antioxid Redox Signal* 15. 6:1583-1606.

Furumoto, K. Ogawara, S. Nagayama, Y. Takakura, M. Hashida, K. 2002. Important role of serum proteins associated on the surface of particles in their hepatic disposition. *Nat Nanotechnol* 17. 5:671-675.

Gao, J. Zeng, L. Yao, L. Wang, Z. Yang, X. 2021. Inherited and acquired corona of coronavirus in the host: Inspiration from the biomolecular corona of nanoparticles. *Nano Today* 10. 39:101-121

Ge C, Du J, Zhao L, Wang L, Liu Y, Li D, Yang Y, Zhou R, Zhao Y, Chai Z, Chen C. Binding of blood proteins to carbon nanotubes reduces cytotoxicity. *Proc Natl Acad Sci* 108 (41) 16968-16973

Geng, J. Li, M. Ren, J. Wang, E. Qu, X. 2011. Polyoxometalates as inhibitors of the aggregation of amyloid β peptides associated with Alzheimer's disease. *Angew Chem* Int Ed Engl. 50. 18:4184-4198.

Ghio, A. J. Sobus, J. R. Pleil, J. D. and Madden, M. C. 2012. Controlled human exposures to diesel exhaust. *Swiss. Med.* 11. 4: 142.156.

Gil, D. Rodriguez, J. Ward, B. Vertegel, A. Ivanov, V. Reukov, V. 2017. Antioxidant Activity of SOD and Catalase Conjugated with Nanocrystalline Ceria. *Bioengineering*. 4. 1:18-25.

Giraldo, J. P. Laundry, M. Faltermeier, S. McNicholas, T. Iverson, N. 2014. Plant nanobionics approach to augment photosynthesis and biochemical sensing. *Nature materials* 13. (2) 400–408.

Giri, S. Karakoti, A. Graham, R. P. Maguire, J. L. Reilly, C. M. Seal, S. 2013. Nanoceria: a rare-earth nanoparticle as a novel anti-angiogenic therapeutic agent in ovarian cancer. *PLoS One* 8:545-578.

Glassman, P. M. Muzykantov, V. R. 2019. Pharmacokinetic and Pharmacodynamic Properties of Drug Delivery Systems. *J Pharmacol Exp Ther*. 370. 3:570-580.

Gojova, J.-T. Lee, H. S. Jung, B. Guo, A. I. Barakat and I. M. Kennedy. 2009. Effect of cerium oxide nanoparticles on inflammation in vascular endothelial cells. *Inhalation Toxicol.*, 21 (5) 123–130.

González-García, E. MacGregor, N. Visalakshan, M. Lazarian, A. Cavallaro, A. 2022. Nanoparticles Surface Chemistry Influence on Protein Corona Composition and Inflammatory Responses. *Nanomaterials* 12. 4:682-774.

Guo, C. Robertson, S. Weber, R. Buckley, A. Warren, J. Hodgson, A. Rappoport, J. Z Ignatyev, K. Meldrum, K. Römer, I. Macchiarulo, S. Chipman, J. K. Marczylo, T. Leonard, M.O. Gant, T. W. Viant, M. R. Smith, R. 2019. Pulmonary toxicity of inhaled nano-sized cerium oxide aerosols in Sprague-Dawley rats. *Nanotoxicology* 13. 6:733-750.

Gutwein, L. G. Webster T. J. 2003. Effects of alumina and titania nanoparticulate on bone cell function. American Ceramic Society 26th Annual Meeting Conference

Habig. W. H. Pabst, M. J. Jakoby, W. B. 1974. Glutathione-S-transferases. The first enzymatic step in mercapturic acid formation. *J Biol Chem* 2. 49:7130–7139

Heckert, E. G. Karakoti, A. S. Seal, S. and Self, W. T. 2008. The role of cerium redox state in the SOD mimetic activity of nanoceria. *Biomaterials* 29. 18:2705–2709.

Heckman, K. DeCoteau, William, E. Ana, R. Kenneth, C. Wendi, D. 2013. Custom Cerium Oxide Nanoparticles Protect Against a Free Radical Mediated Autoimmune Degenerative Disease in the Brain. *ACS nano* 7. 10:538-544

Hetland, R. B. Cassee, F. R, Låg, M, Refsnes, M. Dybing, E. Schwarze, P. E. 2005. Cytokine release from alveolar macrophages exposed to ambient particulate matter: heterogeneity in relation to size, city and season. *Part Fibre Toxicol* 17. 2:4-11.

Hijaz, S. Das, I. Mert, A. Gupta, Z. Al-Wahab, C. Tebbe, S. Dar, J. Chhina, S. Giri, A. Munkarah, S. Seal and R. Rattan. 2016. Folic acid tagged nanoceria as a novel therapeutic agent in ovarian cancer. *BMC Cancer,* 16. 12:220-231.

Hiraiwa, K. Eeden, S. F. 2013. Contribution of lung macrophages to the inflammatory responses induced by exposure to air pollutants. *Mediators Inflamm* 6. 19: 523-535.

Holley, C. 2005. Nanotechnology and packaging. Secure protection for the future. Verpackungs Rundschau. 56: 53–56.

Hoshyar, N. Gray, S. Han, H. Bao, G. 2016. The effect of nanoparticle size on in vivo pharmacokinetics and cellular interaction. *Nanomedicine* 11. 6:673-692.

Hosseini, M. and Mozafari, M. 2020. Cerium Oxide Nanoparticles: Recent Advances in Tissue Engineering. *Materials*, 13. 14: 307-325.

Hu, Q, Tuck, C. Wildman, R. Hague, R. 2016. *Application of Nanoparticles in Manufacturing*. In: Aliofkhazraei M. (eds) Handbook of Nanoparticles.

Iijima, R. Takahashi, H. Namme, R. Ikegami, S. Yamazaki, M. 2004. Novel biological function of sialic acid (N-acetylneuraminic acid) as a hydrogen peroxide scavenger. 12. 561:163-176.

Jain, D. Sharma, M. C. Epari, S. Gupta, N. P. Kolla, S. B. 2009. Hemangioendothelioma of urinary bladder report of rare case. *Urology* 73. 6:1259-1261.

Jakupec, M. A. Unfried, P. Keppler, B. K. 2005. Pharmacological properties of cerium compounds. *Rev Physiol Biochem Pharmacol.* 153. 12:101-111.

Jans, H. and Huo, Q. 2011. Gold nanoparticle-enabled biological and chemical detection and analysis. *Chemical Society reviews.* 41. 6:35-49

Jeevanandam, J. Barhoum, A, Chan, Y. S, Dufresne, A. Danquah. M. K. 2018. Review on nanoparticles and nanostructured materials: history, sources, toxicity and regulations. *J Nanotechnol* 3. 9:1050-1074.

Jin, C. Wang, K. Oppong-Gyebi. A. Hu, J. 2020. Application of Nanotechnology in Cancer Diagnosis and Therapy- A Mini-Review. *Int J Med Sci* 17. 18:2964-2973.

Juan, C. A. Pérez, A. Lastra J. M. Pérez-Lebeña, E. 2022. The Chemistry of Reactive Oxygen Species (ROS) Revisited: Outlining Their Role in Biological Macromolecules (DNA, Lipids and Proteins) and Induced Pathologies. *Int J Mol Sci* 28. 9:4642.

Jung, D. B. Kittelson, M. and Zachariah, R. 2005. The influence of a cerium additive on ultrafine diesel particle emissions and kinetics of oxidation. *Combustion and Flame* 14. 2:276-288.

Kadivar, F. Haddadi, G. Mosleh-Shirazi, M. A. Khajeh, F. Tavasoli, A. Protection effect of cerium oxide nanoparticles against radiation-induced acute lung injuries in rats. *Rep Pract Oncol* 25. 2:206-211.

Kalyanaraman, B. 2013. Teaching the basics of redox biology to medical and graduate students: Oxidants, antioxidants and disease mechanisms. *Redox Biol*. 1. 1:244-257.

Karakoti, A. S, Monteiro-Riviere, N. A. Aggarwal, R. Davis, J. P. Narayan, R. J. Self, W. T. McGinnis, J. Seal, S. 2008. Nanoceria as Antioxidant: Synthesis and Biomedical Applications. *JOM* 60. 3:33-37.

Karin, L. Heckman, Y. Estevez, G. William, D. Stephanie, Y. Samantha, R. Joseph, C Bonnie, Hays-Erlichman. 2019. Variable in Vivo and in Biological Effects of Cerium Oxide Nanoparticle Formulations. *Front. Pharmacol.* 10. 1:59-69.

Karthik, P. Prabaharan, T. 2020. Implementation of nanotechnology in fuel cells, Materials Today: *Proceedings.* 33. 7:2681-2685.

Kennedy, L. Sandhu, J. K. Harper, M. E. Cuperlovic-Culf M. 2020. Role of Glutathione in Cancer: From Mechanisms to Therapies. *Biomolecules* 10. 10:14-29

Khan, M. Mashwani, Z. Ikram, M. Raja, N. Mohamed, A. Ren, G. Omar, A. 2022. Efficacy of Green Cerium Oxide Nanoparticles for Potential Therapeutic Applications: Circumstantial Insight on Mechanistic Aspects. *Nanomaterials* 12. 12:11-27.

Kim, B. G. Choi, D. Y. Kim, M. G. Jang, A. S. Suh, M. W. Lee, J. H. 2022. Effect of Angiogenesis and Lymphangiogenesis in Diesel Exhaust Particles Inhalation in Mouse Model of LPS Induced Acute Otitis Media. *Front Cell Infect Microbiol* 11. 12:82-95.

Klebanoff, S. J. Kettle, A. J. Rosen, H. Winterbourn, C. C. Nauseef, W. M. 2013. Myeloperoxidase: a front-line defender against phagocytosed microorganisms. *J Leukoc Biol* 93. 2:185-198.

Knapen, M. F. Zusterzeel, P. L. Peters, W. H. Steegers, E. A. 1999. Glutathione and glutathione-related enzymes in reproduction: a review. *European journal of Obstertics Gynecology and Reproductive Biology*. 82. 2:171-184

Korsvik, C. Patil, S. Seal, S. Self, W. T. 2007. Superoxide dismutase mimetic properties exhibited by vacancy engineered ceria nanoparticles. *Chem Commun* 14. 10:1056-1068.

Lazarevic-Pasti, T. Leskovac, A. Vasic, V. 2015. Myeloperoxidase Inhibitors as Potential Drugs. *Curr Drug Metab.* 10. 16:168–190.

Lesniak, A. Fenaroli, F. Monopoli, M. P. Åberg, C. Dawson K. A, Salvati, A. 2012. Effects of the presence or absence of a protein corona on silica nanoparticle uptake and impact on cells. *ACS Nano* 6. 7:5845-5857.

Li, H. Xia, P. Pan, S. Qi, Z. Fu, C. Yu, Z. Kong, W. Chang, Y. Wang, K. Wu, D. Yang, X. 2020. The Advances of Ceria Nanoparticles for Biomedical Applications in Orthopaedics. *Int J Nanomedicine*. 29. 15:7199-7214

Li, R. Hou, X. Li, L. Guo, J. Jiang, W. Shang, W. 2022. Application of Metal-Based Nanozymes in Inflammatory Disease: A Review. *Front Bioeng Biotechnol*. 6. 10:920-213.

Li, X. Zhang, R. Hassan, M. M. Cheng, Z. Mills, J. Hou, C. Realini, C. Chen, L. Day, L. Zheng, X. Zhang, D. Hicks, T. M. 2022. Active Packaging for the Extended Shelf-Life of Meat: Perspectives from Consumption Habits, Market

Requirements and Packaging Practices in China and New Zealand. *Foods*. 11. 18:29-38.

Lin, W. Huang, Y. W. Zhou, X. D. Ma, Y. 2006. Toxicity of cerium oxide nanoparticles in human lung cancer cells. *Int J Toxicol*. 25. 6:451-467.

Liou, G. Y. Storz, P. 2010. Reactive oxygen species in cancer. *Free Radic Res.* 44. 5:479-96.

Loh, B, A. Tang, T. Menkhoff, Y. Chay, W and 2003. Applying Knowledge Management in University Research. Governing and Managing Knowledge in Asia, *World Scientific Pub* Co Inc, 3. 28:325-333.

Loos, C. Syrovets, T. Musyanovych, A. Mailänder, V. Landfester, K. Nienhaus, G. U. Simmet, T. 2014. Functionalized polystyrene nanoparticles as a platform for studying bio-nano interactions. *J Nanotechnol* 15. 5:2403-2412.

Lundqvist, M. Stigler, J. Elia, G. Lynch, I. Cedervall, T. Dawson, K. A. 2008. Nanoparticle size and surface properties determine the protein corona with possible implications for biological impacts. *Proc Natl Acad Sci* 105. 38:14265-14270.

Madero-Visbal, B. E. Alvarado, J. F. Colon, C. H. Baker, M. S. Wason, B. Isley, S. Seal, C. M. Lee, S. Das and R. Manon. 2012. Harnessing nanoparticles to improve toxicity after head and neck radiation. ˜*Nanomedicine* 12. 3:1223–1231

Mahmoud, K. Swidan, S. El-Nabarawi, M. 2020. Lipid based nanoparticles as a novel treatment modality for hepatocellular carcinoma: a comprehensive review on targeting and recent advances. *J. Nanobiotechnol* 20.109:384-398.

Majumdar, A. Mangal, N. S. 2013. Hyperprolactinemia. *J Hum Reprod Sci* 6. 3:168-75.

Mansoori, B. Mohammadi, A. Davudian, S. Shirjang, S. and Baradaran, B. 2017. The Different Mechanisms of Cancer Drug Resistance: A Brief Review. *Advanced pharmaceutical bulletin* 7. 3:339–348.

Maritim, A. C. Sanders, R. A. Watkins, J. B. 2003. Diabetes, oxidative stress, and antioxidants: a review. *J Biochem Mol Toxicol*. 17. 1:24-38

Martina, C. Melanie, A. Stephane, R. Virginie, T. Noemie, R. Jerome, R. Jeanne, P. 2020. Nanomaterials from diesel engine exhaust induces DNA damage and oxidative stress in human and rat sperm in vitro. *Nanomaterials* 5. 10: 23-37.

McCord, J. M. and Fridovich, I. 1969. Superoxide dismutase, an enzymatic function for erythrocuprein. *J Biol Chem* 24. 4:6049–6055.

McIlwain, C. C. Townsend, D. M. Tew, K. D. 2006. Glutathione S-transferase polymorphisms: cancer incidence and therapy. Oncogene. 25. 11:1639-1648.

Melissa, S. and Zhao, J. 2013. Cerium oxide nanoparticles: potential applications for cancer and other diseases. *Am J Transl Res* 5. 2:126-131.

Mengzhen, Z. Chao, Z. Xinyun, L. Feng, D. Yaping, Y. 2019. Antibacterial mechanism and activity of cerium oxide nanoparticles. *Science China Materials*. 62. 3:10-22.

Michael, G. Bidir, N. K. Millerjothi, Muyiwa S. Adaramola. 2021. The role of nanoparticles on biofuel production and as an additive in ternary blend fuelled diesel engine: A review, *Energy Reports* 12. 7:3614-3627.

Mleczko, M. Gerkowicz, A. Krasowska, D. 2022. Chronic Inflammation as the Underlying Mechanism of the Development of Lung Diseases in Psoriasis: A Systematic Review. *Int J Mol Sci* 23. 3:1767-1774.

Moldoveanu, B. Otmishi, P. Jani, P. Walker, J. Sarmiento, X. Guardiola, J. Saad, M. Yu, J. 2009. Inflammatory mechanisms in the lung. *J Inflamm Res.* 6. 2:1-11.

Moman, R. N. Gupta, N. Varacallo, M. 2022. *Physiology of Albumin.* In: Treasure Island (FL): StatPearls Publishing

Moron, M. S. Depierre, J. W. Mannervick, B. 1979. Levels of glutathione, glutathione reductase and glutathione-s-transferase activities in rat lung and liver. *Biochim Biophys Acta* 5. 82:67–78.

Muhammad, F. Wang, A. Qi, W. Zhang. S. Zhu, G. 2014. Intracellular antioxidants dissolve man-made antioxidant nanoparticles: using redox vulnerability of nanoceria to develop a responsive drug delivery system. *ACS Appl Mater Interfaces.* 6. 21:19424-19433.

Nelson, B. C. Johnson, M. E. Walker, M. L. Riley, K. R. Sims, C. M. 2016. Antioxidant Cerium Oxide Nanoparticles in Biology and Medicine. Antioxidants 17. 5:15-22.

Nemmar, A. Al-Salam, S. Nuaman, S. A. Kazim, M. Mohamed, F. Beegam, S. Yuvaraju, P. Yasin, J. Ali, B. H. 2021. Exacerbation of Coagulation and Cardiac Injury in Rats with Cisplatin-Induced Nephrotoxicity Following Intratracheal Instillation of Cerium Oxide Nanoparticles. *Cell Physiol Biochem*. 15. 1:1-16.

Nesakumar, N. Sethuraman, S. Krishnan, U. M. Rayappan, J. B. Fabrication of lactate biosensor based on lactate dehydrogenase immobilized on cerium oxide nanoparticles. *J Colloid Interface Sci*. 15. 10:158-164.

Nguyen, V. H. Lee, B. J. 2017. Protein corona: a new approach for nanomedicine design. *Int J Nanomedicine.* 18. 12:3137-3151.

Niemiec, S. M. Hilton, S. A. Wallbank, A. Azeltine, M. Louiselle, A. E. Elajaili, H. Allawzi, A. Xu, J. Mattson, C. Dewberry, L. C. Hu, J. Singh, S. Sakthivel, T. S. Sea, S. Nozik-Grayck, E. Smith, B. Zgheib, C. Liechty, K. W. 2021. Cerium oxide nanoparticle delivery of microRNA-146a for local treatment of acute lung injury. *Nanomedicine.* 5. 34:102-118.

Nita, M. Grzybowski, A. 2016. The Role of the Reactive Oxygen Species and Oxidative Stress in the Pathomechanism of the Age-Related Ocular Diseases and Other Pathologies of the Anterior and Posterior Eye Segments in Adults. *Oxid Med Cell Longev.* 31. 6:34-47.

Niu, J. Azfer, A. Rogers, L. M. Wang, X, Kolattukudy, P. E. 2007. Cardioprotective effects of cerium oxide nanoparticles in a transgenic murine model of cardiomyopathy. *Cardiovasc Res* 73. 3:549-59.

Nyoka, Mpumelelo, Yahya, E. Choonara, Pradeep Kumar, Pierre, P. D. Kondiah, and Viness Pillay. 2020. Synthesis of Cerium Oxide Nanoparticles Using Various Methods: Implications for Biomedical Applications. *Nanomaterials* 10. 2:242-255.

Oliveira, E. Bértolo, E. Núñez, C. Pilla, V. Santos, H. M. Fernández-Lodeiro, J. Fernández-Lodeiro, A. Djafari, J. Capelo, J. L. and Lodeiro, C. 2017. Green and

Red Fluorescent Dyes for Translational Applications in Imaging and Sensing Analytes: A Dual-Color Flag. *Chemistry Open*, 7. 1: 39–52.

Ould-Ouali, L. Noppe, M. Langlois, X. Willems, B. Timmerman, P. Brewster, M. E. Arien, A. 2005. Self-assembling PEGp (CL-co-TMC) copolymers for oral delivery of poorly water-soluble drugs: a case study with risperidone. *J Control Release*, 102. 3:657-668.

Allison, P. Joy, C. Allison, R. Brown, D Phelps, T. and Doktycz, M. 2010. An investigation of the interactions between an E. coli bacterial quorum sensing biosensor and chitosan-based nanocapsules. Appl. Environ. *Microbiol* 76. 10. 7981–7989.

Pagliari, F. Mandoli, C. Forte, G. Magnani, E. Pagliari, S. Nardone, G. Licoccia, S. Minieri, M. Di Nardo, P. Traversa, E. 2012. Cerium oxide nanoparticles protect cardiac progenitor cells from oxidative stress. *ACS Nano* 6. 5:3767-3775.

Palmer, R. M. Ferrige, A. G. Moncada, S. 1987. Nitric oxide release accounts for the biological activity of endothelium derived relaxing factor. *Nature* 3. 27:524–526

Pankhurst, Q. A. Connolly, J. Jones, S. K. 2003. Dobson J: Applications of magnetic nanoparticles in biomedicine. *J Phys D: Appl Phys* 36. 16:177-181.

Panyam, J. Labhasetwar, V. 2004. Sustained cytoplasmic delivery of drugs with intracellular receptors using biodegradable nanoparticles. *Mol Pharm*, 1. 1:77-84.

Park, S. Vohs, J. M. Gorte, R. J. 2000. Direct oxidation of hydrocarbons in a solid-oxide fuel cell. *Nature* 16. 40: 265-267.

Park, B. K. Donaldson, R. Duffin, L. Tran, F. Kelly, I. Mudway, J. P. Morin, R. Guest, P. Jenkinson, Z. Samaras, M. Giannouli, H. Kouridis, and P. Martin. 2008. Hazard and risk assessment of a nanoparticulate cerium oxide-based diesel fuel additive a case study. *Inhalation Toxicol* 10. 20:547-566.

Patra, J. K. Gouda, S. 2013. Application of nanotechnology in textile engineering: An overview. *J. Eng. Technol. Res* 5. 5:104-111.

Peic, A. Podolski-Reni´c, S. Stojkovi´c, B. Matovi´c, D. Zmejkoski, V. Koji´c, G. Bogdanovi´c, A. Pavi´cevi´c, M. Mojovi´c, A. Savi´c, I. Milenkovi´c, A.

Kalauzi and K. Radoti´c. 2015. Anti-cancer effects of cerium oxide nanoparticles and its intracellular redox activity. *Chem.-Biol. Interact.* 2. 32:67–78.

Pelletier, D. A. Suresh, A K. Holton, G. A, McKeown, C. K. Wang, W. Gu, B. Mortensen, N. P. Allison, D. P. Joy, D. C. Allison, M. R. Brown, S. D, Phelps TJ, Doktycz MJ. 2010. Effects of engineered cerium oxide nanoparticles on bacterial growth and viability. *Appl Environ Microbiol*. 76. 24:7981-7999.

Peng, L. He, X. Zhang. P. Zhang, J. Li, Y. Zhang, J. Ma, Y. Ding, Y. Wu, Z. Chai, Z. Zhang, Z. 2014. Comparative pulmonary toxicity of two ceria nanoparticles with the same primary size. *Int J Mol Sci* 10 4:6072-6085.

Pesic, M. Podolski-Renic, A. Stojkovic, S. Matovic, B. Zmejkoski, D. Kojic, V. Bogdanovic, G. Pavicevic, A. Mojovic, M. Savic, A. Milenkovic, I. Kalauzi, A. Radotic, K. 2015. Anti-cancer effects of cerium oxide nanoparticles and its intracellular redox activity. *Chemico-Biol Interaction* 8. 232:85–93.

Pirmohamed, T. Dowding, J. M. Singh, S. Wasserman, B. Heckert, E. Karakoti, A. S. King, J. E. Seal, S. Self, W. T. 2010. Nanoceria exhibit redox state-dependent catalase mimetic activity. *Chem Commun* 28. 16:2736-2748.

Pizzino, G. Irrera, N. Cucinotta, M. Pallio, G. Mannino, F. Arcoraci, V. Squadrito, F. Altavilla, D. Bitto, A. 2017. Oxidative Stress: Harms and Benefits for Human Health. *Oxid Med Cell Longev* 84. 1: 6763.

Pourkhalili, A. Hosseini, A. Nili-Ahmadabadi, S. Hassani, M. Pakzad, M. Baeeri, A. Mohammadirad and M. Abdollahi. 2011. Biochemical and cellular evidence of the benefit of a combination of cerium oxide nanoparticles and selenium to diabetic rats. *World J. Diabetes.* 2. 10: 204–210.

Premont, R. T. Reynolds, J. D. Zhang, R. Stamler, J. S. 2021. Red Blood Cell-Mediated S-Nitrosohemoglobin-Dependent Vasodilation: Lessons Learned from a β-Globin Cys93 Knock-In Mouse. *Antioxid Redox Signal* 34. 12:936-961.

Qi, Z. L. Cheng, Y. H. Xu, Z. Chen, M. L. 2020. Recent Advances in Porphyrin-Based Materials for Metal Ions Detection. *Int J Mol Sci* 14. 21:58-67.

Qiao, K. Xu, L. Tang, J. 2022. The advances in nanomedicine for bone and cartilage repair. *J Nanobiotechnol.* 20. 12:141-157.

Rai, Mahendra, Dos Santos, Júlio César, Soler, Matheus Francisco, Franco Marcelino, Paulo Ricardo, Brumano, Larissa Pereira, Ingle, Avinash P. Gaikwad, Swapnil, Gade, Aniket and da Silva, Silvio Silvério. 2020. Strategic role of nanotechnology for production of bioethanol and biodiesel *Nanotechnology Reviews* 5. 2:231-250.

Raju, G.S. Pavitra, E. Varaprasad, G. L. 2022. Nanoparticles mediated tumor microenvironment modulation: current advances and applications. *J Nanobiotechnol* 20. 3:274-291.

Ramaswamy, S. Weinbauer G. F. 2015. Endocrine control of spermatogenesis: Role of FSH and LH/ testosterone. *Spermatogenesis* 26. 42:e996025.

Rana, S. Yeh, Y. and Rotello, V. 2010. Engineering the nanoparticle-protein interface: applications and possibilities. *Current opinion in chemical biology* 14. 6:828–834.

Ransy, C. Vaz ,C. Lombès, A. Bouillaud, F. 2020. Use of H_2O_2 to Cause Oxidative Stress, the Catalase Issue. *Int J Mol Sci* 30. 21:91-104.

Reitman, S. Frankel, S. 1957. A colorimetric method for the determination of serum level of glutamate-oxaloacetate and pyruvate transaminases. *Am J Clin Pathol* 28. 1:56–63

Rodea-Palomares, S. Gonzalo, J. Santiago-Morales, F. Legan´es, E. Garc´ıa-Calvo, Rosal R. and Fern´andez- Pinas. 2012. An insight into the mechanisms of nanoceria toxicity in aquatic photosynthetic organisms. *Aquat. Toxicol* 122. 123:133–143.

Ronkainen, N. J. Halsall, H. B. Heineman, W. R. 2010. Electrochemical biosensors. *Chem Soc Rev* 39. 5:1747-63.

Rotruck, J. T. Pope, A. L. Ganther, H. E. Swanson. A. B. Hafeman, D. G. Hoekstra, W. G. 1973. Selenium: biochemical role as a component of glutathione peroxidase. *Science* 179:588–590.

Rzigalinski, B. A. 2005. Nanoparticles and cell longevity. *Technol Cancer Res Treat*. 4. 6:651-9.

Saifi, M. A. Seal. S, Godugu, C. 2021. Nanoceria, the versatile nanoparticles: Promising biomedical applications. *J Control Release* 10 338:164-189.

Sallie, R. Tredger, J. M. Williams, R. 1991. Drugs and the liver part 1: testing liver function. *Biopharm Drug Dispos* 8. 12:251–259

Sarabjeet, S. Suri, H. Fenniri and Baljit S. 2007. Nanotechnology-based drug delivery systems. *J of Occup Med and Toxico,* 2. 3:16-25.

Schubert, D. Dargusch, R. Raitano, J. Chan, S. W. 2006. Cerium and yttrium oxide nanoparticles are neuroprotective. *Biochem Biophys Res Commun* 31. 1:86-91.

Sekhon, B. 2010. Food nanotechnology - an overview. *Nanotechnol Sci Appl* 4. 3:1-15.

Senthilkumar, R. P. Bhuvaneshwari, V. Ranjithkumar, R. Sathiyavimal, S. Malayaman, V. Chandarshekar, B. 2017. Synthesis, characterization and antibacterial activity of hybrid chitosan-cerium oxide nanoparticles. *Int J Biol Macromol*.104. 17:46-52.

Sepanjnia, A. Ghasemi, H. Mohseni, R. Ranjbar, A. Shabani, F. Salimi, F. Kheiripour. N. 2020. Effect of Cerium Oxide Nanoparticles on Oxidative Stress Biomarkers in Rats' Kidney, Lung, and Serum. *Iran Biomed J.* 24. 4:251-266.

Sha, Li. Hor-Yue Tan, Ning Wang, Zhang-Jin Zhang, Lixing Lao, Chi-Woon Wong Yibin Feng 2015. The Role of Oxidative Stress and Antioxidants in Liver Diseases. *Int J Mol Sci* 10. 16:26087–26124.

Shashi, K. and Murthy, 2007. Nanoparticles in modern medicine: State of the art and future challenges. *Int J. Nanomed* 2. 2:129–141.

Shen, Y, and White, E. 2001. p53-dependent apoptosis pathways. *Adv Cancer Res* 12. 82:55-84.

Shi, H. Magaye. R. Castranova, V. Zhao, J. 2013. Titanium dioxide nanoparticles: a review of current toxicological data. *Part Fibre Toxicol* 15. 10:15-22.

Singh, K. R. Nayak, V. Sarkar, T. Singh, R. P. 2020. Cerium oxide nanoparticles: properties, biosynthesis and biomedical application. *RSC Adv* 21. 10:27194-27214.

Singh, K. R. Nayak, V. Sarkar, T. Singh, R. P. 2020. Cerium oxide nanoparticles: properties, biosynthesis and biomedical application. *RSC Adv* 21. 10.:27194-27214.

Singh, S. Dosani, T. Karakoti, A. S. Kumar, A. Seal, S. Self, W. T. 2011. A phosphate-dependent shift in redox state of cerium oxide nanoparticles and its effects on catalytic properties. *Biomaterials.* 32. 28:6745-6753.

Singh, S. and Namrata, P. 2021. Antioxidant metal oxide nanozymes: role in cellular redox homeostasis and therapeutics. *Pure and Applied Chemistry* 93. 2:64-77.

Sirelkhatim, A. Mahmud, S. Seeni, A. Kaus, N. Ann, L. Bakhori, S. 2015. Review on Zinc Oxide Nanoparticles: Antibacterial Activity and Toxicity Mechanism. *Nanomicro Lett* 7. 3:219-242.

Skibińska, K. Kołczyk-Siedlecka, K. Kutyła, D. Gajewska. M. Żabiński P. 2021. Synthesis of Co-Fe 1D Nanocone Array Electrodes Using Aluminum Oxide Template. *Materials* 14. 7:1717.

Snow, S. J. Mcgee, J. Miller, D. B 2014. Inhaled diesel emissions generated with cerium oxide nanoparticle fuel additive induce ad verse pulmonary and systemic effects. *Toxicol Sci* 142:403–417.

Song, Y. Driessens, N. Costa, M. De-Deken, X. Detours, V. Corvilain, B. Maenhaut, C. Miot, F. Van Sande, J. Many, M. C. Dumont, J. E. 2007. Roles of hydrogen peroxide in thyroid physiology and disease. *J Clin Endocrinol Metab* 92. 10:3764-73.

Spicer, C. D. Jumeaux, C. Gupta, B. Stevens, M. M. 2018. Peptide and protein nanoparticle conjugates: versatile platforms for biomedical applications. *Chem Soc Rev* 47. 10:3574-3620.

Stark, G. 2005. Functional consequences of oxidative membrane damage. *J Membr Biol* 205. 1:1-16.

Su, L. J. Zhang, J. H. Gomez, H. Murugan, R. Hong, X. Xu, D. Jiang, F. Peng, Z. Y. 2019. Reactive Oxygen Species-Induced Lipid Peroxidation in Apoptosis, Autophagy, and Ferroptosis. *Oxid Med Cell Longev* 10:342-355.

Sudha, T. Bharali, D. J. Yalcin, M. Darwish, N. Coskun, M. Keating, K. A, 2017. Targeted delivery of paclitaxel and doxorubicin to cancer xenografts via the nanoparticle of nano-diamino-tetrac. *Int J Nanomedicine* 15. 12:1305-1315.

Sukhanova, A. Bozrova, S. Sokolov, P. Berestovoy, M. Karaulov, A. Nabiev, I. 2018. Dependence of Nanoparticle Toxicity on Their Physical and Chemical Properties. *Nanoscale Res Lett* 7 13:44-58.

Szymanski, C. J. Munusamy, P. Mihai, C. Xie, Y. Hu, D. Gilles, M. K. Tyliszczak, T. Thevuthasan, S. Baer, D. R. 2017. Shifts in oxidation states of cerium oxide nanoparticles detected inside intact hydrated cells and organelles. *Biomaterials.* 10. 62:147-54.

Taha, M, Elazab, T. Badawy, A. M. Saati A. A. Qusty, N. F. Al-Kushi, A. Sarhan, A. Osman, A. Farage, A. E. 2022. Activation of SIRT-1 Pathway by Nanoceria Sheds Light on Its Ameliorative Effect on Doxorubicin-Induced Cognitive Impairment (Chemobrain): Restraining Its Neuroinflammation, Synaptic Dysplasticity and Apoptosis. *Pharmaceuticals* 15. 8:918.

Tarnuzzer, R. W. Colon, J. Patil, S. and Seal, S. 2005. Vacancy engineered ceria nanostructures for protection from radiation-induced cellular damage. *Nano letters* 5. 4:2573–2577.

Tewabe, A. Abate, A. Tamrie, M. Seyfu, A. Abdela, Siraj, E. 2021. Targeted Drug Delivery - From Magic Bullet to Nanomedicine: Principles, Challenges, and Future Perspectives. *J Multidiscip Health* 5. 14:1711-1724.

Thakur, N. Manna, P. and Das, J. 2019. Synthesis and biomedical applications of nanoceria, a redox active nanoparticle. *Journal of nanobiotechnology,* 17. 1:84-96.

Tharkar Priyanka, Varanasi Ramya, Wong Wu Shun Felix, Jin Craig T., Chrzanowski Wojciech 2010. Nano-Enhanced Drug Delivery and Therapeutic Ultrasound for Cancer Treatment and Beyond. *Front. Bioeng. Biotechnol* 22. 8:485-500.

Thiel, R. J. 2000. Natural vitamins may be superior to synthetic ones. *Med Hypotheses* 55. 6:461-469.

Trush, M.A. Egner, P. A. Kensler, T. W. 1994. Myeloperoxidase as a biomarker of skin irritation and inflammation. *Food Chem Toxicol* 12. 32:143–147.

Tsai. S. M. Duran-Robles, E. Goshia, T. Mesina, M. Garcia, C. Young, J. Sibal, A. Chiu, M. H. Chin, W. C. 2018. CeO_2 nanoparticles attenuate airway mucus secretion induced by TiO_2 nanoparticles. *Sci Total Environ* 1:631-632.

Tsapras, P. and Nezis, I. P. 2017. Caspase involvement in autophagy. *Cell Death Differ*. 24. 8:1369-1379.

Tung, N. M. and Garber. J. E. 2018. BRCA1/2 testing: therapeutic implications for breast cancer management. *Br J Cancer* 19. 2:141-152.

Valavanidis, A. Vlachogianni, T. Fiotakis, K. Loridas, S. 2013. Pulmonary oxidative stress, inflammation and cancer: respirable particulate matter, fibrous dusts and ozone as major causes of lung carcinogenesis through reactive oxygen species mechanisms. *Int J Environ Res Public Health* 10. 9:3886-907.

Váradi, L. Luo, J. L. Hibbs, D. E. Perry, J. D. Anderson, R. J. Orenga, S. Groundwater, P. W. 2017. Methods for the detection and identification of pathogenic bacteria: past, present, and future. *Chem Soc Rev* 46. 16:4818-4832

Wagner, A. M. Knipe, J. M. Orive, G. Peppas, N. A. 2019. Quantum dots in biomedical applications. *Acta Biomater* 15. 94:44-63.

Wang, J. Chen, Y. Gao, N. 2013. Inhibitory effect of glutathione on oxidative liver injury induced by dengue virus serotype 2 infections in mice. *PLoS One* 8. 1:55407–55407

Wang, L. Hu, C. Shao, L. 2017. The antimicrobial activity of nanoparticles: present situation and prospects for the future. *Int J Nanomedicine* 14. 12:1227-1249.

Wang L. 2017. Engineering the Genetic Code in Cells and Animals: Biological Considerations and Impacts. *Acc Chem Res* 50. 11:2767-2775.

Wang, W. J. Y. Howe, Y. Li, X. Qiu, D. C. Joy, M. P. Paranthaman, M. J. Doktycz, and B. Gu. 2010. A surfactant and template free route for synthesizing ceria nanocrystals with tunable morphologies. *J. Mater. Chem* 20:7776-7781.

Wason, M. S. Colon, J. Das, S. Seal, S. Turkson. J. Zhao, J. Baker, C. H. 2013. Sensitization of pancreatic cancer cells to radiation by cerium oxide nanoparticle-induced ROS production. *Nanomedicine* 9. 4:558-69.

Wen, L. Li, M. Lin, X. Li, Y. Song, H. Chen, H. 2022. AgNPs Aggravated Hepatic Steatosis, Inflammation, Oxidative Stress, and Epigenetic Changes in Mice With NAFLD Induced by HFD. *Front Bioeng Biotechnol* 19. 10:912178.

Wieczfinska, J. Sitarek, P. Skała, E. Kowalczyk, T. Pawliczak, R. 2019. Inhibition of NADPH Oxidase-Derived Reactive Oxygen Species Decreases Expression of Inflammatory Cytokines in A549 Cells. *Inflammation* 42. 6:2205-2214.

Wyrobek, A. J. Heddle, J. A. Bruce, W. R. 1975. Chromosomal abnormalities and the morphology of mouse sperm heads. *Can J Genet Cytol* 17. 4:675-81.

Xia, T. Kovochich, M. Brant, J. Hotze, M. Sempf, J. Oberley, T. Sioutas, C. Yeh, J. I. Wiesner, M. R. Nel, A. E. 2006. Comparison of the abilities of ambient and

manufactured nanoparticles to induce cellular toxicity according to an oxidative stress paradigm. *Nano Lett.* 6. 8:1794-807.

Xia, X. R. Monteiro-Riviere N. Riviere, J. E. 2010. An index for characterization of nanomaterials in biological systems. *Nat Nanotechnol* 5. 9:671-685.

Xu, G. Shi, Y. 2007. Apoptosis signalling pathways and lymphocyte homeostasis. *Cell Res* 17:759–771.

Ya-hong, Z. Ying-liang, W. Shinichi, T. Satoshi, O. Takashi, I. 2011. Reactive oxygen species contribute to oridonin-induced apoptosis and autophagy in human cervical carcinoma HeLa cells. *Acta Pharmacologica Sinica* 12. 32:1266–1275.

Yang, Y. Zhang, M. Song, H. Yu, C. 2020. Silica-Based Nanoparticles for Biomedical Applications: From Nanocarriers to Biomodulators. *Acc Chem Res* 18 8:1545-1556.

Yetisgin, A. A. Cetinel, S. Zuvin, M. Kosar. A. Kutlu O. 2020. Therapeutic Nanoparticles and Their Targeted Delivery Applications. *Molecules* 25 9:2193.

Younus, H. 2018. Therapeutic potentials of superoxide dismutase. *Int J Health Sci* 12. 3:88-93.

Yue, W, Moustafa, R. Ali, K. Ning, F. Mostafa A. El-Sayed. 2019. Gold nanoparticles in biological optical imaging, *Nano Today*. 3. 24:120-140.

Zhang, D. Ma, X. L. Gu, Y. Huang, H. Zhang, G.W. 2020. Green Synthesis of Metallic Nanoparticles and Their Potential Applications to Treat Cancer. *Front Chem* 29. 8:799

Zhang, D. Tan. T. Gao, L. Zhao, W. Wang, P. 2007. Preparation of azithromycin nanosuspensions by high pressure homogenization and its physicochemical characteristics studies. *Drug Dev Ind Pharm* 33. 5:569-575.

Zhang, Y. Wu, X. Hou, C. Shang, K. Yang, K. Tian, Z. Pei, Z. Qu, Y. and Pei, Y. 2018. Dual-responsive dithio-polydopamine coated porous CeO_2 nanorods for targeted and synergistic drug delivery. *Intl J Nanomed* 15. 13:2161–2173.

Zhao, H. Wu, L. Yan, G. 2021. Inflammation and tumor progression: signalling pathways and targeted intervention. *Sig Transduct Target Ther* 6. 9: 263-278.

Zholobak, V. Ivanov, K, and Shcherbakov, B. 2016. Interaction of nanoceria with microorganisms. *Therapy* 3. 5:419–450.

Zubieta-Calleja, G. R. Paulev, P. E. Zubieta-Calleja, L. Zubieta-Castillo, G. 2007. Altitude adaptation through hematocrit changes. *J Physiol Pharmacol*. 5. 2:811-8.

APPENDICES

Appendix 3.1

Preparation of rinsing buffer (1.15%KCl):

A 1.15 g potassium chloride was taken, weighed and liquified in 100ml dH_20 kept at 4^0c

Appendix 3.2

Preparation of homogenizing Buffer (0.01M Phosphate buffer, pH7.4)

a $Na_2HPO_4.12H_2O$ (7.1628g) was liquified in 200mL of dH_20.

b. $NaH_2PO_4.2H_2O$ (1.5603g) (Mol.Wt. 358.22) was dissolved in 100mL dH_20.

Also, the preparation of 0.1M PO buffer solution was performed by mixing 200 ml of $Na_2HPO_4.12H_2O$ to 100 ml $NaH_2PO_4.2H_2O$ together. pH was regulated with a few droplets of HCl and sodium hydroxide to 7.4.

Appendix 3.3

Reagent and calculation for haemoglobin

(1) Drabkin,s Solutions

1.0 g sodium hydrogen carbonate and 198.0 mg potassium ferricyanide were dissolved in distilled water and made up to 1000 cm

Calculation:

$$\text{Hb concentration (g/100mL)} = \frac{\text{Abs of test X B= Conc. standard x Dil. F}}{\text{Abs of Standard}}$$

DF = 201 while Conc of standard = 0.0572g/100ml

Appendix 3.4

Reagent and calculation for determination of Red blood cell count:

(i) Haymen's solution

0.25g of Mercury chloride ($HgCl_2$; Hopkins and Williams Ltd, England), 0.25g of Sodium sulphate (Na_2SO_4: BDH chemicals Ltd, England), and 0.5g of sodium chloride

were dissolved in liquified in dH_20 and levelled up to 100 ml. This mixture was isotonic with blood and prevented roleaux formation and coagulation.

Calculation:

Volume of distilled blood over each small square =

Volume of diluted blood over 80 small squares=

Blood was diluted 1:200

If N red cells were present in 1/50 nm^3 of diluted blood,

Then 50N red cells would be in $1mm^3$ of diluted blood

50N x 200 (10,000N) red cells would be present in $1mm^3$ of diluted blood

Note: The red cell containing area was situated in the centre of the counting chamber and bounded by three thoma ruling.

Appendix 3.5

Reagents for determination of lipid peroxidation

(a) 10% Trichloroacetic acid (TCA)

TCA (10g) (Sigma Chemicals Co, London)was liquefied inside 100mL of dH_20, kept at 40C.

(b) 0.75% Thiobarbituric acid (TBA) in 0.1M HCl

TBA (0.75g) (Sigma Chemicals) was liquefied inside 10mL of 0.1M HCl.

Total suspension was performed placing it inside a shaking hot bath. It was prepared fresh.

(c) 0.1M Tris buffer(pH 7.4)

1.12g potassium chloride was first dissolved inside a beaker and later followed by dissolving 2.36g Tris-base in another beaker. Both solution were later mixed and dH_20 was added to make 100ml mark.

Calculation

$$\text{MDA (units/mg protein)} = \frac{\text{Absorbance x Volume of mixture}}{E_{532nm} \text{ x Volume of Sample x mg Protein}}$$

Appendix 3.6

Reagents for the determination of superoxide dismutase activity

1. 0.05 M Carbonate Buffer, pH 10.2

$Na_2CO_3.10H_2O$ (14.3 g) and 4.2 g of $NaHCO_3$ were dissolved in 900 mL of distilled water and then made up to 1 litre.

2. 0.3 M of adrenaline.

Adrenaline (0.0137 g) was dissolved in 200 mL distilled water and then made up to 250 mL. This solution was prepared just before the experiment.

Calculation

$$\text{Increase in absorbance per minute} = \frac{A\,3 - A\,0}{2.5}$$

Where $A\,0$ = absorbance after 0 seconds

$A\,3$ = absorbance after 150 seconds

$$\%\ \text{Inhibition} = \frac{\text{Increase in absorbance of substrate X 100}}{\text{Increase in absorbance of blank}}$$

1 unit of SOD activity was given as the amount of SOD necessary to cause 50% inhibition of the oxidation of adrenaline.

Appendix 3.7

Reagents for determining of catalase activity.

1. Buffer System

Dipotassium hydrogen phosphate trihydrate ($K_2HPO_4.3H_2O$) (0.696g) and potassium dihydrogen phosphate (0.265g) were liquified in 90mL dH_20 and pH set at 7.4. The solution was then levelled up to 100mL mark by dH_20.

2. Hydrogen peroxide (19mM)

Thirty percent H_20_2 (194µl) was mixed with 50mL (0.05M) phosphate buffer, and pH set at 7.4. The solution was then levelled up to 100mL mark by dH_20. [

Calculation

$$\text{Catalase activity} = \frac{AA_{240}/\text{min} \times \text{reaction volume} \times \text{dilution factor}}{0.0436 \times \text{sample volume} \times \text{mg protein/mL}}$$

$$= \mu\text{mole } H_2O_2/\text{min/mg protein}$$

Appendix 3.8

Chemicals

1. 1 chloro, 2 4-DinitroBenzene (3.37 mg) was liquified using 1mL ethanol.

2. Glutathione (30.73 mg) was liquified using 1mL of (0.1M) phosphate buffer(pH 6.5)

3. Buffer system

The buffer system preparation involves the dissolution of 4.96g Dipotassium Hydrogen Phosphate (K_2HPO_4) with 9.73 g Dihydrogen Phosphate, (KH_2PO_4) in dH_20 and pH set at 6.4. The solution was then levelled up to 100mL mark by dH_20.

Appendix 3.9

Reagents for determination of glutathione peroxidase activity

1. Sodium Azide, NaN_3 (0.0325 g) was liquified with 50 mL dH_2O

2. Reduced Glutathione GSH (0.0123g) was liquified with 10 mL Phosphate Buffer.

3. Hydrogen Peroxide, H_2O_2, (0.028 mL) was liquified with 100 mL dH_2O.

4. Tricholoroacetic acid, TCA (2g) was liquified with 20 mL dH_2O

5. Dipotassium Hydrogen orthophosphate K_2HPO_4 (5.23g) was liquified with 100 mL dH_2O

5. 5, 5`-Dithiobis (2- DinitroBenzoic acid), (0.04g) was liquified with 100 mL phosphate buffer.

6. The Buffer system K_2HPO_4 (0.992 g) and 1.946 g KH_2PO_4 was liquified in 200 mL of pH set at 7.4. The solution was then levelled up to 100mL mark by dH_20.

Calculation:

GSH consumed = 245.84 – GSH remaining

$$\text{Glutathione peroxidase activity} = \frac{\text{GSH consumed}}{\text{mg protein}}$$

Appendix 3.10

Reagents for the determination of reduced glutathione.

1. Reduced Glutathione (GSH) working standard

GSH was liquified with 0.1 M Phosphate buffer, pH set at 7.4. The solution was then levelled up to 100mL mark by dH_20 and then stored at 4^0C

0.1 M Phosphate buffer (pH 7.4)

a. $Na_2HPO_4.12H_2O$ (7.1628g) was liquified with 200 mL dH_20.

b. $NaH_2PO_4.2H_2O$ (1.5603 g) was liquified with 100 mL dH_20.

The preparation of 0.1 M phosphate buffer was performed with the addition of 200 mL of (a) to 100 mL of (b) and pH set at 7.4

[5, 5` -Dithiobis-(2-Nitrobenzoate) (DTNB)]

The reagent preparation was performed with the dissolution of 40 mg of Ellman's reagent into 0.1 M phosphate buffer and levelled up to 100 mL mark. The stability of this solution can be maintained for about three weeks while in the refrigerator

3 Sulphosalicyclic acid ($C_7H_6O_6S.2H_2O$) was prepared following the dissolution of 4 g of sulphosalicyclic acid into little quantity of dH_20 and levelled up to 100mL mark. The stability of this solution can be maintained for about three weeks while in the refrigerator.

Appendix 3.11

Reagents for the determination of myeloperoxidase activity

1. o-dianisidine

16.7 mg of o-dianisidine was liquified with 100 ml phosphate buffer.

2. Buffer system

0.496 g dipotassium hydrogen phosphate and 0.973 g of potassium dihydrogen phosphate was liquified inside dH_20 and and levelled up to 100 mL mark

3. Diluted H_2O_2

4 µl of H_2O_2 was added to 96 µl of distilled water to make 100 µl of diluted H_2O_2.

Calculation

$$\text{MPO activity} = \frac{\Delta Abs\ (t_2\text{-}t_1) / \text{min} \times \text{volume of mixture} \times \text{dilution factor}}{(11.3 \times 10^{-3}) \times \text{volume of sample} \times \text{mg protein}}$$

Appendix 3.12

Preparation of reagents for the determination of the Sialic acid content

(1). Sodium Per iodate

2.67mg of sodium per-iodate was dissolved in 5ml of 1.0M H_2SO_4

(2). Sodium meta arsenite

120mg of sodium meta arsenite was dissolved in 3ml of 0.5N Hcl

(3). Thiobarbituric Acid (TBA)

172.8mg of TBA was dissolved in 12ml of dH_20.

(4). Acidified Butanol

5% Hcl in butanol. 5ml of Hcl and 95ml of butanol were mixed together.